THEORETICAL INVESTIGATIONS
OF
EXTERNALLY PRESSURIZED GAS-BEARINGS

Hiroshi Yabe

(1965)

THEORETICAL INVESTIGATIONS
OF
EXTERNALLY PRESSURIZED GAS-BEARINGS

Hiroshi Yabe

(1965)

Abstract

Descriptions are concerned with the static bearing characteristics such as the pressure distribution, load capacity, and volume rate of flow of the externally pressurized gas-bearings for some bearing configurations.

The complex potential theory is applied to the thrust gas-bearings with multiple supply holes to yield the bearing characteristics, and the thrust collar gas-bearings with slit-supply are also investigated as well.

Externally pressurized thrust and journal gas-bearings with porous bearing surface are analyzed with consideration of the gas-flow in the porous material by applying an extension of Darcy's law.

These theoretical results are compared with experimental ones and good agreements are observed between them.

Contents

Introduction

The externally pressurized gas-bearings are recently investigated and applied to many devices especially for supporting high speed rotors owing to their advantages of small static and dynamic friction.

The externally pressurized bearing has a restrictor generally such as a capillary or an orifice at the fluid supply so that large bearing stiffness may be achieved. In order to design the most reasonable restrictor, one should know the bearing characteristics such as load capacity and volume rate of flow.

In the followings, these characteristics are investigat theoretically in connection with bearing clearance and supp pressure for various bearing configurations.

Externally pressurized thrust gas-bearing is rather disadvantageous for its small load capacity. The recess to hold high supply pressure is apt to make the operation less stable because of self-excited vibration.

A simple method to improve the load capacity is to arrange multiple supply holes on the bearing surface so tha the average pressure may increase fairly well. For the thr collar type of gas-bearing, multiple supply holes must be required because of the bearing construction. These types

thrust gas-bearings are investigated in Part I by means of the complex potential theory to yield the pressure distribution, volume rate of flow, and load capacity, which are compared with experimental results.

The technique of complex potential theory is also applied to the rectangular pad-type thrust gas-bearing with multiple supply holes.

The load capacity may increase with increase of number of supply holes which are spaced circumferentially in the thrust collar bearing surface. This leads to a gas-bearing with slit-supply which is considered as innumerable supply holes arranged in a line.

In Part II, externally pressurized thrust collar gas-bearing with single or double slit-supply is analyzed theoretically to obtain a design chart concerning load capacity and volume rate of flow.

In Part III, externally pressurized porous gas-bearing is investigated theoretically. The porous bearing can be assumed to consist of a mesh structure incorporating innumerable tubes of fluid supply, hence it may be a limiting bearing structure where infinite supply holes are arranged on the entire bearing surface. The porous bearing surface serves to restrict the gas flow and also to dissipate the

energy of vibrations. So this type of gas-bearing is expected to have comparatively large load capacity and to make stable operation.

Externally pressurized porous gas-bearing is analyzed fundamentally for two cases of journal and thrust bearings. The analysis can be applied to the other types of porous bearings, namely, porous thrust and journal gas-bearings with flat and solid parts, porous thrust collar gas-bearing, and so on.

The theory may be verified with experimental results with very good qualitative agreement and fairly good quantitative agreement.

Part I Analysis of Externally Pressurized Gas-Bearing by Means of the Complex Potential Theory

Chapter 1 Introduction

In practical applications of externally pressurized gas-bearings, it is desirable to obtain the exact pressure distribution in the bearing clearance in order to determine the volume rate of flow, which in turn leads to a determination of the size of the restrictor (such as a capillary or an orifice), and in order to calculate the load capacity.

The complex potential theory is one of the most applicable methods to obtain these characteristics of the externally pressurized bearing, and it has been applied to the journal bearing[1] and to the thrust bearing with several bearing shapes[2]. The theoretical pressure distribution coincided well with experimental results, but the load capacity was hard to determine analytically because of difficulty of mathematical integration of the pressure over the bearing area.

In Part I, externally pressurized thrust bearings are analyzed by means of the complex potential theory for several bearing configurations, namely, circular thrust gas-bearing, thrust collar gas-bearing, rectangular pad-type thrust bearing,

and some modifications of them as well. The bearings have multiple supply holes and no recess since the recess causes the instability of the bearing.

By using the suitable potential function which satisfies the boundary conditions of the particular bearing, pressure distribution and volume rate of flow are obtained theoretically for both an incompressible and a compressible fluid, while load capacity is obtained theoretically for an incompressible fluid.

Experiments are made to be compared with theoretical results and very good agreements are observed between them.

Chapter 2 General Theory

2-1 Basic Equations

Upon applying the usual assumptions in gas-bearing theory, Navier-Stokes equations reduce to the Reynolds equation for compressible viscous flow:

$$\frac{\partial}{\partial x}\left(\frac{\rho h^3}{\mu}\cdot\frac{\partial p}{\partial x}\right)+\frac{\partial}{\partial y}\left(\frac{\rho h^3}{\mu}\cdot\frac{\partial p}{\partial y}\right)=6\left\{U_x\frac{\partial(\rho h)}{\partial x}+U_y\frac{\partial(\rho h)}{\partial y}\right\} \qquad (1.2.1)$$

The symbols are notated in page 203-209.

Assuming that the gas flow is polytropic with index n and that μ is constant, Eq. (1.2.1) becomes

$$\frac{\partial}{\partial x}\left(h^3\frac{\partial p^{\frac{1+n}{n}}}{\partial x}\right)+\frac{\partial}{\partial y}\left(h^3\frac{\partial p^{\frac{1+n}{n}}}{\partial y}\right)=6\mu\left(\frac{1+n}{n}\right)\left\{U_x\frac{\partial(hp^{\frac{1}{n}})}{\partial x}+U_y\frac{\partial(hp^{\frac{1}{n}})}{\partial y}\right\} \quad (1.2.2)$$

If $U_x = U_y = 0$ or the sliding speed is very small compared with gas flowing velocity due to the pressure gradient, then the right-hand side of Eq. (1.2.2) vanishes. With the assumption of h=const., Eq. (1.2.2) becomes

$$\frac{\partial^2(p^{\frac{1+n}{n}})}{\partial^2 x}+\frac{\partial^2(p^{\frac{1+n}{n}})}{\partial^2 y}=0 \quad (1.2.3)$$

For the case of an incompressible fluid, Eq. (1.2.1) becomes as follows with the same assumptions,

$$\frac{\partial^2 p}{\partial x^2}+\frac{\partial^2 p}{\partial y^2}=0 \quad (1.2.4)$$

These are represented by the following Laplacian equation,

$$\frac{\partial^2 P}{\partial x^2}+\frac{\partial^2 P}{\partial y^2}=0 \quad (1.2.5)$$

where $P = p$ for an incompressible fluid

$P = p^{\frac{1+n}{n}}$ for a compressible fluid (1.2.6)

Eq. (1.2.5) is also expressed by the cylindrical coordinates

$$\frac{\partial}{\partial r}\left(r\frac{\partial P}{\partial r}\right)+\frac{1}{r}\cdot\frac{\partial^2 P}{\partial\theta^2}=0 \quad (1.2.7)$$

The problem of solving Eq. (1.2.5) or (1.2.7) can be

transformed into the problem of finding a suitable complex potential in the plane of complex number $Z = x + iy = re^{i\theta}$.

If a complex potential is obtained, the real part of the potential function gives the form of the pressure distribution for an incompressible fluid case, and the imaginary part gives the stream function. The pressure distribution must satisfy the boundary conditions of the actual bearing.

2-2 Transformation to Compressible Fluid

The compressible solution can be easily obtained from the incompressible solution by transformation through Eq. (1.2.6). If the letter P is substituted for p of the solution, P satisfies Eq. (1.2.5) or (1.2.7) and gives the pressure distribution in the form of $p^{\frac{1+n}{n}}$ where p is the real pressure for the compressible fluid case. But K's, which are constants determined by the boundary conditions mentioned in later sections, must satisfy the boundary conditions for the real pressure. Considering the relation between p and P in Eq. (1.2.6), p_o and p_a in K's must be changed to P_o and P_a, respectively, through the relations

$$P_o = p_o^{\frac{1+n}{n}}, \qquad P_a = p_a^{\frac{1+n}{n}} \tag{1.2.8}$$

where p_o and p_a correspond to the boundary pressures for

a compressible fluid case. Thus the solution for a compressible fluid can be expressed by

$$p = P^{\frac{n}{1+n}} \qquad (1.2.9)$$

where P is corresponding solution obtained for the incompressible fluid case using the correct boundary conditions.

Chapter 3 Analysis of Externally Pressurized Circular Thrust Gas Bearing with Multiple Supply Holes

3-1 Complex Potential and Pressure Distribution

In this Chapter, such an externally pressurized circular thrust bearing is analyzed that has multiple supply holes spaced circumferentially as shown later in Fig. 1.3.2.

At the first step, an analysis is made on a bearing with single supply hole located anywhere in the bearing as shown in Fig. 1.3.1: A variety of multiple supply holes can be obtained by the proper use of superposition.

In Fig. 1.3.1, we put a point source at radius a and a sink with the same strength q at radius r_1^2/a by the mirror image principle so that the solution may satisfy the boundary condition everywhere on the bearing periphery.

The complex potential function for this case can be given by

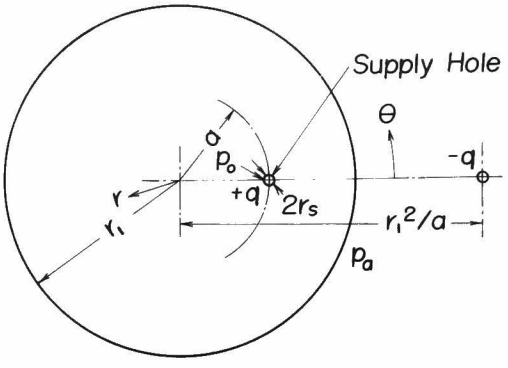

Fig. 1.3.1 Configuration of a circular thrust bearing with single supply hole

$$w = \frac{8}{2\pi}\left[\log(Z-a) - \log\left(Z-\frac{r_1^2}{a}\right)\right] \qquad (1.3.1)$$

By separating the complex potential w into real and imaginary parts, the pressure distribution p for an incompressible fluid can be obtained from the real part in terms of dimensionless variables,

$$p = K_1 \log \frac{R_a^2R^2+1-2R_aR\cos\theta}{R^2+R_a^2-2R_aR\cos\theta} + K_2 \qquad (1.3.2)$$

where $R = r/r_1$ and $R_a = a/r_1$

K_1 and K_2 are constants determined by the following boundary conditions:

$$\left.\begin{aligned} p &= p_a \quad \text{at} \quad R = r/r_1 = 1 \\ p &= p_o \quad \text{at} \quad R = R_a - R_s = (a - r_s)/r_1,\ \theta = 0 \end{aligned}\right\} \quad (1.3.3)$$

Then

$$\left.\begin{aligned} K_1 &= \frac{p_o - p_a}{2\log \dfrac{1 - R_a(R_a - R_s)}{R_s}} \\ K_2 &= p_a \end{aligned}\right\} \quad (1.3.4)$$

It should be noted that the boundary conditions are satisfied only at one point of the inner edge of the supply hole. However, if Z is near to a in Eq. (1.3.1), the curve of constant pressure is given as a circular form so that this pressure distribution may satisfy the condition of the supply hole when R_s is small enough compared with unity.

In the above boundary condition, the value of the pressure p_o just after the inlet hole is used. The p_o is not constant but varies as the change of the bearing clearance because of the pressure drop across the inlet restrictor, such as a capillary or an orifice if one is used. However it should be noted that the inlet pressure p_o, when the bearing load is given, is determined by the bearing load and is independent of the bearing clearance. Thus, the results below may be applied to obtain gas flow, bearing clearance, and stiffness when the external restrictor is used.

For the case with multiple supply holes, the pressure

distribution can be obtained by a proper superposition of the solution for a single supply hole. When there are k supply holes, each of which has radius r_{sj} and is located at $r = a_j$, $\theta = \theta_j$ $(j = 0, 1, \ldots, k-1)$, the resulting pressure distribution for an incompressible fluid is

$$p = \sum_{j=0}^{k-1} K_{1j} \log \frac{R_{aj}^2 R^2 + 1 - 2R_{aj} R\cos(\theta - \theta_j)}{R^2 + R_{aj}^2 - 2R_{aj} R\cos(\theta - \theta_j)} + K_2 \qquad (1.3.5)$$

where K_{1j} and K_2 are determined by the following boundary conditions:

$$\left.\begin{aligned} &p = p_a \quad \text{at} \quad R = 1 \\ &p = p_{oj} \quad \text{at} \quad R = R_{aj} - R_{sj},\ \theta = \theta_j\ (j = 1, 2, \ldots k-1) \end{aligned}\right\} (1.3.6)$$

When all of the k supply holes have the same dimensions

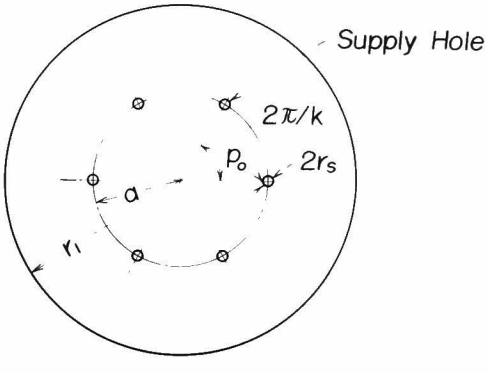

Fig. 1.3.2 Configuration of a circular thrust bearing with multiple supply holes

and are located at the same radius (R_a) with equal angular spacing of $2\pi/k$, as shown in Fig. 1.3.2, all of K_{1j} become equal to be $K_{1(k)}$, and the pressure distribution is

$$\left.\begin{aligned} p &= K_{1(k)} \sum_{j=0}^{k-1} \log \frac{R_a^2 R^2 + 1 - 2R_a R \cos(\theta - \theta_j)}{R^2 + R_a^2 - 2R_a R \cos(\theta - \theta_j)} + K_{2(k)} \\ &= K_{1(k)} \log \frac{R_a^{2k} R^{2k} + 1 - 2R_a^k R^k \cos k\theta}{R^{2k} + R_a^{2k} - 2R_a^k R^k \cos k\theta} + K_{2(k)} \end{aligned}\right\} \quad (1.3.7)$$

This reduction is shown in Appendix I.

The constants $K_{1(k)}$ and $K_{2(k)}$ are determined by the same boundary conditions as Eq. (1.3.3); then

$$\left.\begin{aligned} K_{1(k)} &= \frac{p_o - p_a}{2 \log \dfrac{1 - R_a^k (R_a - R_s)^k}{R_a^k - (R_a - R_s)^k}} \\ K_{2(k)} &= p_a \end{aligned}\right\} \quad (1.3.8)$$

Later on, this symmetrical case is analyzed; the results for an asymmetrical case may be obtained by modifying the results.

3-2 Examples of Theoretical Pressure Distribution

Figures 1.3.3 and 1.3.4 show examples of theoretical pressure distribution for the following bearing:

Number of supply holes, $k = 6$

Radial position of supply hole, $R_a = 0.5$

Radius of supply hole, $R_s = 0.01$

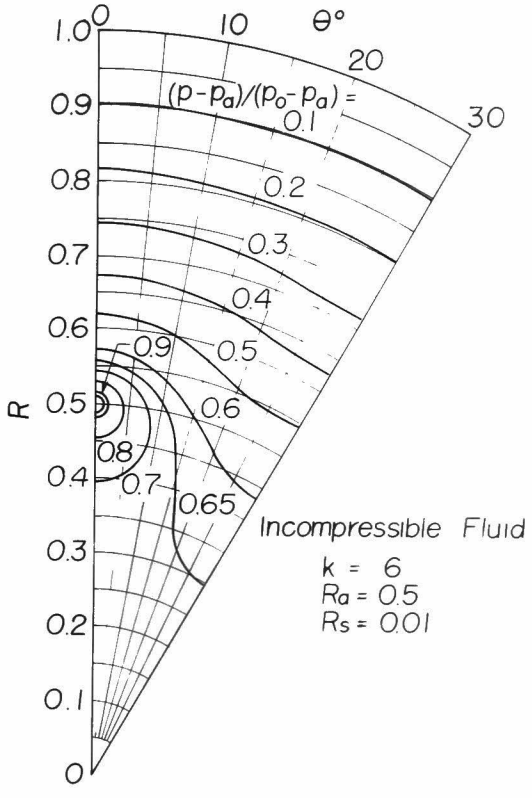

Fig. 1.3.3 Constant pressure curves with an incompressible fluid

Figure 1.3.3 shows the constant pressure lines on the bearing surface for an incompressible fluid. The pressure at central clearance space within the circle of the supply holes is kept at a considerably high value so that load

capacity can be much greater than that of the bearing with a single central supply hole.

The pressure distributions for radial and circumferential directions are shown in Fig. 1.3.4 for both an incompressible and a compressible fluid. For the latter, it is assumed that the gas flows isothermally and that $p_0 - p_a$ is taken to be 1 kg per square centimeter.

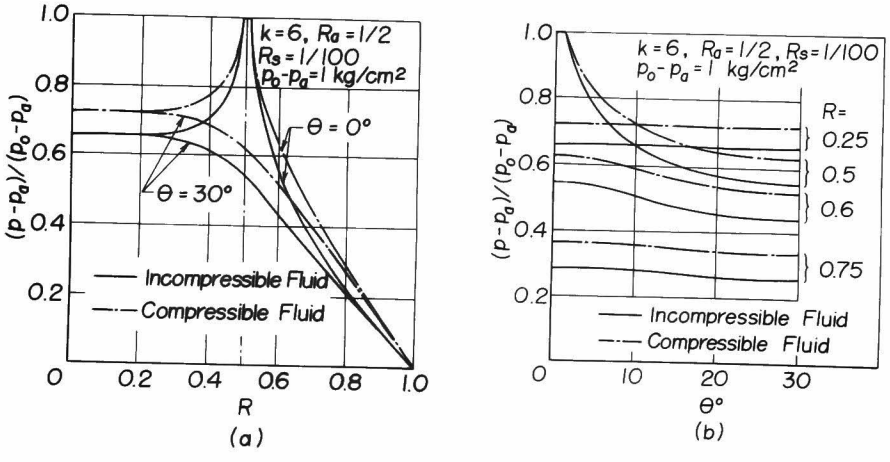

Fig. 1.3.4 Example of pressure distribution for an incompressible and a compressible fluid.

3-3 Load Capacity with an Incompressible Fluid

First, the load capacity of the bearing with a single supply hole is calculated. Denoting ϕ as

$$\phi = \exp\left(\frac{p - K_2}{K_1}\right) \tag{1.3.9}$$

then, Eq. (1.3.2) can be written as

$$R^2 - \frac{(\phi-1)R_a}{\phi - R_a^2}\cdot 2R\cos\theta + \left[\frac{(\phi-1)R_a}{\phi-R_a^2}\right]^2 = \left[\frac{1-R_a^2}{\phi-R_a^2}\right]^2\phi \quad (1.3.11)$$

Equation (1.3.10) shows the equipotential line for a given p.

It should be noted that this is the equation of a circle in polar coordinates, where the center and the radius of the circle are given by, respectively:

$$\left.\begin{array}{l} R = \dfrac{(\phi-1)R_a}{\phi - R_a^2}\ , \quad \theta = 0 \\ \dfrac{1-R_a^2}{\phi-R_a^2}\sqrt{\phi}\, r_i \end{array}\right\} \quad (1.3.11)$$

The load capacity can be obtained by integrating the pressure over the bearing area. Consequently the load capacity is given by the volume of a three-dimensional figure with the coordinates (x,y,p) as shown in Fig. 1.3.5, so that it can also be obtained by integrating the area $S(p)$ enclosed by a constant pressure line with respect to the pressure, that is,

$$W_{(1)} = \int_0^{r_i}\int_0^{2\pi}(p-p_a)\,r\,dr\,d\theta = \int_{p_a}^{p_o} S(p)\,dp \quad (1.3.12)$$

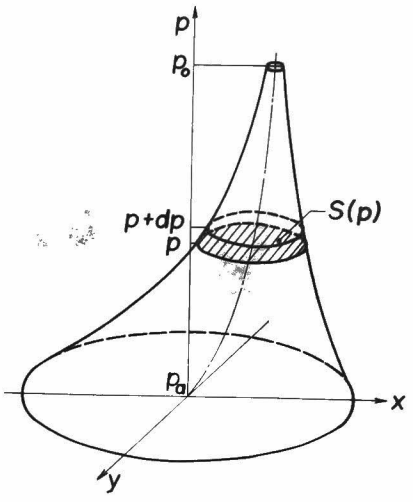

Fig. 1.3.5 Schematic figure of pressure distribution

The constant pressure lines are circular as mentioned above, hence

$$S(p) = \pi\left[\frac{1 - R_a^2}{\phi - R_a^2}\sqrt{\phi}\, r_1\right]^2 \tag{1.3.13}$$

then, the load capacity $W_{(1)}$ for a single supply hole is

$$W_{(1)} = \pi r_1^2 \int_{p_a}^{p_0}\left[\frac{1 - R_a^2}{\phi - R_a^2}\right]^2 \phi\, dp \tag{1.3.14}$$

$$= \pi r_1^2 K_1 (1 - R_a^2)[1-(R_a - R_s)^2] / [1 - R_a(R_a - 2R_s)]$$

as shown in Appendix II.

For the case with multiple supply holes, the load capacity is calculated by using Eq. (1.3.14),

$$W_{(k)} = \pi r_1^2 k K_{1(k)} (1-R_a)[1-(R_a-R_s)^2] \Big/ [1-R_a(R_a-2R_s)] \quad (1.3.15)$$

This reduction is shown in Appendix III.

3-4 Volume Rate of Flow

The volume rate of flow can be calculated from the outflow from the bearing periphery.

For an incompressible fluid, it becomes

$$Q_{incomp.} = -\frac{h^3}{6\mu}\int_0^{2\pi} \left| R\frac{\partial p}{\partial R}\right|_{R=1} d\theta = \frac{\pi k h^3}{3\mu} K_{1(k)} \quad (1.3.16)$$

For the case of a compressible fluid, the pressure gradient is given by

$$\left|\frac{\partial p}{\partial R}\right|_{R=1} = \frac{n}{1+n} p_a^{-\frac{1}{n}} \left|\frac{\partial P}{\partial R}\right|_{R=1}$$

Substituting this into Eq. (1.3.16), the volume rate of flow, $Q_{comp.}$ which corresponds to the pressure p_a, has the following relationship with $Q_{incomp.}$

$$Q_{comp.} = \frac{p_o^{\frac{1+n}{n}} - p_a^{\frac{1+n}{n}}}{p_o - p_a} \cdot \frac{n}{1+n} \cdot p_a^{-\frac{1}{n}} \cdot Q_{incomp.} \quad (1.3.17)$$

where $K_{1(k)}$ in $Q_{incomp.}$ should again be modified by changing p_o and p_a to P_o and P_a as indicated by Eq. (1.2.8).

3-5 Some Examples of Theoretical Bearing Characteristics

Load capacity and volume rate of flow are calculated theoretically from Eqs. (1.3.8), (1.3.15), and (1.3.16) for an incompressible fluid for several numbers and radii of supply holes.

Figs. 1.3.6 and 1.3.7 show the dimensionless load capacity $[W_{(k)}/\pi r_1^2 (p_o - p_a)]$ and volume rate of flow $[Q_{incomp.}/\pi R^3 (p_o - p_a)(3\mu)^{-1}]$ for the case of $k = 6$ versus radial position of supply holes for several numbers and for several radii of supply holes, respectively.

Volume rate of flow increase with increases of R_a, R_s, and k but load capacity takes the largest value for the optimum radial position of supply holes for given k and R_s. This optimum position is given in Fig. 1.3.8 for several values of R_s. At the calculation for Fig. 1.3.8, the volume rate of flow and the angular stiffness of the bearing are not taken into consideration. When the bearing is designed with less value of R_a, one may obtain less volume rate of flow, while with larger value of R_a, larger angular stiffness may be obtained.

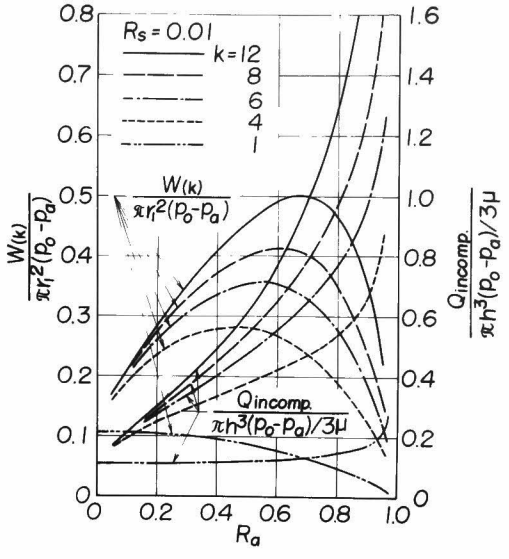

Fig. 1.3.6 Bearing characteristics for several numbers of supply holes

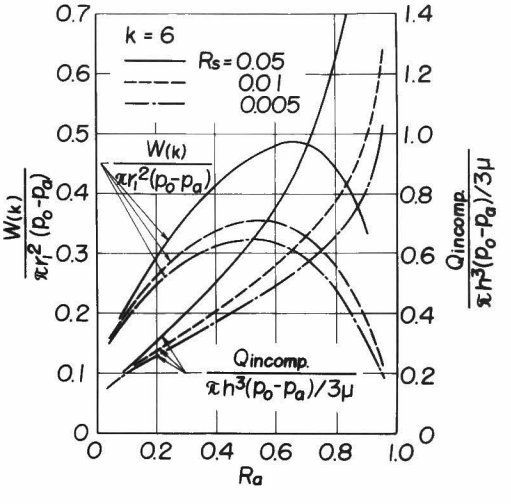

Fig. 1.3.7 Bearing characteristics for several radii of supply holes

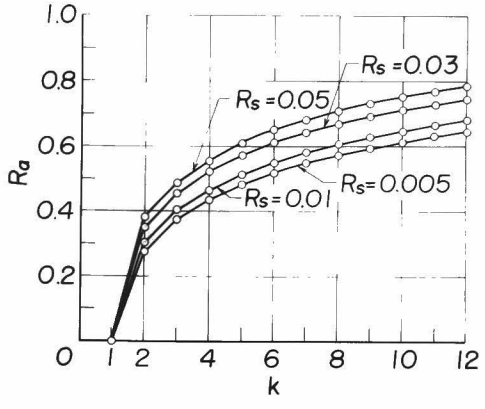

Fig. 1.3.8 Optimum radial position of supply holes

3-6 Boundary Condition at Supply Hole

Eq. (1.3.3) represents the real boundary condition only at an inner point of the supply hole. The following boundary conditions could also be used instead of Eq. (1.3.3):

$$\left.\begin{aligned} p = p_a \quad &\text{at} \quad R = 1 \\ p = p_o \quad &\text{at} \quad R = R_a + R_s, \ \theta = 0 \end{aligned}\right\} \qquad (1.3.18)$$

which gives the real pressure at an outer point of the supply hole.

When the radius of the supply hole is small, the differen between the results is negligible. But the pressure distribution deviates from the real one when there are more supply

holes with larger radius.

For example, Fig. 1.3.9 shows theoretical constant pressure curves for the value of p_o with these boundary conditions, which should correspond to the form of large supply hole with $r_s/r_i = 0.05$ and $a/r_i = 0.5$. Condition (1.3.3) satisfies fairly well the real condition but gives the solution with a smaller supply hole located at inner radial position, while condition (1.3.18) seems not to be such a reasonable boundary condition to be applied because the deviation becomes larger.

However, though their radial positions and sizes are different from the real one, it should be noted that these shapes are almost circular. So the deviation may be corrected approximately by modifying the position of source in the complex potential function.

If the source is put in the bearing surface (Z-plane) at radius R_a^* ($= a^*/r_i$) instead of R_a ($= a/r_i$), and the sink is put at $R = 1/R_a^*$ by the mirror image principle, then the pressure distribution becomes

$$p = K_{1(k)}^* \log \frac{R_a^{*2k} R^{2k} + 1 - 2R_a^{*k} R^k \cos k\theta}{R^{2k} + R_a^{*2k} - 2R_a^{*k} R^k \cos k\theta} + K_{2(k)}^* \qquad (1.3.19)$$

The radius R_a^* is chosen to give the pressure p_o at both inner and outer edges of the supply holes. Then R_a^* must be

$$R_a^{*k} = \frac{1+(R_a+R_s)^k(R_a-R_s)^k}{(R_a+R_s)^k+(R_a-R_s)^k} - \frac{\{[1-(R_a+R_s)^{2k}][1-(R_a-R_s)^{2k}]\}^{\frac{1}{2}}}{(R_a+R_s)^k+(R_a-R_s)^k} \quad \left.\right\} (1.3.20)$$

as shown in Appendix IV.

The constants $K_{1(k)}^*$ and $K_{2(k)}^*$ are determined by the boundary conditions (1.3.3) or (1.3.18) to be

$$\left.\begin{aligned} K_{1(k)}^* &= \frac{p_o - p_a}{2\log \dfrac{1-R_a^{*k}(R_a-R_s)^k}{R_a^{*k}-(R_a-R_s)^k}} \\ &= \frac{p_o - p_a}{2\log \dfrac{1-R_a^{*k}(R_a+R_s)^k}{-R_a^{*k}+(R_a+R_s)^k}} \\ K_{2(k)}^* &= p_a \end{aligned}\right\} \quad (1.3.21)$$

Either of conditions (1.3.3) and (1.3.18) gives the same value of $K_{1(k)}^*$ and $K_{2(k)}^*$. Then

$$\left.\begin{aligned} W_{(k)}^* &= \pi r_1^2 k K_{1(k)}^* (1-R_a^{*2})[1-(R_a-R_s)^2]/[1-2R_a^*(R_a-R_s)+R_a^{*2}] \\ Q_{incomp.} &= \frac{\pi R_k h^3}{3\mu} K_{1(k)}^* \end{aligned}\right\} (1.3.22)$$

The chain line in Fig. 1.3.9 is the form of supply hole for this case, which is seen to satisfy the real condition very well.

Figure 1.3.10 shows the effect of boundary conditions on load capacity and volume rate of flow in dimensionless form for $R_s = 0.01$ and 0.05. For small values of R_s (such as 0.01)

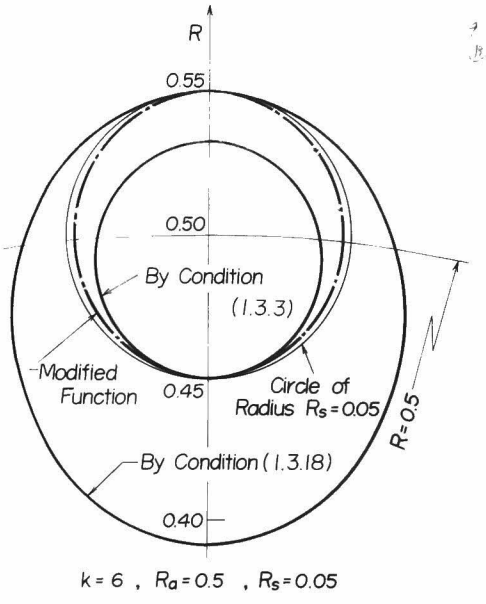

Fig. 1.3.9 Theoretical shapes of supply holes with various boundary conditions

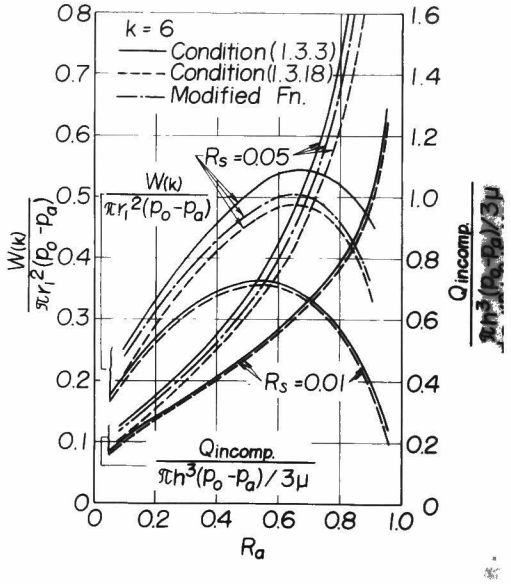

Fig. 1.3.10 Bearing characteristics depending on various boundary conditions

there is little difference between the results with conditions (1.3.3) and (1.3.18), but for $R_s = 0.05$ the difference becomes appreciable, which could have been predicted from the data in Fig. 1.3.9. For the latter case, the modified functions (1.3.19)-(1.3.22) seem to be reasonably good.

3-7 Experimental Investigation

(a) Experimental Apparatus

Fig. 1.3.11 shows the apparatus of the experiments for the pressure distribution and volume rate of flow (Apparatus I). The upper plate (No.2) and the bearing plate (No.1) are fixed parallelly by adjusting screws to compose a bearing clearance which is measured by three dial gages. The compressed air is fed to the annular groove behind the bearing plate, and then to the bearing clearance through the supply holes spaced circumferentially. The pressure in the bearing clearance is measured by a U-tube mercury manometer connected to the clearance through a small hole of 0.5mm diameter drilled in the upper plate. The under bearing surface can be rotated and slided by fine screws to measure the pressure distribution on the entire bearing surface.

This apparatus is used for measuring the pressure distribution and volume rate of flow because the bearing clearance is fixed.

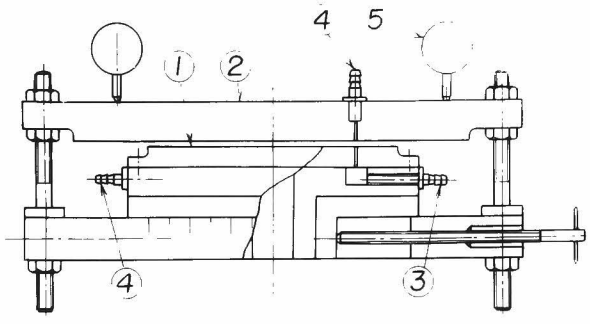

1 Bearing Plate
2 Upper Plate
3 Air Supply
4 To the Manometer
5 Dial Gage

Fig. 1.3.11 Experimental apparatus (I)

The experiments are made on the static condition.

For investigating the load capacity experimentally, the apparatus shown in Fig. 1.3.12 is used. (Apparatus II). The rotor has a thrust bearing with multiple supply holes through which the compressed air is supplied into bearing clearance.

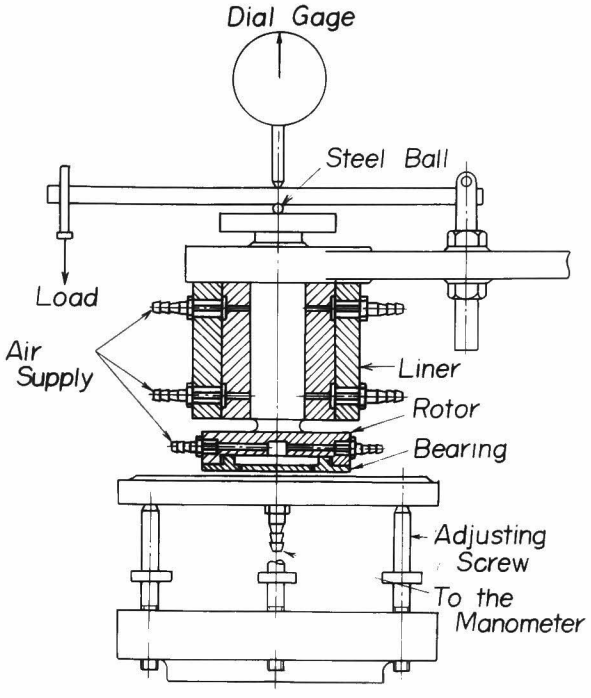

Fig. 1.3.12 Experimental apparatus (II)

The pressure just after the supply holes is measured by a U-tube mercury manometer connected with a small hole of 0.2mm diameter drilled in the stator. The roter is guided in the liner by an externally pressurized journal air-bearing in order to prevent their contact.

The load is put on the top of the rotor by a lever and load weights.

The bearing clearance is measured by a dial gage placed on the top of the apparatus.

(b) Pressure Distribution

The pressure distributions are measured by the apparatus I. The configurations of the bearings employed in the experiments are shown in Fig. 1.3.13.

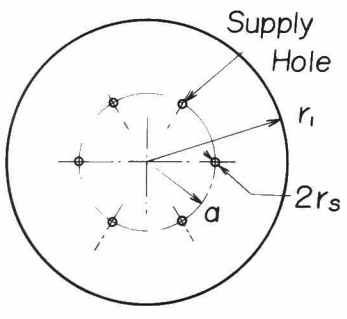

No.	$2r_1$ (mm)	$2a$ (mm)	$2r_s$ (mm)	k
1	120	60	1.2	6
2	120	60	1.2	4
3	120	60	1.2	8
4	120	60	6.0	6
5	120	40	1.2	6
6	120	80	1.2	6

Fig.1.3.13 Bearings employed in experiments for pressure distribution and volume rate of flow

The typical bearing dimensions are

$2r_1$ = 120 mm

a = 30 mm

$2r_s$ = 1.2 mm

k = 6

$h = 15\ \mu$

$p_o - p_a = 0.5\ kg/cm^2$

Figs. 1.3.14-1.3.18 are the experimental results of the pressure distribution. In each group of figures, there are three kinds of pressure distributions which are

(a) On the position of $\Theta = 0$ (radial direction through the supply hole)

(b) On the position of $\Theta = \pi/k$ (radial direction just between the supply holes)

(c) On the position of R = Ra (circumferential direction through the supply hole)

Fig. 1.3.14 is the pressure distribution for the typical bearing of Fig. 1.3.13. No.1 under $p_o - p_a = 0.5\ kg/cm^2$ and for several bearing clearances. (h = 15, 30, 40 and 50 microns).

Figs. 1,3,15-1.3.18 are for various values of p_o, various numbers of supply holes, various radii of supply holes, and for various radial position of supply holes, respectively.

In these figures, the thick lines are the theoretical pressure distributions calculated from the above theory with polytropic index n = 1.0 (isothermal condition is applied). The experimental results coincide very well with theoretical one which confirms the theory especially for the case with low supply pressure with small bearing clearance.

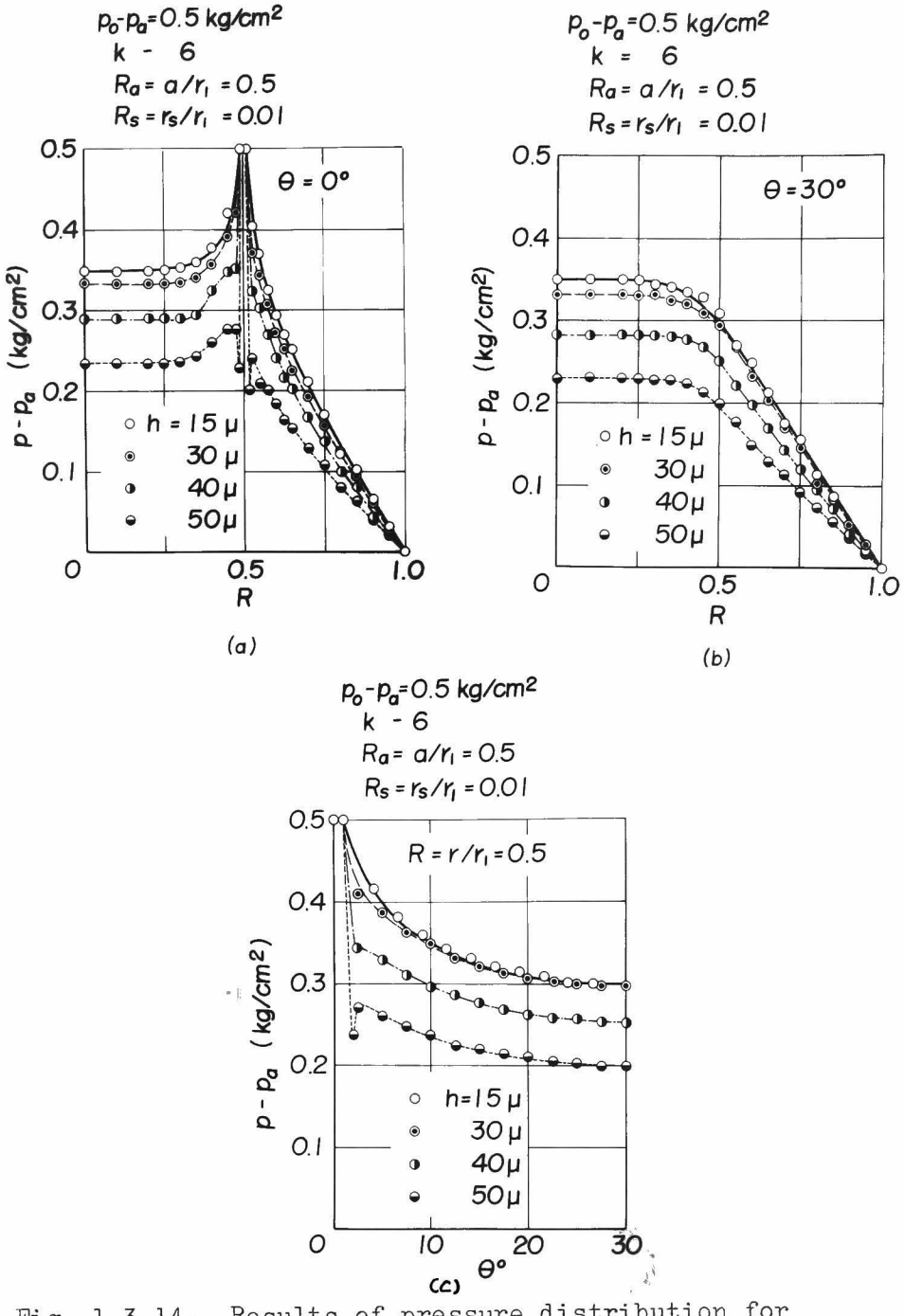

Fig. 1.3.14. Results of pressure distribution for various values of h

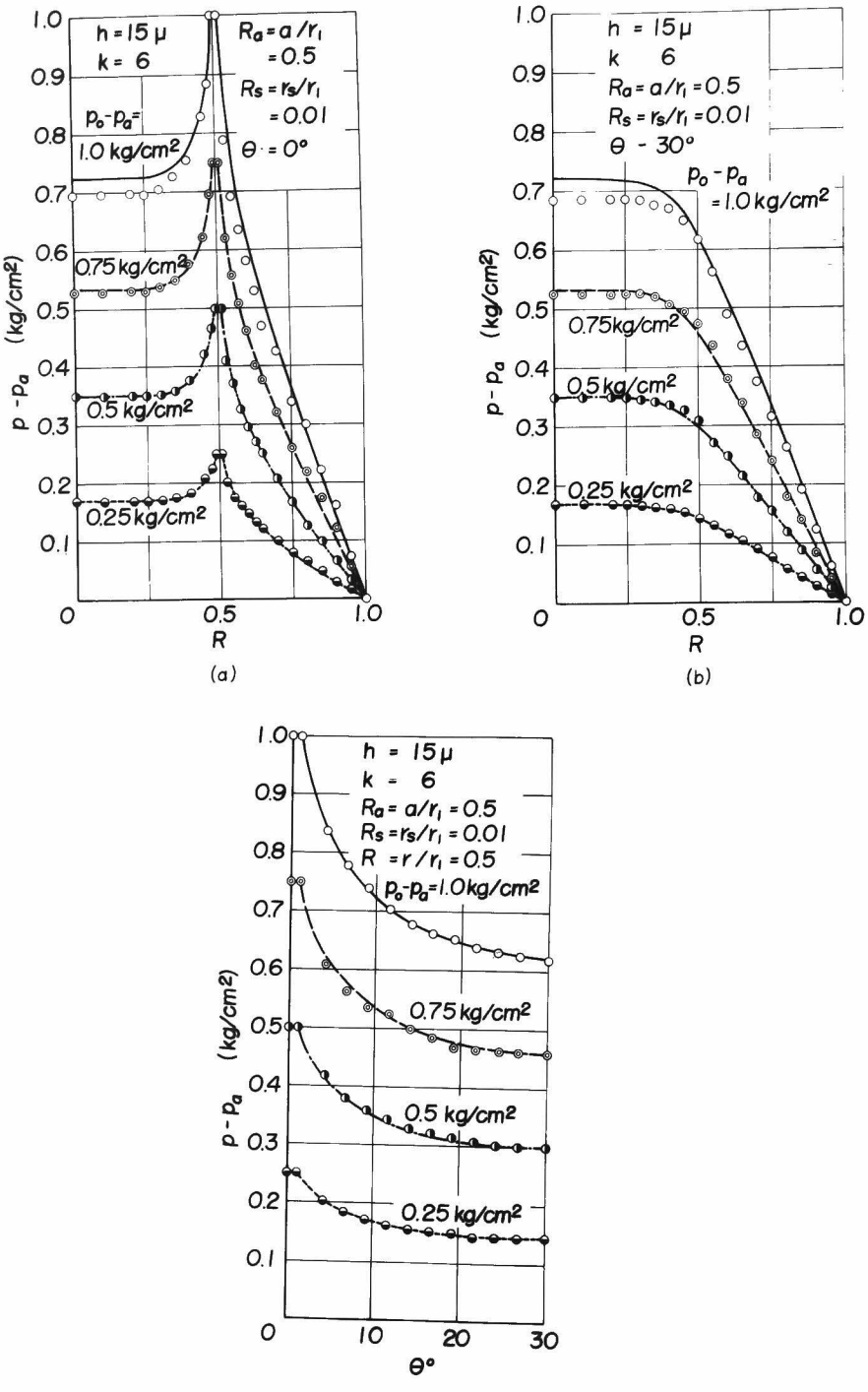
h = 15 μ
k = 6
Ra = a/r1 = 0.5
Rs = rs/r1 = 0.01
θ = 0°
po - pa = 1.0 kg/cm2
0.75 kg/cm2
0.5 kg/cm2
0.25 kg/cm2
p - pa (kg/cm2)
R
(a)
h = 15 μ
k 6
Ra = a/r1 = 0.5
Rs = rs/r1 = 0.01
θ - 30°
po - pa = 1.0 kg/cm2
0.75kg/cm2
0.5 kg/cm2
0.25 kg/cm2
p - pa (kg/cm2)
R
(b)
h = 15 μ
k = 6
Ra = a/r1 = 0.5
Rs = rs/r1 = 0.01
R = r/r1 = 0.5
po-pa=1.0kg/cm2
0.75 kg/cm2
0.5 kg/cm2
0.25 kg/cm2
p - pa (kg/cm2)
θ°
(c)

Fig. 1.3.15

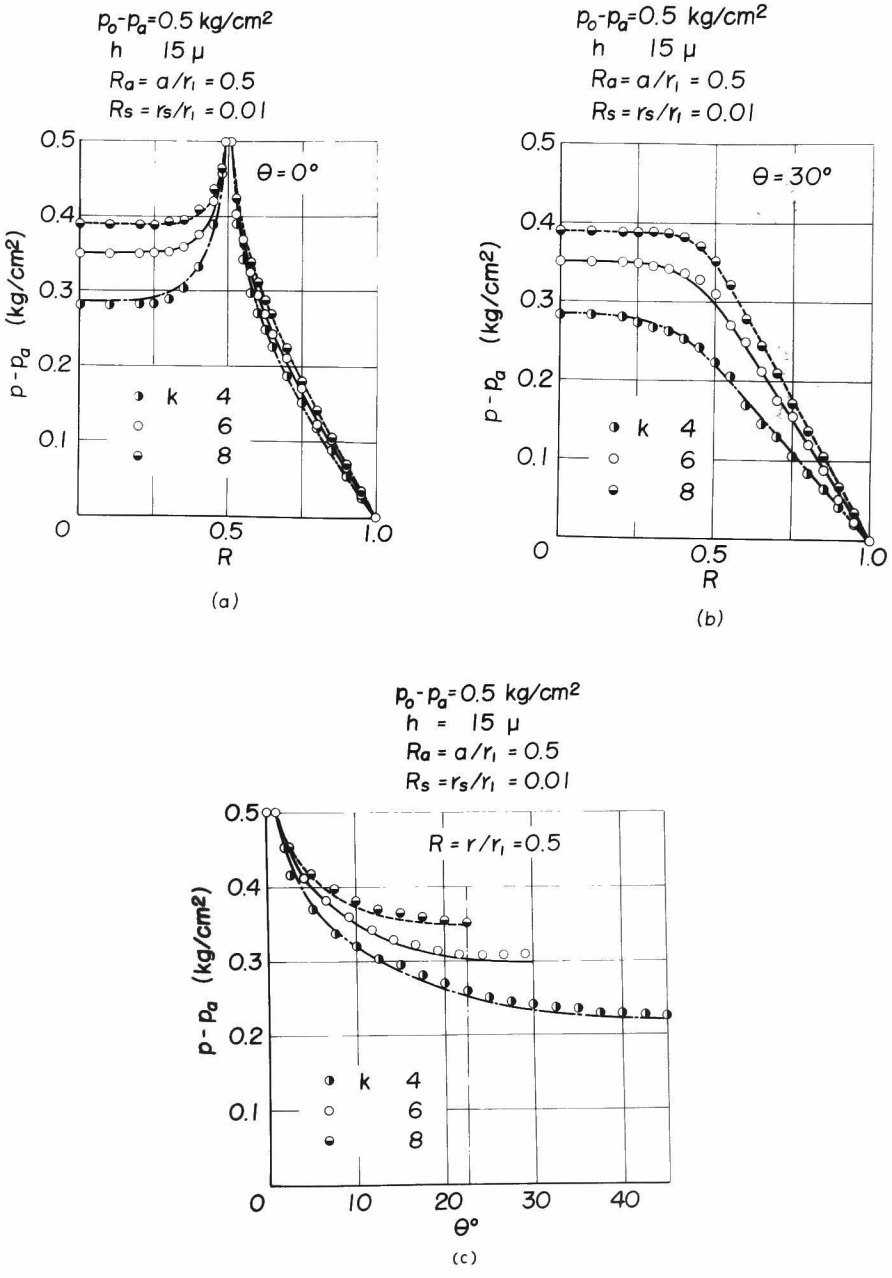
$p_o - p_a = 0.5$ kg/cm²
h 15 μ
$R_a = a/r_1 = 0.5$
$R_s = r_s/r_1 = 0.01$
θ = 0°
θ = 30°
$p - p_a$ (kg/cm²)
R
k 4
6
8
(a)
(b)
$R = r/r_1 = 0.5$
θ°
(c)

Fig. 1.3.16

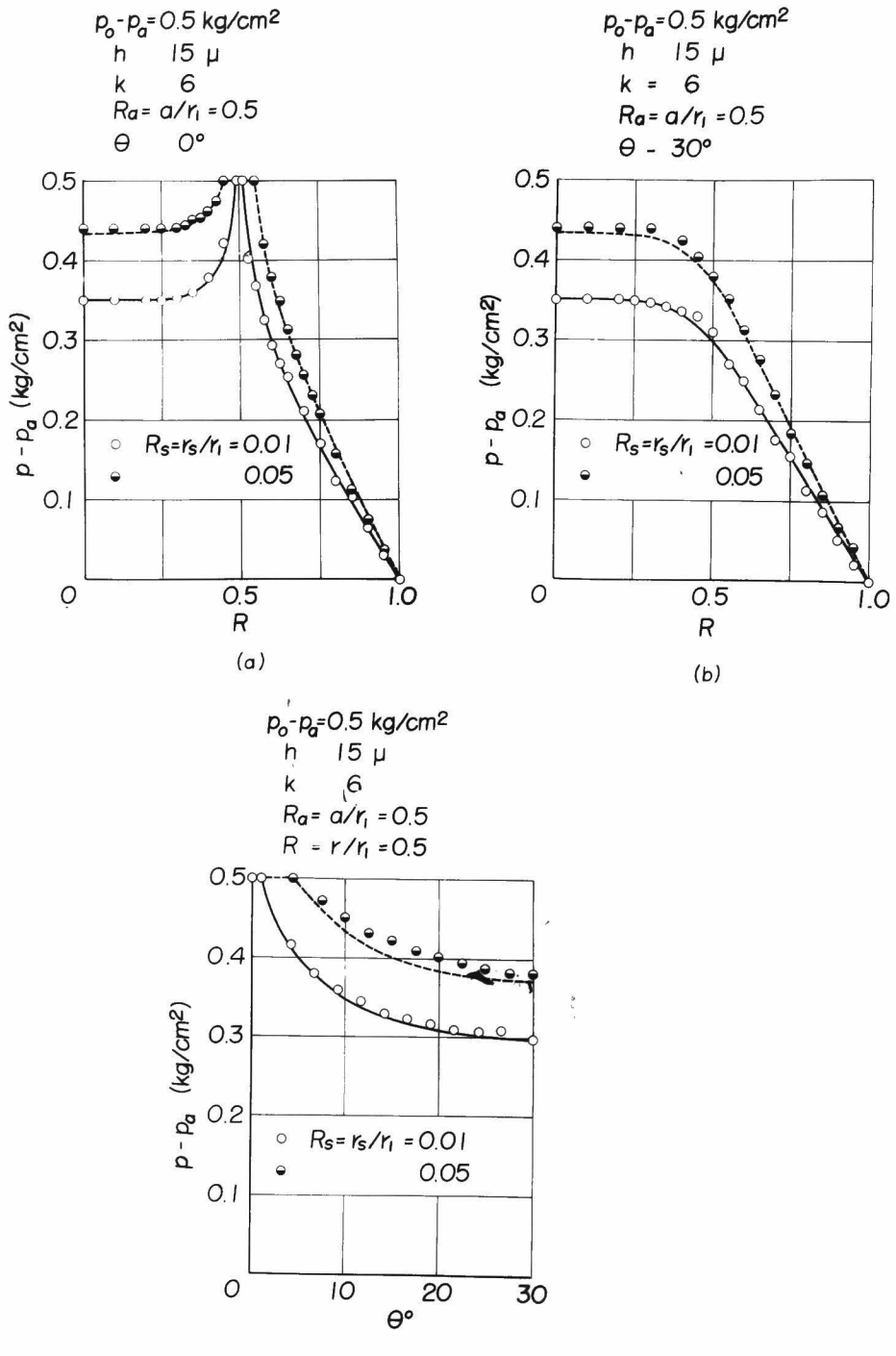
$p_o - p_a = 0.5$ kg/cm²
h 15 μ
k 6
$R_a = a/r_1 = 0.5$
θ 0°
$p - p_a$ (kg/cm²)
$R_s = r_s/r_1 = 0.01$
0.05
R
(a)
$p_o - p_a = 0.5$ kg/cm²
h 15 μ
k = 6
$R_a = a/r_1 = 0.5$
θ - 30°
$p - p_a$ (kg/cm²)
$R_s = r_s/r_1 = 0.01$
0.05
R
(b)
$p_o - p_a = 0.5$ kg/cm²
h 15 μ
k 6
$R_a = a/r_1 = 0.5$
R = $r/r_1 = 0.5$
$p - p_a$ (kg/cm²)
$R_s = r_s/r_1 = 0.01$
0.05
θ°
(c)

Fig. 1.3.17

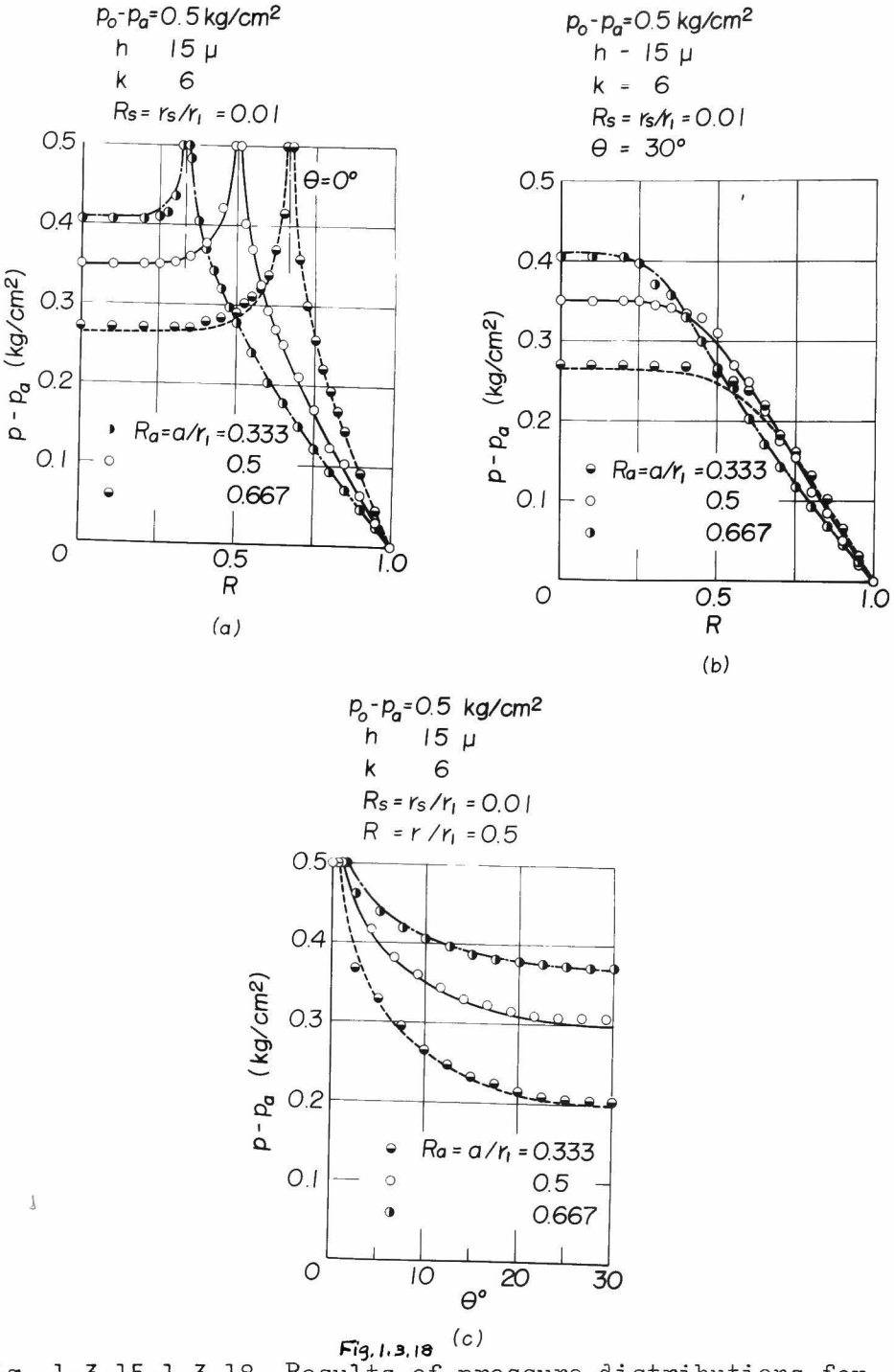

Fig. 1.3.15-1.3.18 Results of pressure distributions for various values of bearing parameters

But, for the cases with large bearing clearance or high supply pressure, the experimental results fall somewhat from the theoretical ones. These deviations are larger as the values of supply pressure and bearing clearance increase. These pressure falls are considered to be due to the inertia effects of the lubricant so that the adiabatic condition may be applied.

When the clearance becomes very large, for example h = 50 microms, the pressure fall develops to the pressure depression as shown in Fig. 1.3.14 (a). (In Fig. 1.3.14, the thin lines are only experimental). This phenomenum can be observed also for an externally pressurized circular thrust gas-bearing with a central single supply hole.(3) It may be explained by a flow model that the choked condition is achieved at the supply hole, and then, the supersonic flow region and the shock wave may follow. After the shock wave the pressure can be recovered as shown in figure. The theory(3) also shows that the large bearing clearance and high supply pressure may cause the pressure depression, which can be observed also in these experimental results.

The pressure loss at the supply holes will be investigated later concerning the load capacity.

(c) Load Capacity

Load capacity is investigated experimentally by using the apparatus II. The fluid is compressed air.

The bearings employed in the experiments are shown in Fig. 1.3.19.

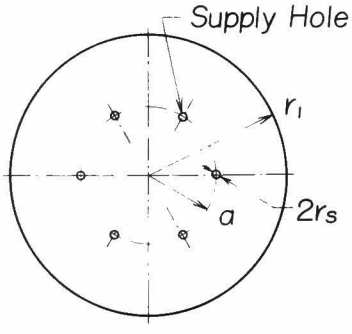

No.	$2r_i$(mm)	2a(mm)	$2r_s$(mm)	k
1	60	30	1.2	6
2	60	30	1.2	4
3	60	30	1 2	8
4	60	30	3.0	6
5	60	20	1.2	6
6	60	40	1.2	6

Fig. 1.3.19 Bearings employed in experiments for load capacity

Figs. 1.3.20 and 1.3.21 are the experimental results of the load capacity for various values of the bearing dimensions, radius of supply holes, radial position of supply holes and so forth, respectively. Experimental load capacity is shown in dimensionless form $f_w = W/\pi r_i^2 (p_o - p_a)$ versus the bearing clearance h.

Fig. 1.3.20 is typical results which are measured by using the bearing No.1 under several values of load. The thin broken line in the figure is the theoretical one for an

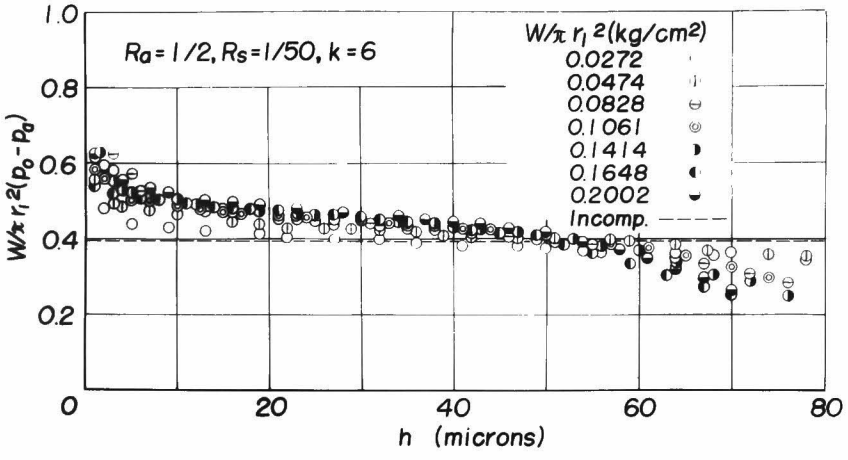

Fig. 1.3.20 Typical results of load capacity

incompressible fluid.

For a small bearing clearance, experimental results of f_w take higher values than the theoretical one because of the compressibility of the fluid. But, for larger clearance, the pressure fall after the supply holes becomes considerably effective so that the values of f_w may fall down even under the compressible theoretical one. These inclinations become remarkable as the load, and then the supply pressure increases.

For the clearance of 30-60 microns, which seems to be used practically, these effects cancel each other so that the theoretical incompressible solution may be an approximate value of f_w .

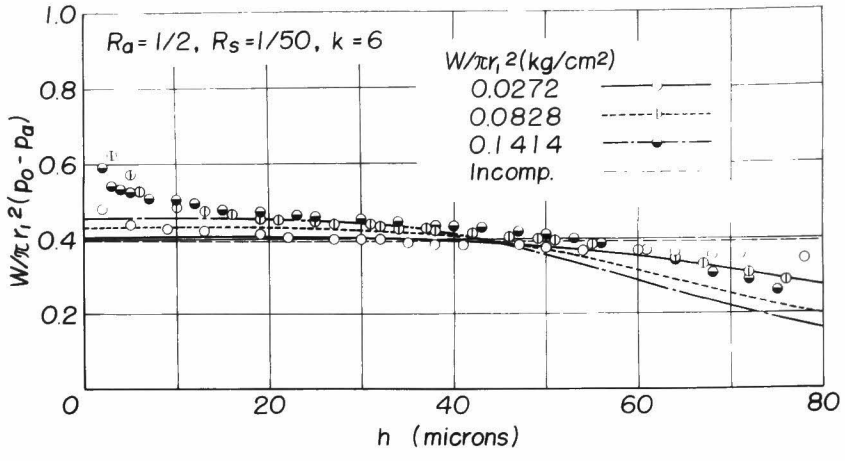
Ra = 1/2, Rs = 1/50, k = 6
W/πr1 2(kg/cm2)
0.0272
0.0828
0.1414
Incomp.
W/πr1 2(p0 - pa)
h (microns)
0
20
40
60
80
0.2
0.4
0.6
0.8
1.0

(a)

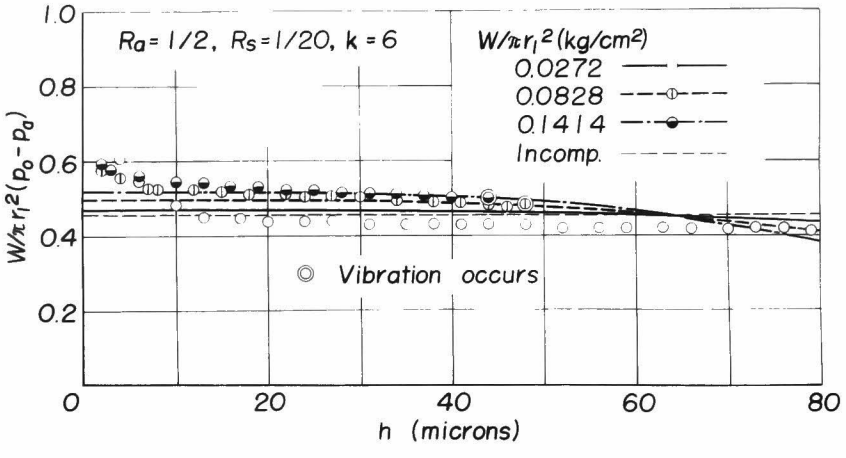
Ra = 1/2, Rs = 1/20, k = 6
W/πr1 2(kg/cm2)
0.0272
0.0828
0.1414
Incomp.
◎ Vibration occurs
W/πr1 2(p0 - pa)
h (microns)
0
20
40
60
80
0.2
0.4
0.6
0.8
1.0

(b)

Fig. 1.3.21

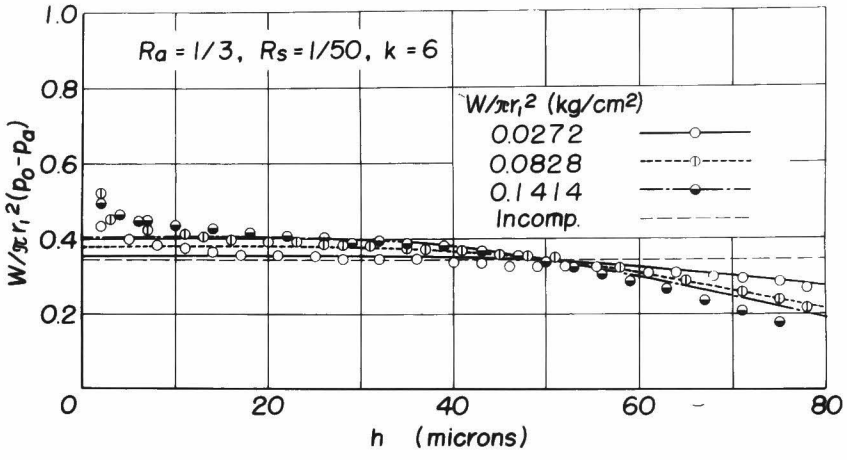
Ra = 1/3, Rs = 1/50, k = 6
W/πr1² (kg/cm²)
0.0272
0.0828
0.1414
Incomp.
W/πr1²(p0-pa)
h (microns)
0
20
40
60
80
0.2
0.4
0.6
0.8
1.0

(c)

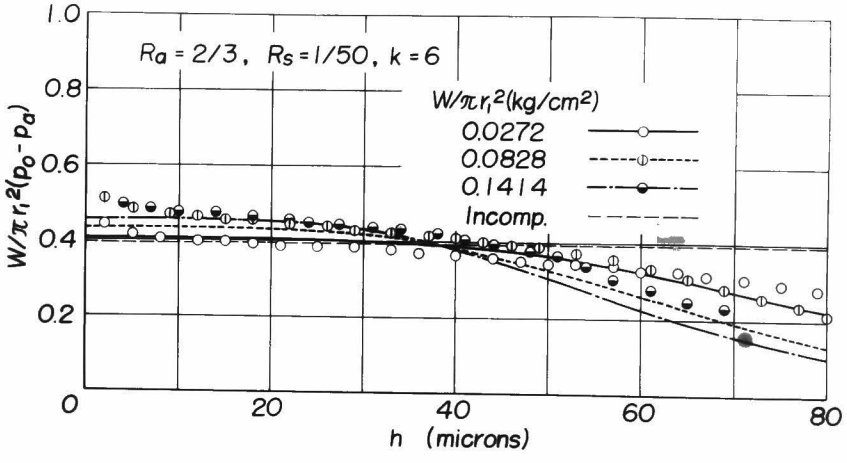
Ra = 2/3, Rs = 1/50, k = 6
W/πr1²(kg/cm²)
0.0272
0.0828
0.1414
Incomp.
W/πr1²(p0-pa)
h (microns)
0
20
40
60
80
0.2
0.4
0.6
0.8
1.0

(d)

Fig. 1.3.21

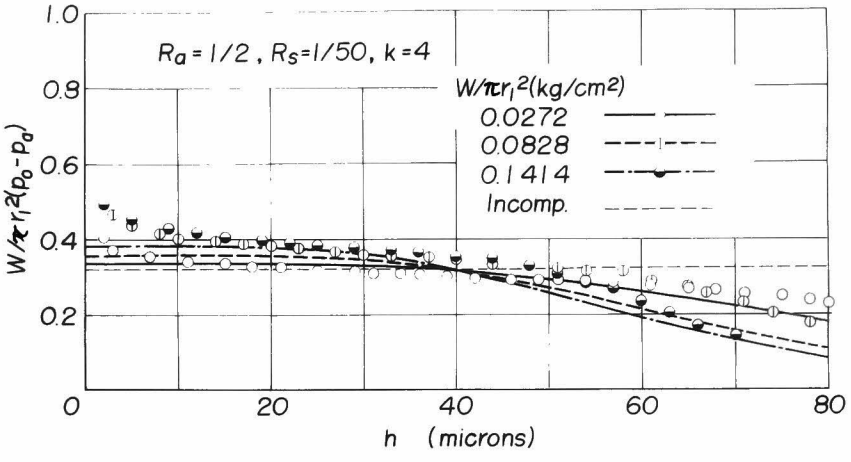

(e)

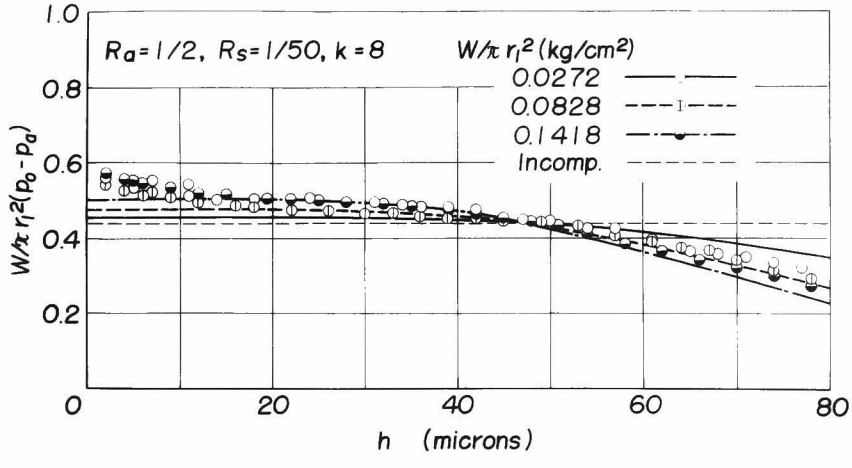

(f)

Fig. 1.3.21 Results of load capacity for various values of bearing parameters

(c)-(i) Effect of Compressibility of the Fluid

The pressure distribution with consideration of the compressibility of the fluid can not be easily integrated theoretically on the bearing area.

In order to estimate the load capacity of the gas-bearing of this type, an approximate solution is introduced as reduced in Appendix V, resulting

$$W_{comp.} = \frac{p_o + p_a}{2p_a} \times W_{incomp.} \qquad (1.3.23)$$

which may be valid when the supply pressure is not so high. When the pressure fall at supply hole is taken into account, this equation must be

$$W_{comp.} = \frac{p_o'' + p_a}{2p_a} \times W_{incomp.} \qquad (1.3.23)'$$

where p_o'' is modified pressure after supply hole which is mentioned in the following section.

(c)-(ii) Pressure Fall at Supply Holes.

The pressure fall at supply holes may be explained by considering the flow pattern in the bearing clearance.

At the practical bearing, the stream lines are presumed as shown in Fig. 1.3.22, in which the flow from the supply hole may turn into the direction of the bearing clearance, and there the energy loss must occur because of the entrance

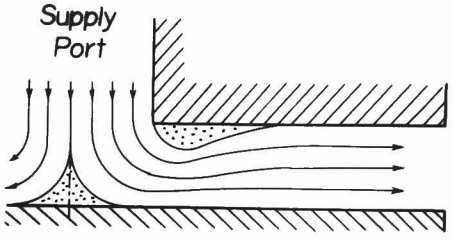

Fig. 1.3.22 Flow pattern in the practical bearing

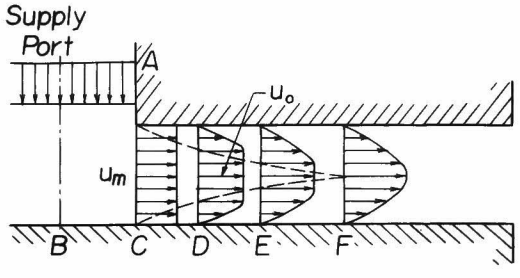

Fig. 1.3.23 Assumed schematic flow pattern in the bearing

effects as separation or contraction of the effective flow area.

To analyze the flow, the flow pattern as shown schematically in Fig. 1.3.23 is assumed approximately, in which the lubricant flows into bearing clearance from supply holes (section A), then it flows out to the bearing periphery (B-F). B is the stagnation point with no flow velocity towards the bearing clearance. At section C, the velocity distribution is uniform as shown in the figure. From section C, the boundary layers begin to develop to section F which refers to the fully developed profile of flow velocity.

At the supply holes, the pressure fall may occur on account of two causes; one is due to the accelerating energy of the lubricant from the stagnation point (B) to the bearing lubricant flow (section C), and the other the energy consumption for the development of the boundary layers and the change of velocity distribution profile.

For the former, the acceleration of the lubricant, Bernoulli's theorem can be applied between B and C in the figure neglecting the friction loss, resulting the following pressure fall;

$$p_o - p_o' = \frac{1}{2}\rho_o u_m^2 \qquad (1.3.24)$$

where p_o : pressure at the stagnation point B

p_o': pressure at section C

ρ_o : density of the fluid at section C

u_m : average flow velocity at section C

For the latter, the change of velocity distribution, one can estimate approximately the pressure fall assuming that the friction on the bearing wall is very small so that the entrance length for the development of the velocity profile may be neglected, resulting

$$p_o' - p_o'' = \frac{1}{5}\rho_o u_m^2 \qquad (1.3.25)$$

This equation is reduced in Appendix VI.

The further investigation is made in Appendix VII with consideration of the friction loss at the entrance length.

The pressure fall at the supply holes can be estimated from the total effects of Eqs. (1.3.24) and (1.3.25), then

$$p_o - p_o'' = \lambda \frac{1}{2}\rho_o u_m^2 = \lambda \frac{1}{2}\rho_o \left(\frac{Q_o}{2\pi k r_s h}\right)^2 \qquad (1.3.26)$$

where λ is coefficient of pressure fall and is taken as $\lambda = 1.4$ by the above investigations, and Q_o is volume vate of flow corresponding to pressure p_o''. ρ_o is the density of the fluid corresponding to pressure p_o'' approximately.

The pressure distribution, which includes the secondary effects of compressibility and pressure fall, is shown in Fig. 1.3.24 schematically.

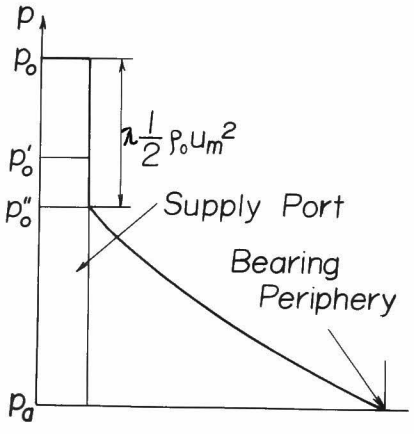

Fig. 1.3.24 Schematic pressure distribution with consideration of secondary effects

Fig. 1.3.21 shows the experimental results of load capacity for various bearing parameters such as radius of supply holes, radial position of supply holes and number of supply holes.

In these figures, the theoretical curves are drawn with consideration of both effects of compressibility and pressure fall at supply holes.

The theoretical values show a good conformity with the experimental results both qualitatively and quantitatively even for comparatively large bearing clearance and high

supply pressure though the above compensation terms do not concern the shock or pressure depression near the supply holes.

(d) Volume Rate of Flow

The volume rate of flow is also experimented by using the experimental apparatus I in which the bearing clearance is fixed to be constant by fine screws. The bearings employed are the same that used in the above experiments concerning the pressure distribution.

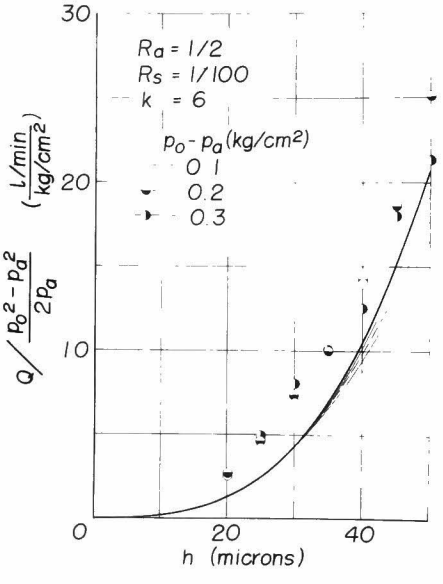

(a)

Fig. 1.3.25

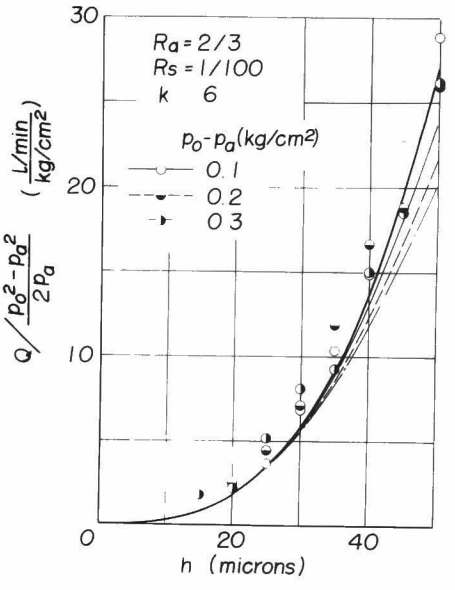

(b)

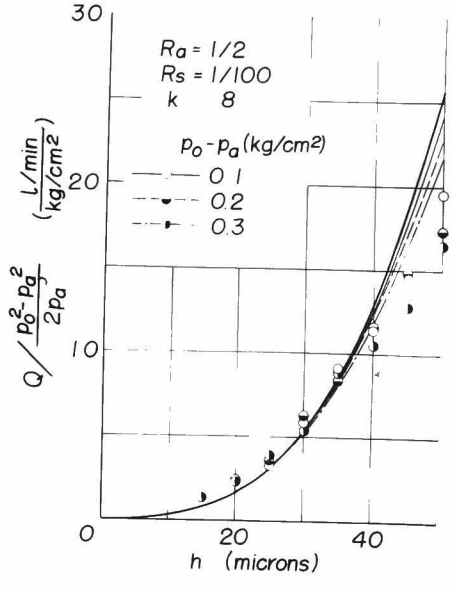

(c)

Fig. 1.3.25 Results of volume rate of flow for various bearing parameters

Fig. 1.3.25 is the experimental results of volume rate of flow for various bearing configurations such as the radial position and number of supply holes. In these figures the volume rates are arranged in the form of $Q/\frac{p_o^2-p_a^2}{2p_a}$ against the bearing clearance h, because a compressible flow rate with $n = 1.0$ is expressed theoretically from Eqs. (1.3.16) and (1.3.17) as

$$Q_{comp.} = \frac{p_o+p_a}{2p_a} \cdot Q_{incomp.}$$

$$= \frac{p_o+p_a}{2p_a} \cdot \frac{\pi k h^3}{3\mu} K_{1(k)}$$

$$= \frac{\pi k h^3}{3\mu \Phi(R_a-R_s,0)} \cdot \frac{(p_o+p_a)(p_o-p_a)}{2p_a}$$

where $\Phi(R_a-R_s, 0)$ is such a function as given in Appendix V, then $Q_{comp.}$ is proportional to $(p_o^2-p_a^2)/2p_a$ or $Q/\frac{p_o^2-p_a^2}{2p_a}$ is considered theoretically to be independent with p_o or p_a.

The thick lines in the figures are the theoretical curves which is proportional to h^3.

The pressure fall at supply hole is also taken into account which lessens the flow rate. When the pressure falls down to p_o'' as obtained in the above section, the volume rate of flow becomes

$$Q = \frac{\pi k h^3}{3\mu \Phi(R_a-R_s,0)} \cdot \frac{p_o''^2-p_o^2}{2p_a}$$

in which the pressure fall is estimated as

$$p_o - p_o'' = \lambda \frac{\rho_o}{2} u_m^2 = \lambda \frac{\rho_o}{2} \left(\frac{Q_o}{2\pi k r_s h} \right)^2$$

Then

$$\frac{Q}{\frac{p_o^2 - p_a^2}{2p_a}} = \frac{\pi k h^3}{3\mu \Xi (R_a - R_s, 0)} \cdot \frac{p_o''^2 - p_a^2}{p_o^2 - p_a^2}$$

The theoretical curves with consideration of the pressure fall effect are also drawn by thin lines in the figures.

The experimental results coincide very well with theoretical ones qualitatively and fairly well quantitatively, but pressure fall effect is not so obvious in the experimental results.

The bearing clearance is very hard to be kept constant because of the bearing elastic deformation by the gas film pressure so that the volume rate of flow may be affected by it considerably, which may cause the quantitative errors in experiments.

Chapter 4 Analysis of Externally Pressurized Thrust Collar Gas-Bearing with Multiple Supply Holes

4-1 Complex Potential and Pressure Distribution

In this Chapter, externally pressurized thrust collar

gas-bearings with several gas supply holes are investigated by using the complex potential theory. The gas supply holes of these bearings are spaced circumferentially and communicate directly with the film without feeding into recesses.

(a) Single Supply Hole

For the first step, an externally pressurized thrust collar bearing with only one supply hole as shown in Fig. 1.4.1(a) is analyzed; the bearing with multiple supply holes as shown in Fig. 1.4.1(b) investigated by an appropriate superposition of the results.

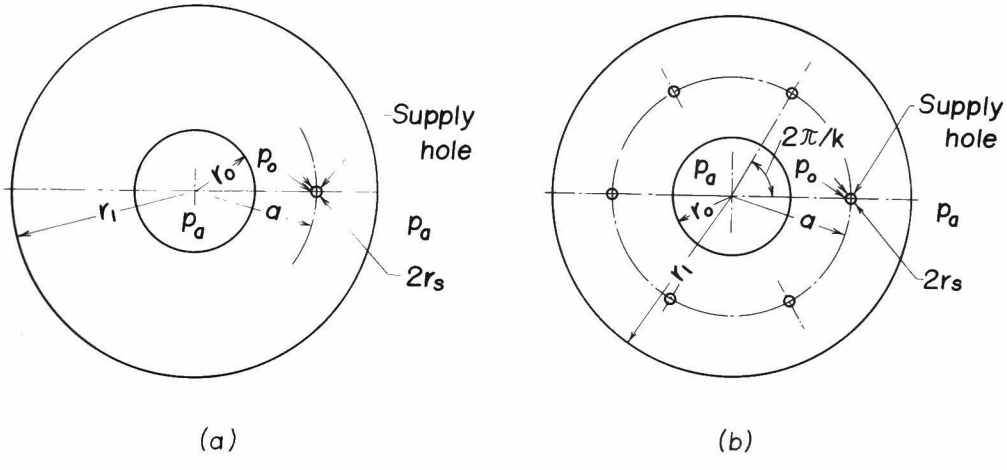

Fig. 1.4.1 Configurations of thrust collar bearings

Now consider the following analytic function on Z-plane;

$$w = w(Z) = \frac{q}{2\pi}\left[\log\sin\frac{\pi\log(Z/a)}{2\log(r_0/r_1)} - \log\sin\frac{\pi\log(aZ/r_0^2)}{2\log(r_0/r_1)}\right] \quad (1.4.1)$$

where r_0 : radius to inner periphery

r_1 : radius to outer periphery

a : radius to supply hole

q : strength of source

Substituting $Z_0 (= r_0 e^{i\theta})$ which represents the inside circle of the bearing edge, the analytic function vanishes its real part and only has imaginary part as follows;

$$w_0 = w(r_0 e^{i\theta}) = i\frac{q}{2\pi}\Psi_0(A_0, B_j)$$

where

$$\left.\begin{aligned} A_0 &\equiv \frac{\pi\log(r_0/a)}{2\log(r_0/r_1)} = \frac{\pi\log(R_0/R_a)}{2\log R_0} \\ B_j &= \frac{\pi(\theta+2\pi j)}{2\log(r_0/r_1)} = \frac{\pi(\theta+2\pi j)}{2\log R_0} \quad (j = 0, \pm 1, \pm 2, \ldots) \end{aligned}\right\} \quad (1.4.2)$$

in which $R_0 = r_0/r_1$, $R_a = a/r_1$.

as shown in Appendix VIII.

Similarly substituting $Z_1 (= r_1 e^{i\theta})$, which designates the outside circle of the bearing edge, into Eq. (1.4.1), w becomes

$$w_1 = w(r_1 e^{i\theta}) = i\frac{q}{2\pi}\Psi(A_1, B_j) \quad (1.4.3)$$

where

$$A_1 \equiv \frac{\pi \log (r_1/a)}{2 \log (r_0/r_1)} = -\frac{\pi \log R_a}{2 \log R_0}$$

as shown in Appendix IX.

Thus the real parts of w_0 and w_1 become zero so that the analytic function given by Eq. (1.4.1) can satisfy the boundary conditions at both edges of the bearing, and gives a suitable complex potential function for the bearing.

Dividing w into two parts of w^{I} and w^{II}, and substituting $Z = re^{i\theta}$ into Eq. (1.4.1) to obtain the real part of w which gives the pressure distribution,

$$w^{\mathrm{I}} = \frac{g}{2\pi} \log \sin \frac{\pi \log (Z/a)}{2 \log (r_0/r_1)}$$

$$= \frac{g}{2\pi} \log \left[\sin \frac{\pi \log (r/a)}{2 \log (r_0/r_1)} \cosh \frac{\pi (\theta + 2\pi j)}{2 \log (r_0/r_1)} + \cos \frac{\pi \log (r/a)}{2 \log (r_0/r_1)} \sinh \frac{\pi (\theta + 2\pi j)}{2 \log (r_0/r_1)} \right] \qquad (1.4.4)$$

Real part of w^{I} is

$$\mathcal{R}(w^{\mathrm{I}}) = \frac{g}{4\pi} \log \left[\sin^2 A \cosh^2 B_j + \cos^2 A \sinh^2 B_j \right] = \frac{g}{4\pi} \log \left[\sin^2 A + \sinh^2 B_j \right] \qquad (1.4.5)$$

where $$A \equiv \frac{\pi \log r/a}{2 \log r_0/r_1} = \frac{\pi \log R/R_a}{2 \log R_0}$$

in which $R = r/r_1$

Now

$$w^{\mathrm{II}} = \frac{g}{2\pi} \log \sin \frac{\pi \log aZ/r_0^2}{2 \log r_0/r_1} \qquad (1.4.6)$$

Real part of w^{II} becomes

$$\mathcal{R}(w^{II}) = \frac{8}{4\pi} \log \left[\sin^2 A' + \sinh^2 B_j \right] \tag{1.4.7}$$

where $A' \equiv \dfrac{\pi \log (ar/r_o^2)}{2 \log (r_o/r_i)} = \dfrac{\pi \log (RR_a/R_o^2)}{2 \log R_o}$

Therefore, the pressure distribution for an incompressible fluid can be expressed as

$$p = K_1 \sum_{j=-\infty}^{\infty} \left\{ \log (\sin^2 A' + \sinh^2 B_j) - \log (\sin^2 A + \sinh^2 B_j) \right\} + K_2 \tag{1.4.8}$$

where K_1 and K_2 are constants to be determined by the following boundary conditions;

$$\left.\begin{aligned} p &= p_o \quad \text{at} \quad r = a - r_s \,, \quad \theta = 0 \\ p &= p_a \quad \text{at} \quad r = r_o \ \text{or} \ r_i \end{aligned}\right\} \tag{1.4.9}$$

where r_s is rudius of the gas supply hole.

Using the boundary conditions into Eq. (1.4.8), K_1 and K_2 are given by

$$K_1 = \frac{p_o - p_a}{\sum_{j=-\infty}^{\infty} \log \dfrac{\sin^2 A_s' + \sinh^2 B_j}{\sin^2 A_s + \sinh^2 B_j}} \tag{1.4.10}$$

$$K_2 = p_a$$

where

$$A_s \equiv \frac{\pi \log (a - r_s)/a}{2 \log (r_o/r_i)} = \frac{\pi \log (1 - R_s/R_a)}{2 \log R_o}$$

$$A_s' \equiv \frac{\pi \log a(a-r_s)/r_0^2}{2\log(r_0/r_i)} = \frac{\pi \log R_a(R_a-R_s)/R_0^2}{2\log R_0}$$

in which $R_s = r_s/r_i$

It should be noted that the boundary conditions are satisfied only at one point of the edge of the gas supply hole. However, if ξ is near to a in Eq. (1.4.1), the curve of constant pressure is given by a circular form so that this pressure distribution may satisfy the condition of the gas supply hole, if r_s is small enough compared to the bearing dimensions.

In the summation of Eq. (1.4.8), since the terms of $j \neq 0$ are negligibly small in comparison with the term of $j = 0$, the pressure distribution can be expressed by

$$p = K_{1,0}\{\log(\sin^2 A' + \sinh^2 B_0) - \log(\sin^2 A + \sinh^2 B_0)\} + K_2 \qquad (1.4.11)$$

$$K_{1,0} = \frac{p_0 - p_a}{2\log(\sin A_s'/\sin A_s)}$$

(b) Multiple Gas Supply Holes

When there are several gas supply holes in each sector which are equally spaced circumferentially, as shown in Fig. 1.4.2, the pressure distribution is obtained by superposing the solution which corresponds to the case of one supply hole in each sector.

If there are k arrays of supply holes circumferentially

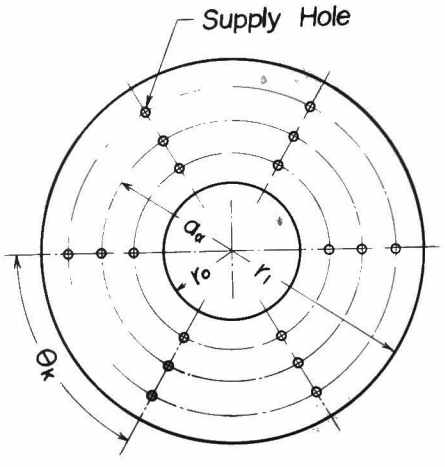

Fig. 1.4.2 Configuration of the bearing with multiple supply holes

and k' supply holes in each array in radial direction, the pressure distribution is given by

$$p = \sum_{\alpha=1}^{k'} \sum_{\beta=1}^{k} K_{1(\alpha,\beta)} \sum_{j=-\infty}^{\infty} \log \frac{\sin^2 A'_\alpha + \sinh^2 B_{j\beta}}{\sin^2 A_\alpha + \sinh^2 B_{j\beta}} + K_{2(\alpha,\beta)}$$
$$= \sum_{\alpha=1}^{k'} \sum_{\beta'=1}^{k} K_{1(\alpha,\beta)} \log \frac{\sin^2 A'_\alpha + \sinh^2 B_{\beta'}}{\sin^2 A_\alpha + \sinh^2 B_{\beta'}} + K_{2(\alpha,\beta)} \qquad (1.4.12)$$

where

$$A_\alpha = \frac{\pi \log(r/a_\alpha)}{2\log(r_0/r_1)} = \frac{\pi \log R/R_{a\alpha}}{2\log R_0}$$

$$A'_\alpha = \frac{\pi \log(a_\alpha r/r_0^2)}{2\log(r_0/r_1)} = \frac{\pi \log(R_{a\alpha} R/R_0^2)}{2\log R_0} \qquad (\alpha = 1, 2, \ldots, k')$$

$$B_{j\beta} = \frac{\pi[\theta + 2\pi j - (\beta-1)\theta_k]}{2\log(r_0/r_1)} = \frac{\pi[\theta + 2\pi j - (\beta-1)\theta_k]}{2\log R_0}$$

$$B_{\beta'} = \frac{\pi[\theta - (\beta'-1)\theta_k]}{2\log(r_0/r_1)} = \frac{\pi[\theta - (\beta'-1)\theta_k]}{2\log R_0}$$

$$\theta_k = \frac{2\pi}{k} \quad : \text{angular interval}$$

The boundary conditions to determine the constants $K_{1(\alpha,\beta)}$ and $K_{2(\alpha,\beta)}$ are

$$p = p_o \quad \text{at} \quad r = a_\alpha - r_{s\alpha}, \quad \theta = (\beta - 1)\theta_k$$

$$p = p_a \quad \text{at} \quad r = r_o \quad \text{or} \quad r_i$$

$$(\alpha = 1, 2, \ldots, k'; \ \beta = 1, 2, \ldots, k)$$

(c) The Bearing with Radial Grooves

If the bearing has radial grooves between the gas supply holes, as shown in Fig. 1.4.3, the pressure distribution on one sector can be obtained by taking alternate sources and sinks spaced θ_k as shown in Fig. 1.4.4.

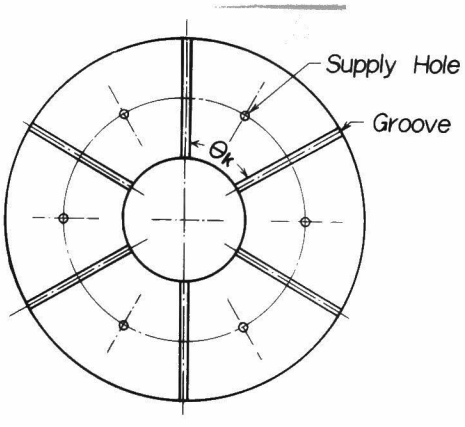

Fig. 1.4.3 Thrust collar bearing with radial grooves between supply holes

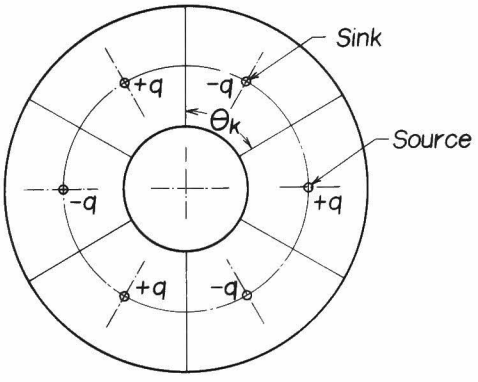

Fig. 1.4.4 Arrangement of sources and sinks in the case of $\Theta_k = 60^\circ$

The angle Θ_k can be taken as the angle of real sector in a particular bearing, so that k may be an arbitrary real number.

The pressure distribution obtained similarly as Eq. (1.4.12) is

$$p = \sum_{\alpha=1}^{k'} \sum_{\beta'=-\infty}^{\infty} (-1)^{\beta'-1} K_{1(\alpha,\beta)} \log \frac{\sin^2 A'_\alpha + \sinh^2 B_{\beta'}}{\sin^2 A_\alpha + \sinh^2 B_{\beta'}} + K_{2(\alpha,\beta)} \quad (1.4.13)$$

Eq. (1.4.13) is valid for a sector bounded by $r_o \leqq r \leqq r_i$ and $-\frac{\Theta_k}{2} \leqq \Theta \leqq \frac{\Theta_k}{2}$. The boundary conditions to determine the constants $K_{1(\alpha,\beta)}$ and $K_{2(\alpha,\beta)}$ are

$$p = (-1)^{\beta'-1} p_o \quad \text{at} \quad r = a_\alpha - r_{s\alpha}, \ \Theta = (\beta'-1)\Theta_k$$

$$p = p_a \quad \text{at} \quad r = r_o \ \text{or} \ r_i$$

$$(\alpha = 1, 2, \ldots, k'; \ \beta' = 0, \pm 1, \pm 2, \ldots)$$

4-2 Some Examples of Theoretical Pressure Distribution

The bearing dimensions are chosen for calculations as follows;

$$r_o/r_i = R_o = 1/3$$

$$a/r_i = R_a = 2/3$$

$$r_s/r_i = R_s = 1/75$$

$$p_o - p_a = 1 \text{ kg/cm}^2$$

The number of supply holes is taken to one as shown in Fig. 1.4.1(a) and six as shown in Fig. 1.4.1(b) or Fig. 1.4.3. The case of one supply hole is fundamental since the case of multiple supply holes is obtained by superposition of it.

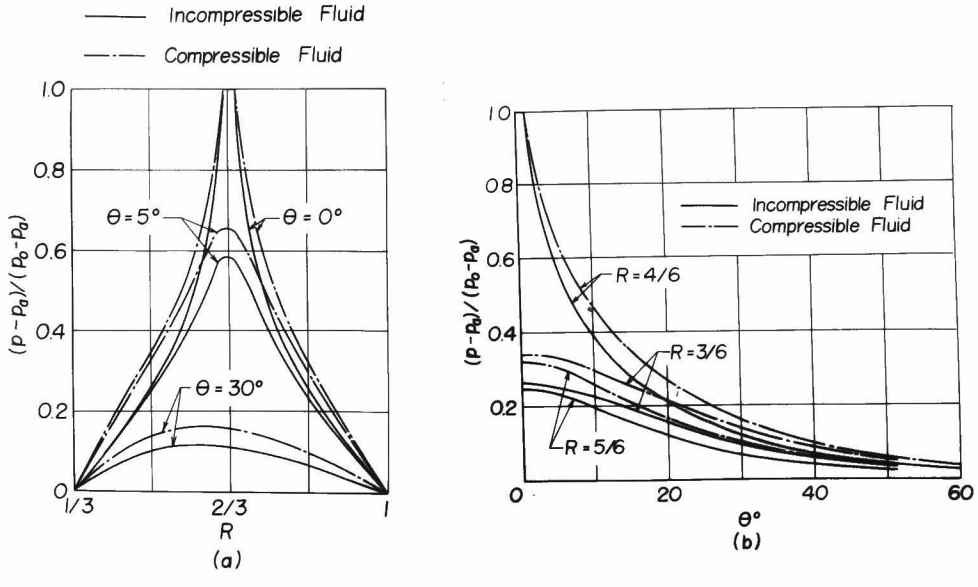

Fig. 1.4.5 Pressure distributions for the case of one supply holes

Fig. 1.4.5(a) shows the pressure distribution calculated on the circle of radii with $R = r/r_1 = 3/6, 4/6,$ and $5/6$ and Fig. 1.4.5(b) shows the pressure distributions on the radii locating on $\theta = 0^\circ$, 5° and 30° for the case of one supply hole.

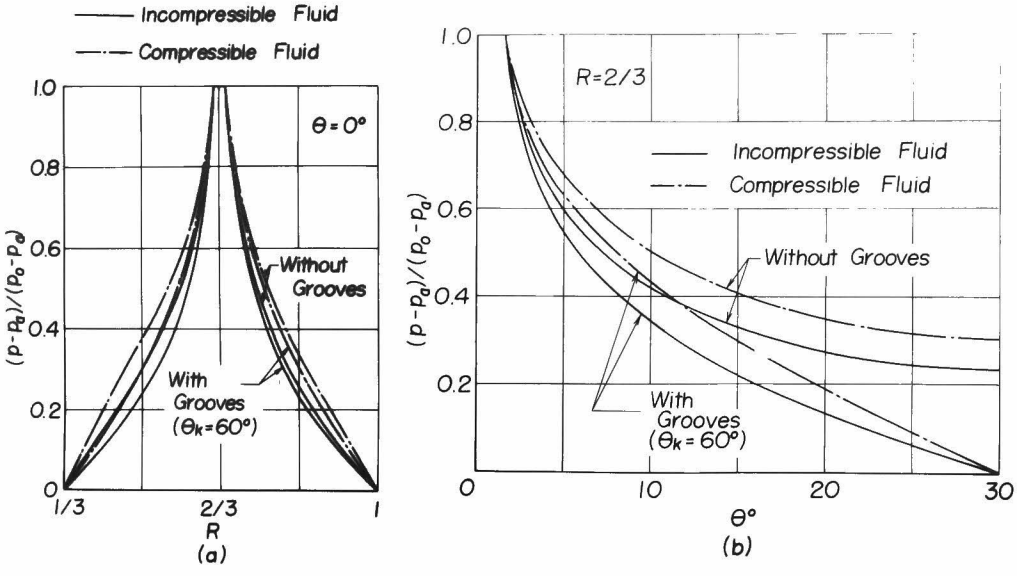

Fig. 1.4.6 Pressure distributions for the case of six supply holes

Fig. 1.4.6 shows the pressure distribution for the case of six supply holes spaced equally in the circumferential direction.

4-3 Load Capacity with Incompressible Fluid

(a) Potential Function in Series

The pressure of Eq. (1.4.8) is hard to be integrated

with respect to the bearing surface in order to yield the load capacity, though Eq. (1.4.8) can be conveniently used for the evaluation of the pressure distribution.

In the followings an externally pressurized thrust collar bearing with single supply hole as shown in Fig. 1.4.7 is analyzed concerning the load capacity.

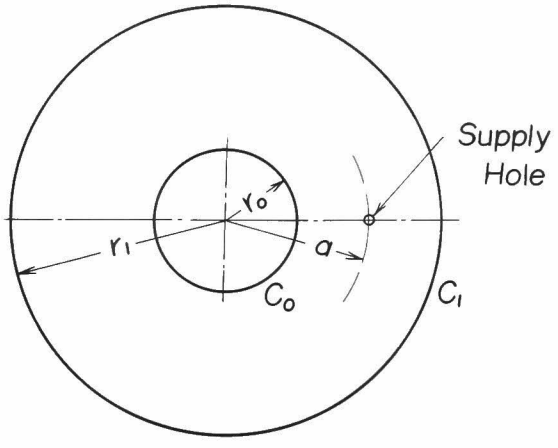

Fig. 1.4.7 Schematic diagram of a thrust collar bearing

At the first step, a single point source of strength q is put at $Z = a$, where Z represents a complex plane containing the bearing surface. The complex potential function is

$$w_1(Z) = \frac{q}{2\pi} \log\left(1 - \frac{Z}{a}\right) \qquad (1.4.14)$$

This point source function cannot satisfy the boundary conditions, or the potential cannot be constant at bearing peripheries C_0 and C_1. For the first correction of potential, two point sinks of strength -q are put; one is at the inverse point of a with C_0 $(Z=r_0^2/a)$ in order to cancel the potential $w_1(Z)$ and to make constant, the other at $Z=r_1^2/a$ in order to cancel $w_1(Z)$ on the peripfery C_1, resulting

$$w_{20}(Z) = -\frac{q}{2\pi}\log\left(1-\frac{aZ}{r_0^2}\right) \tag{1.4.15}$$

$$w_{21}(Z) = -\frac{q}{2\pi}\log\left(1-\frac{aZ}{r_1^2}\right) = -\frac{q}{2\pi}\log\left[1-\left(\frac{r_1}{r_0}\right)^{-2}\left(\frac{aZ}{r_0^2}\right)\right] \tag{1.4.16}$$

respectively.

$w_{20}(Z)$ compensates the function $w_1(Z)$ on C_0, but its effect on C_1 is not considered; in order to cancel $w_{20}(Z)$ on C_1, the following potential must be added

$$w_{31}(Z) = \frac{q}{2\pi}\log\left(1-\frac{r_0^2 Z}{ar_1^2}\right) = \frac{q}{2\pi}\log\left[1-\left(\frac{r_1}{r_0}\right)^{-2}\left(\frac{Z}{a}\right)\right] \tag{1.4.17}$$

Similarly in order to cancel $w_{21}(Z)$ on C_0, a source must be added

$$w_{30}(Z) = \frac{q}{2\pi}\log\left(1-\frac{r_1^2 Z}{ar_0^2}\right) = \frac{q}{2\pi}\log\left[1-\left(\frac{r_1}{r_0}\right)^2\left(\frac{Z}{a}\right)\right] \tag{1.4.18}$$

An array of infinite sources and sinks must be put according to the similar reduction so that the potential

may be canceled by each other to be constant on the bearing peripferies C_0 and C_1, that is

$$w_{40}(Z) = -\frac{q}{2\pi}\log\left(1-\frac{a r_1^2 Z}{r_0^4}\right) = -\frac{q}{2\pi}\log\left[1-\left(\frac{r_1}{r_0}\right)^2\left(\frac{aZ}{r_0^2}\right)\right] \quad (1.4.19)$$

$$w_{41}(Z) = -\frac{q}{2\pi}\log\left(1-\frac{a r_0^2 Z}{r_1^4}\right) = -\frac{q}{2\pi}\log\left[1-\left(\frac{r_1}{r_0}\right)^{-4}\left(\frac{aZ}{r_0^2}\right)\right] \quad (1.4.20)$$

and so forth. Denoting $w_m(Z)$ as summation of these sources and sinks, namely

$$w_m(Z) = w_1(Z) + w_{20}(Z) + w_{21}(Z) + w_{30}(Z) + \cdots + w_{2(m+1)0}(Z) \quad (1.4.21)$$

$$= \frac{q}{2\pi}\log\prod_{j=-m}^{m}\left[1-\left(\frac{r_1}{r_0}\right)^{2j}\left(\frac{Z}{a}\right)\right] - \frac{q}{2\pi}\log\prod_{j=-m}^{m}\left[1-\left(\frac{r_1}{r_0}\right)^{2j}\left(\frac{aZ}{r_0^2}\right)\right]$$

When m tends to infinity, one can obtain the potential function which may be constant on both of C_0 and C_1.

Complementary solution of Eq. (1.2.5) may be added by the boundary condition that the pressure at the bearing edges is p_a (ambient pressure):

$$w_0(Z) = A_{01}\log Z + A_{02} \quad (1.4.22)$$

Then, potential function $w(Z)$ is obtained as

$$w(Z) = \lim_{m\to\infty}\left[w_m(Z) + w_0(Z)\right] \quad (1.4.23)$$

Eq. (1.4.23) may be considered as an expansion of Eq. (1.4.8) in series, and is used for the calculation of load capacity

instead of Eq. (1.4.8).

The pressure distribution can be obtained from the real part of Eq. (1.4.23) as

$$p = \lim_{m\to\infty}\left\{\frac{q}{4\pi}\sum_{j=-\infty}^{\infty}\log\frac{1-2R_o^{2j}(R/R_a)\cos\theta+R_o^{4j}(R/R_a)^2}{1-2R_o^{2j}(R_aR/R_o)\cos\theta+R_o^{4j}(R_aR/R_o)^2} + A_{o1}\log r + A_2\right\} + K_2 \qquad (1.4.24)$$

where $R = r/r_1$, $R_a = a/r_1$, and $R_o = r_o/r_1$

When the boundary condition of Eq. (1.4.9) is applied, the strength q has the following relation with K_1 of Eq. (1.4.10)

$$K_1 = -\frac{q}{4\pi} \quad \text{and} \quad K_2 = p_a \qquad (1.4.25)$$

(b) Evaluation of Potential Function on the Bearing Peripheries

The real part of function $w_m(Z)$ is

$$\mathcal{R}\{w_m\} = \frac{q}{4\pi}\sum_{j=-m}^{m}\log\frac{1-2\left(\frac{r_1}{r_o}\right)^{2j}\left(\frac{r}{a}\right)\cos\theta+\left(\frac{r_1}{r_o}\right)^{4j}\left(\frac{r}{a}\right)^2}{1-2\left(\frac{r_1}{r_o}\right)^{2j}\left(\frac{ar}{r_o^2}\right)\cos\theta+\left(\frac{r_1}{r_o}\right)^{4j}\left(\frac{ar}{r_o^2}\right)^2} \qquad (1.4.26)$$

Substituting $r=r_o$, one can obtain the potential on bearing periphery C_o as

$$\mathcal{R}\{w_m\}_{r=r_o} = \frac{q}{4\pi}\sum_{j=-m}^{m}\log\left(\frac{r_1}{r_o}\right)^{4j}\left(\frac{r_o}{a}\right)^2 \qquad (1.4.27)$$

The potential is constant everywhere on C_o because this equation is independent of θ.

In the other hand, by substituting $r=r_i$ into Eq. (1.4.26 the potential on C_i becomes

$$\left.\begin{aligned}\mathcal{R}\{w_m\}_{r=r_i} &= \frac{q}{4\pi}\sum_{j=-m}^{m}\log\left(\frac{r_i}{r_o}\right)^{4j}\left(\frac{r_i}{a}\right)^2 \\ &+ \frac{q}{4\pi}\log\frac{1-2\left(\frac{r_i}{r_o}\right)^{2m}\left(\frac{r_i}{a}\right)\cos\theta+\left(\frac{r_i}{r_o}\right)^{4m}\left(\frac{r_i}{r_o}\right)^2}{1-2\left(\frac{r_i}{r_o}\right)^{2m}\left(\frac{ar_i}{r_o^2}\right)\cos\theta+\left(\frac{r_i}{r_o}\right)^{4m}\left(\frac{ar_i}{r_o^2}\right)^2}\end{aligned}\right\} \quad (1.4.28)$$

The first term is independent on θ to be constant, and the potential deviates from the real bearing boundary condition by the second term, which contains the variable θ . But the deviation becomes negligible for sufficiently large number of m because $(r_i/r_o)^{2m}$ can be neglected compared with $(r_i/r_o)^{4m}$. Now, the complementary solution $w_o(Z)$ is added to make the potential to match the ambient condition both on inner and outer bearing peripheries. Then the real part of $w_o(Z)$, $A_{o1}\log r + A_{o2}$, should satisfy the following conditions:

$$\left.\begin{aligned}A_{o1}\log r_o + A_{o2} + w_m^o &= 0 \quad (\text{on } C_o) \\ A_{o1}\log r_i + A_{o2} + w_m^i &= 0 \quad (\text{on } C_i)\end{aligned}\right\} \quad (1.4.29)$$

where

$$\left.\begin{aligned}w_m^o = \mathcal{R}\{w_m\}_{r=r_o} &= \frac{q}{4\pi}\sum_{j=-m}^{m}\log\left(\frac{r_i}{r_o}\right)^{4j}\left(\frac{r_o}{a}\right)^2 \\ &= \frac{q}{4\pi}(2m+1)\log\left(\frac{r_o}{a}\right)^2\end{aligned}\right\} \quad (1.4.30)$$

$$\left.\begin{aligned}w_m^i = \mathcal{R}\{w_m\}_{r=r_i,\,\theta=0} &= \frac{mq}{\pi}\log\left(\frac{r_o}{a}\right) \\ &+ \frac{q}{2\pi}\log\frac{1-\left(\frac{r_i}{r_o}\right)^{2m}\left(\frac{r_i}{r_o}\right)}{1-\left(\frac{r_i}{r_o}\right)^{2m}\left(\frac{ar_i}{r_o^2}\right)}\end{aligned}\right\} \quad (1.4.31)$$

For sufficiently large number of m, w_m' becomes

$$w_m' \cong \frac{q}{2\pi}(m+1)\log\frac{r_0}{a} \qquad (1.4.31)'$$

Obtaining A_{01} and A_{02} from these equations, the complementary solution becomes

$$\left.\begin{aligned} A_{01}\log r + A_{02} &= \frac{q}{2\pi}\cdot\frac{\log a/r_0}{\log r_1/r_0}\log\frac{r\cdot r_1^{2m+1}}{r_0^{2m+2}} \\ &= -\frac{q}{2\pi}\cdot\frac{\log R_a/R_0}{\log R_0}\log(R/R_0^{2m+2}) \end{aligned}\right\} \qquad (1.4.32)$$

(c) Load Capacity(Incompressible Fluid Case)

Now consider the following potential function which represents a single source at $Z = \bar{a}$,

$$\bar{w} = \frac{q}{2\pi}\log\left(1-\frac{\bar{z}}{\bar{a}}\right) \qquad (1.4.33)$$

Denoting $\bar{p}$ to be the potential of this source resulting

$$\bar{p} = \mathcal{R}\{\bar{w}\} = \frac{q}{4\pi}\log\left\{\left(\frac{r}{\bar{a}}\right)^2 - 2\left(\frac{r}{\bar{a}}\right)\cos\theta + 1\right\} \qquad (1.4.34)$$

Then, $\bar{p}$ is integrated on the region inner than a circle of radius $\bar{r}$, that is

$$\left.\begin{aligned} \bar{W} &= \int_0^{\bar{r}}\int_0^{2\pi}\bar{p}\, r\,dr\,d\theta \\ &= \frac{q}{4\pi}\int_0^{\bar{r}} r\int_0^{2\pi}\log\left\{\left(\frac{r}{\bar{a}}\right)^2 - 2\left(\frac{r}{\bar{a}}\right)\cos\theta + 1\right\}d\theta\,dr \end{aligned}\right\} \qquad (1.4.35)$$

The integration with respect to θ can be calculated as

$$\left.\begin{aligned}\int_0^{2\pi}\log\left\{\left(\frac{r}{\bar{a}}\right)^2-2\left(\frac{r}{\bar{a}}\right)^2\cos\theta+1\right\}d\theta&=0 \qquad (r\leqq\bar{a})\\ &=4\pi\log(r/\bar{a}) \qquad (r>\bar{a})\end{aligned}\right\} \quad (1.4.36)$$

This is reduced in Appendix X .

Then Eq. (1.4.35) becomes as follows:

$$\overline{W} = 0 \qquad (\bar{r}\leqq\bar{a}) \qquad (1.4.37)$$

$$\begin{aligned}\overline{W} &= \varrho\int_{\bar{a}}^{\bar{r}} r\log\left|\frac{r}{\bar{a}}\right| dr\\ &= \varrho\left\{\frac{\bar{r}^2}{2}\log\frac{\bar{r}}{\bar{a}}-\frac{1}{4}(\bar{r}^2-\bar{a}^2)\right\} \quad (\bar{r}>\bar{a}) \qquad (1.4.38)\end{aligned}$$

The integration of $\bar{p}$ on the annular region as shown in Fig. 1.4.8 is obtained from the results of Eqs. (1.4.37) and (1.4.38) as follows:

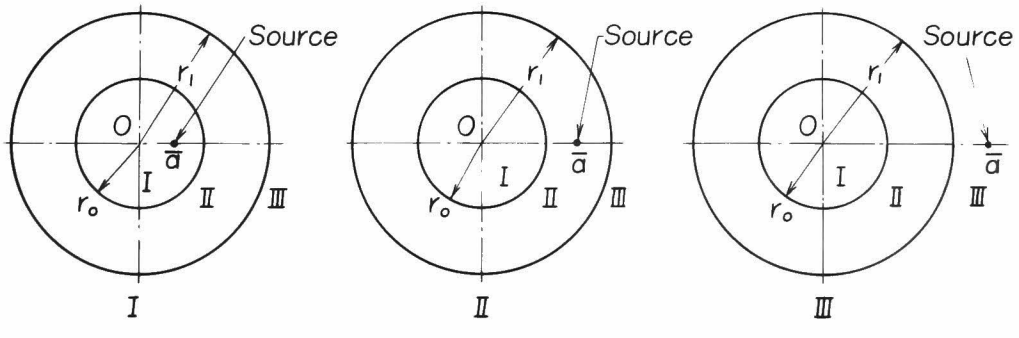

Fig. 1.4.8 Positions of source for obtaining load capacity

(i) when the source locates in inner region (I)

$$W_I = \beta\left\{\frac{r_1^2}{2}\log\frac{r_1}{a} - \frac{r_0^2}{2}\log\frac{r_0}{a} - \frac{1}{4}(r_1^2 - r_0^2)\right\} \qquad (1.4.39)$$

(ii) when the source locates in the annular region (II)

$$W_{II} = \beta\left\{\frac{r_1^2}{2}\log\frac{r_1}{a} - \frac{1}{4}(r_1^2 - a^2)\right\} \qquad (1.4.40)$$

(iii) when the source locates in outer region (III)

$$W_{III} = 0 \qquad (1.4.41)$$

Lastly, the integration of the term of complementary function, $\bar{p}_c = \mathcal{R}\{w_0\} = A_{01}\log r + A_{02}$, in the region II is

$$\left.\begin{aligned} W_c &= \int_{r_0}^{r_1} 2\pi r\,(A_{01}\log r + A_{02})\,dr \\ &= 2\pi\left[A_{01}\left\{\frac{r_1^2}{2}\log r_1 - \frac{r_0^2}{2}\log r_0\right\} - \left(\frac{A_{01}}{2} - \frac{A_{02}}{2}\right)(r_1^2 - r_0^2)\right] \end{aligned}\right\} \qquad (1.4.42)$$

The pressure distribution of Eq. (1.4.24) can be integrated within the annular bearing surface for each term of it by using Eqs. (1.4.39)-(1.4.42), resulting

$$W' = -\frac{\beta}{4}\left\{(r_1^2 - r_0^2)\frac{\log(a/r_0)}{\log(r_1/r_0)} - (a^2 - r_0^2)\right\} \qquad (1.4.43)$$

The pressure distribution is truncated at the supply hole so that its effect must be subtracted from the load capacity of Eq. (1.4.43). The pressure distribution of

truncated part can be approximated by

$$p = \frac{q}{4\pi} \log \frac{r}{r_s} + p_o \tag{1.4.44}$$

where the boundary condition of $p=p_o$ at $r=r_s$ is applied, and assuming that the coordinates are taken for the supply hole to locate at the origin. Then, the effect of truncated part is

$$W_{tr.} = \int_o^{r_s} 2\pi r (p - p_o)\, dr = -\frac{q r_s^2}{8} \tag{1.4.45}$$

The load capacity W is obtained as

$$\begin{aligned} W &= W' - W_{tr.} \\ &= -\frac{q}{4}\left[(r_i^2 - r_o^2)\frac{\log(a/r_o)}{\log(r_i/r_o)} - \left(a^2 - r_o^2 + \frac{r_s^2}{2}\right)\right] \end{aligned} \tag{1.4.46}$$

For the case with multiple supply holes, the load capacity can be obtained by the appropriate superposition; for the bearing with $k \times k'$ supply holes, the load capacity is

$$W_{(k,k')} = -\frac{k\sum_{\alpha=1}^{k'} q_{(\alpha,\beta)}}{4}\left[(r_i^2 - r_o^2)\frac{\log(a/r_o)}{\log(r_i/r_o)} - \left(a^2 - r_o^2 + \frac{r_s^2}{2}\right)\right] \tag{1.4.47}$$

where

$$q_{(\alpha,\beta)} = -4\pi K_{I(\alpha,\beta)} \tag{1.4.48}$$

4-4 Volume Rate of Flow

The quantity of flow can be calculated from the outflow from the bearing edges.

For the incompressible fluid, it becomes

$$Q_{incomp.} = -\frac{kh^3}{6\mu}\left\{\int_0^{\frac{\pi}{k}} \left| r\frac{\partial p}{\partial r}\right|_{r=r_o} d\theta + \int_0^{\frac{\pi}{k}} \left| r\frac{\partial p}{\partial r}\right|_{r=r_i} d\theta\right\} \quad (1.4.49)$$
$$= \frac{\pi k h^3}{3\mu}\sum_{\alpha=1}^{k'} K_{1(\alpha,\beta)}$$

in the case of the bearing without radial grooves,

$$Q_{incomp.} = -\frac{kh^3}{6\mu}\left\{\int_0^{\frac{\pi}{k}} \left| r\frac{\partial p}{\partial r}\right|_{r=r_o} d\theta + \int_0^{\frac{\pi}{k}} \left| r\frac{\partial p}{\partial r}\right|_{r=r_i} d\theta + 2\int_{r_o}^{r_i} \left|\frac{1}{r}\frac{\partial p}{\partial \theta}\right|_{\theta=\frac{\pi}{k}} dr\right\}$$
$$= \frac{\pi k h^3}{3\mu}\sum_{\alpha=1}^{k'} K_{1(\alpha,\beta)} \quad (1.4.50)$$

in the case of the bearing with radial grooves.

For the case of a compressible fluid, the pressure gradient is given by

$$\left|\frac{\partial p}{\partial r}\right|_{r=r_o,\,r_i} = \left(\frac{n}{1+n}\right) p_a^{-\frac{1}{n}} \left|\frac{\partial P}{\partial r}\right|_{r=r_o,\,r_i}$$

Substituting this into Eqs. (1.4.49) and (1.4.50), the volume rate of flow, $Q_{comp.}$, which corresponds to the pressure p_a has the following relationship with $Q_{incomp.}$,

$$Q_{comp.} = \frac{p_o^{\frac{1+n}{n}} - p_a^{\frac{1+n}{n}}}{p_o - p_a} \cdot \frac{n}{1+n} \cdot p^{-\frac{1}{n}} \cdot Q_{incomp.} \quad (1.4.51)$$

4-5 Some Examples of Theoretical Bearing Characteristics

Fig. 1.4.9 shows some theoretical characteristics of the bearings, load capacity and volume rate of flow, with some bearing parameters, such as number of supply holes, radius of supply holes and ratio of bearing radii, respectively. In these figures, the bearing characteristics are shown

in dimensionless forms;

$$f_W = \frac{W_{(k)}}{\pi(r_1^2 - r_0^2)(p_o - p_a)} \quad , \quad f_Q = \frac{Q_{incomp.}}{\pi h^3 (p_o - p_a)(3\mu)^{-1}} \qquad (1.4.52)$$

k' is taken to be one.

For any bearing, the supply holes must locate at inner position than the middle of the thrust collar in order to maximize the load capacity. The volume rate of flow may also vary with the value of R_a but this is not so conclusive at the bearing design because the value of f_Q is almost constant as long as the supply holes are arranged near the middle of the thrust collar.

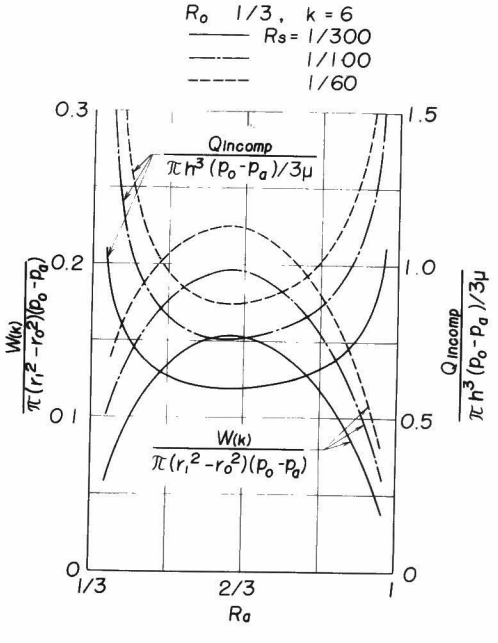

(a)

Fig. 1.4.9

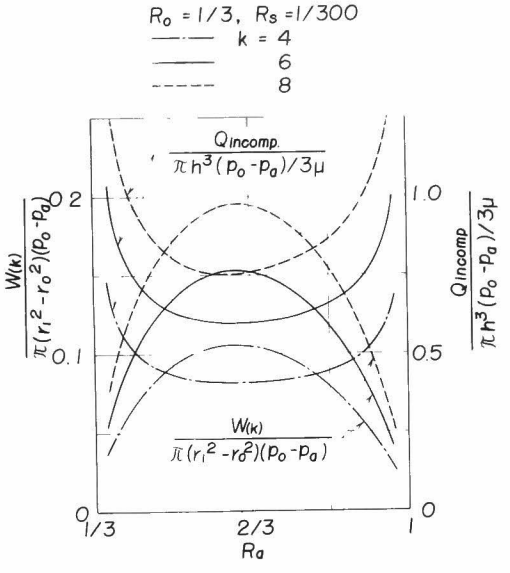

(b)

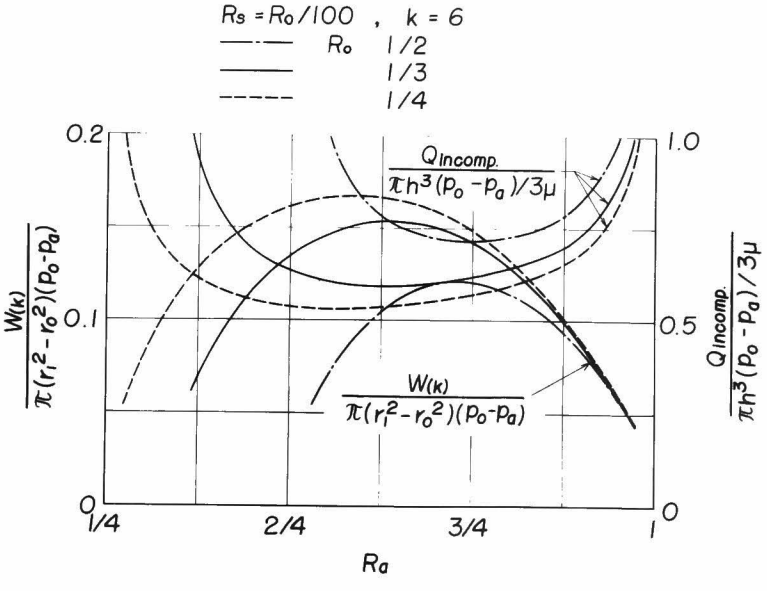

(c)

Fig. 1.4.9 Bearing characteristics for various bearing parameters

4-6 Experimental Investigations

In order to verify the foregoing theory, the pressure distributions, load capacities, and volume rates of flow are investigated experimentally by using the same apparatus as in Chapter 3.

(a) Pressure Distribution

Pressure distributions of the thrust collar gas-bearings are measurdd experimentally by using experimental apparatus I for three bearing configurations which are with a single supply hole, with 6 supply holes without radial grooves between supply holes, and with 6 supply holes with grooves, respectively as shown in Fig. 1.4.10.

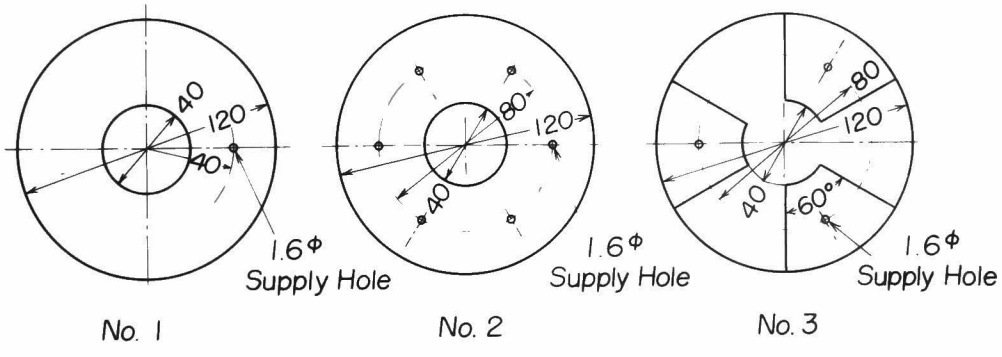

Fig. 1.4.10 Bearings employed in experiments for pressure distribution and volume rate of flow

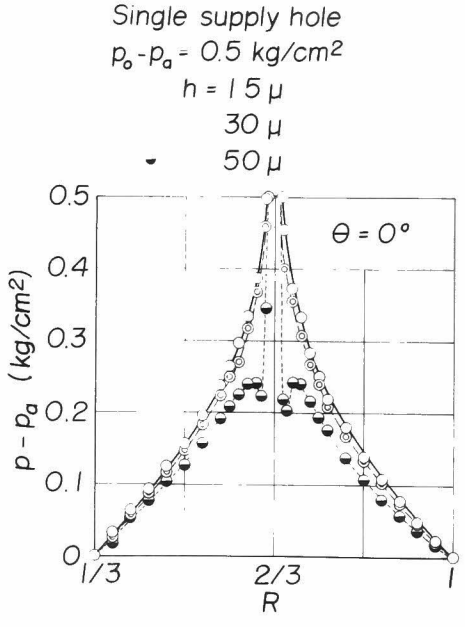
Single supply hole
$p_o - p_a$ = 0.5 kg/cm²
h = 15 μ
30 μ
50 μ
θ = 0°
p - p_a (kg/cm²)
0.5
0.4
0.3
0.2
0.1
0
1/3
2/3
1
R

(a)

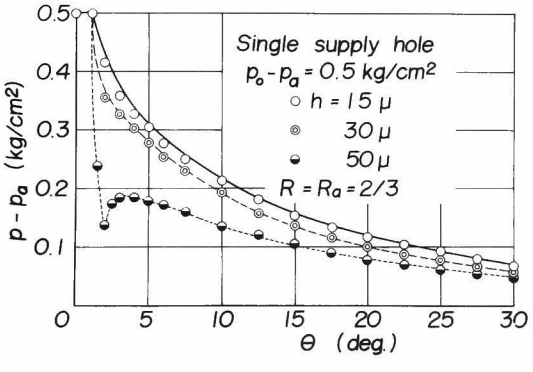
Single supply hole
$p_o - p_a$ = 0.5 kg/cm²
h = 15 μ
30 μ
50 μ
R = R_a = 2/3
p - p_a (kg/cm²)
0.5
0.4
0.3
0.2
0.1
0
5
10
15
20
25
30
θ (deg.)

(b)

Fig. 1.4.11

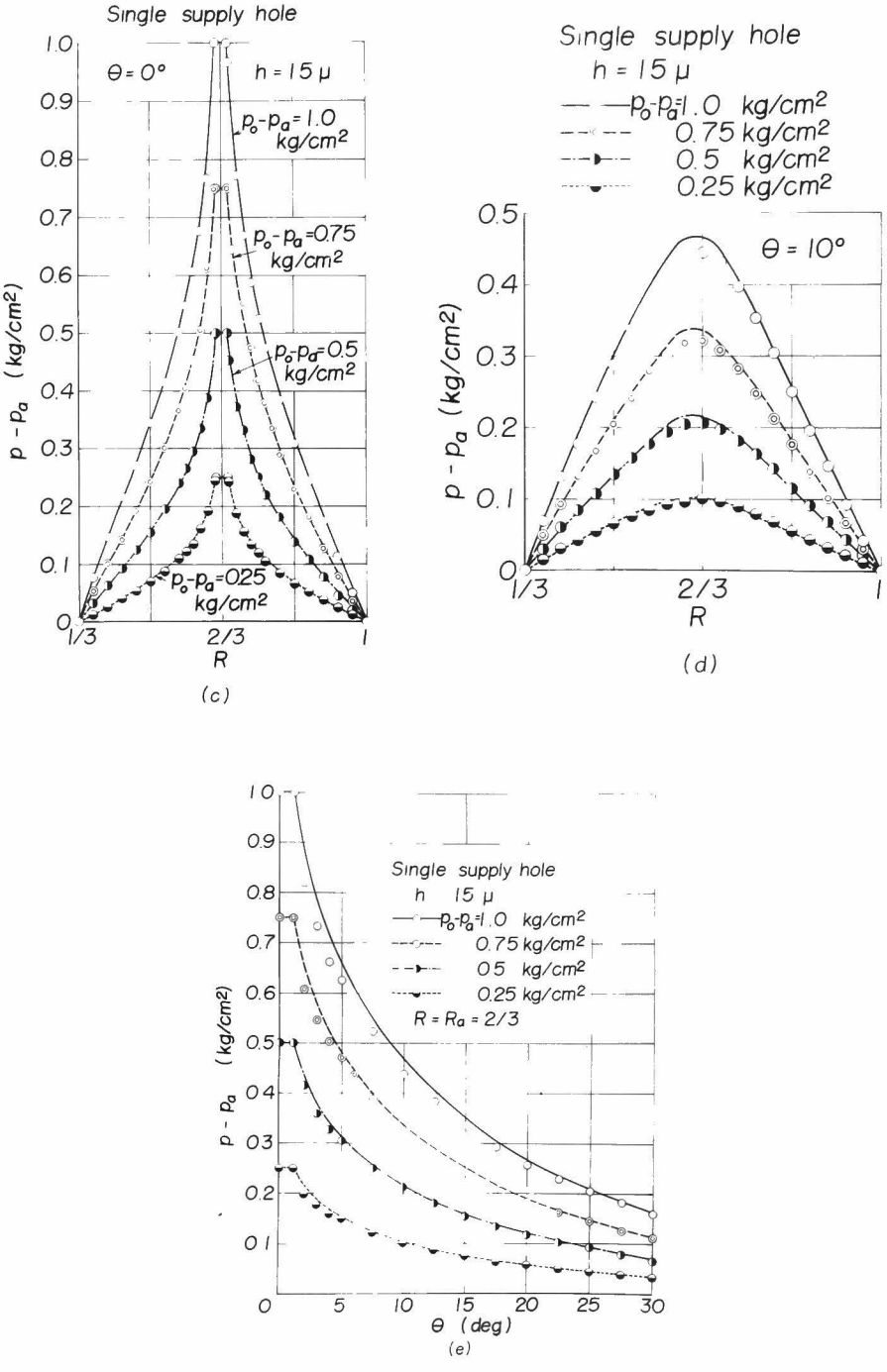
Single supply hole
Θ = 0°
h = 15 μ
$p_o - p_a$ = 1.0 kg/cm²
$p_o - p_a$ = 0.75 kg/cm²
$p_o - p_a$ = 0.5 kg/cm²
$p_o - p_a$ = 025 kg/cm²
p - p_a (kg/cm²)
R
(c)
Single supply hole
h = 15 μ
$p_o - p_a$ = 1.0 kg/cm²
0.75 kg/cm²
0.5 kg/cm²
0.25 kg/cm²
Θ = 10°
p - p_a (kg/cm²)
R
(d)
Single supply hole
h 15 μ
$p_o - p_a$ = 1.0 kg/cm²
0.75 kg/cm²
0.5 kg/cm²
0.25 kg/cm²
R = R_a = 2/3
p - p_a (kg/cm²)
Θ (deg)
(e)

Fig. 1.4.11

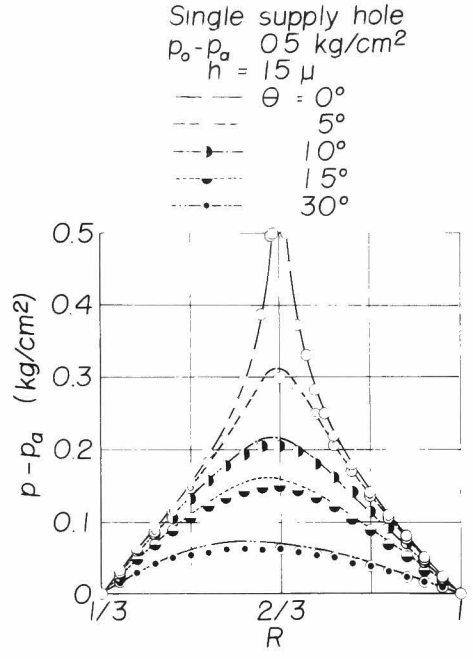
Single supply hole
$p_o - p_a$ 0.5 kg/cm²
h = 15 μ
θ = 0°
5°
10°
15°
30°
0.5
0.4
0.3
0.2
0.1
0
p - pa (kg/cm²)
1/3
2/3
1
R

(f)

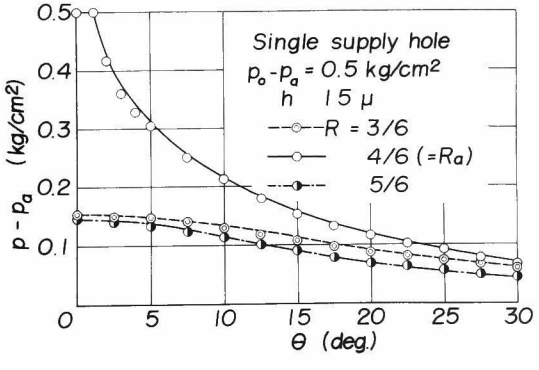
Single supply hole
$p_o - p_a$ = 0.5 kg/cm²
h 15 μ
R = 3/6
4/6 (=Ra)
5/6
0.5
0.4
0.3
0.2
0.1
0
p - pa (kg/cm²)
0
5
10
15
20
25
30
θ (deg.)

(g)

Fig. 1.4.11

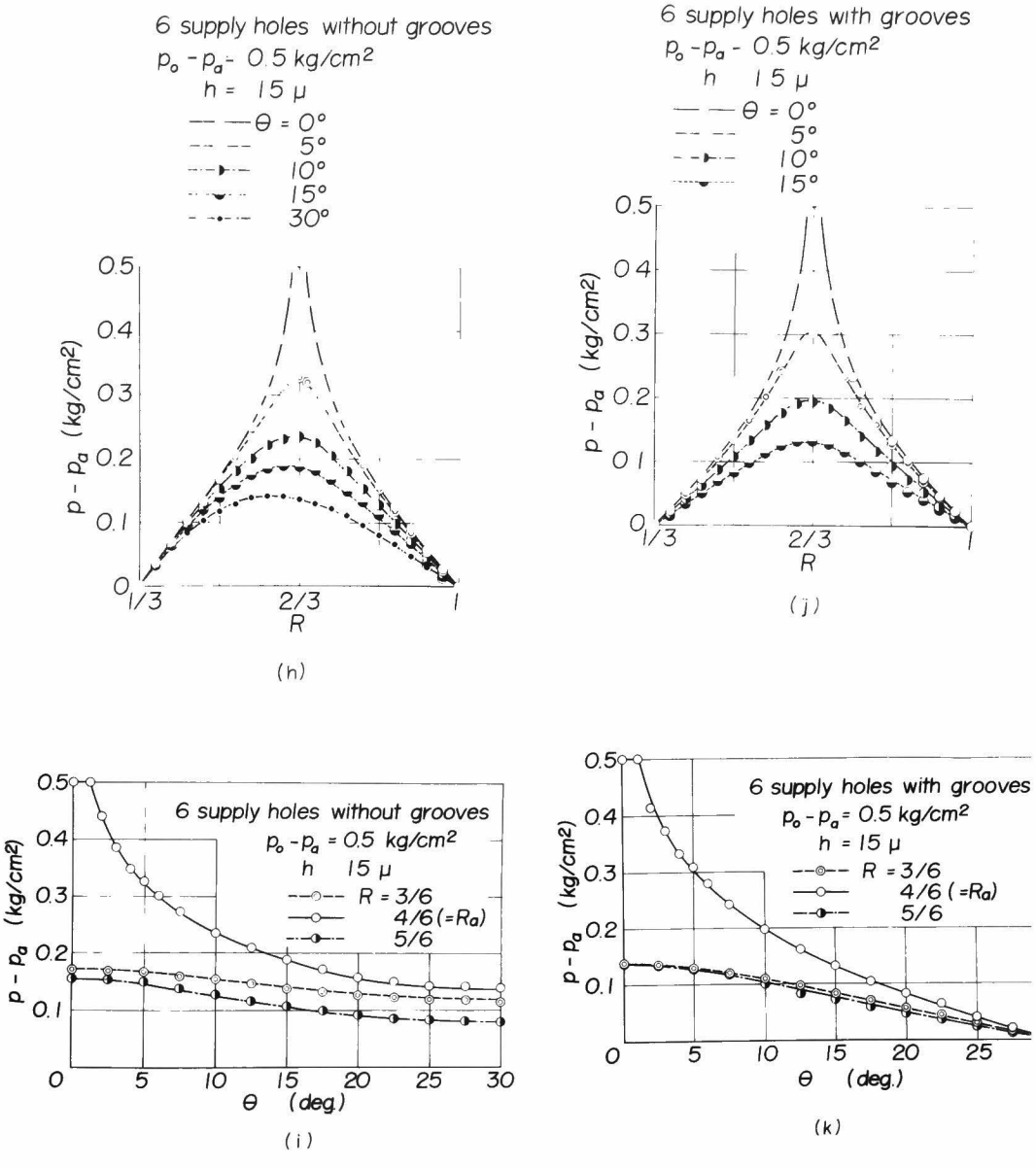

Fig. 1.4.11 Results of pressure distributions

Fig. 1.4.11 is the experimental results for some bearing parameters. In these figures, the thick lines show the theoretical curves calculated by the foregoing theory assuming n = 1.0 (isothermal condition).

For the particular case with a large bearing clearance or high supply pressure, the pressure loss at the supply holes may occur as also mentioned in Chapter 3. Furthermore the pressure depressions are also observed near the supply holes for the case of larger bearing clearance (for example h=50 microns) such as shown in Fig. 1.4.11(a) in which thin lines are only experimental.

However, for the whole, the experimental results coincide very well with theoretical ones for any case of the bearings especially for a small bearing clearance and comparatively low supply pressure where a fully viscous flow may be presumed.

(b) Load Capacity

Load capacity is also investigated experimentally by using the experimental apparatus II mentioned in Chapter 3. Configurations of the employed bearings are shown in Fig. 1.4.12, all of which have no radial grooves between supply holes.

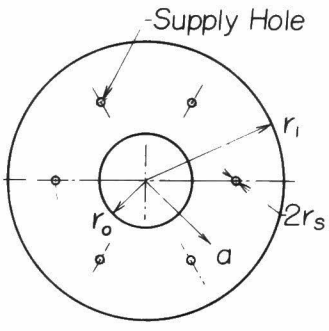

No.	$2r_i$ (mm)	$2r_o$ (mm)	$2a$ (mm)	$2r_s$ (mm)	k
1	90	30	60	1.5	6
2	90	30	60	1.5	4
3	90	30	60	1.5	8
4	90	30	70	1.5	6
5	90	30	50	1.5	6
6	90	30	60	3.0	6
7	60	30	45	1.5	6

Fig. 1.4.12 Bearings employed in experiments for load capacity

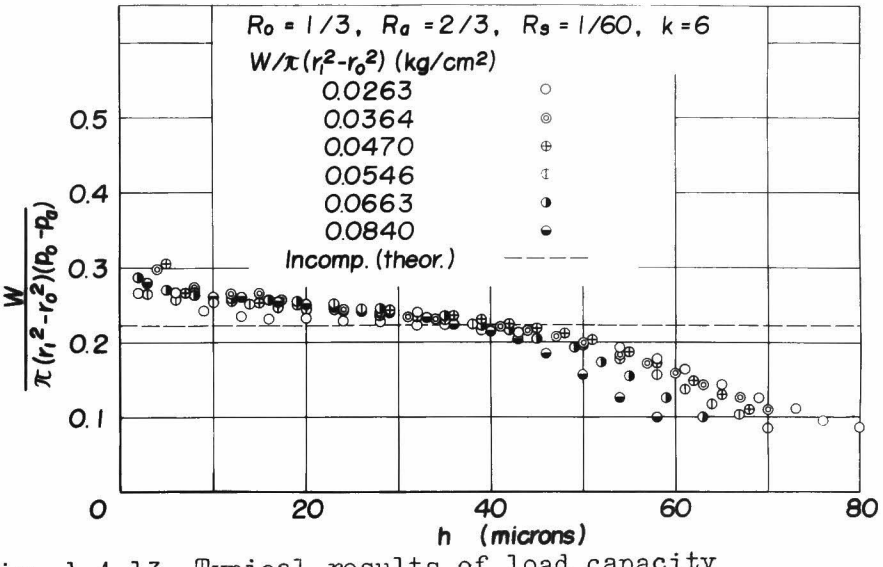

Fig. 1.4.13 Typical results of load capacity

Figs. 1.4.13 and 1.4.14 are the results of experiments in which the dimensionless load capacity $W/\pi(r_i^2-r_o^2)(p_o-p_a)$ is shown versus the bearing clearance with some bearing

parameters such as bearing load, radial position, radius and number of supply holes, and ratio of inner and outer bearing radii, respectively.

Fig. 1.4.13 is a typical results of experiments using the bearing specimen No.1. The load capacity is larger than the theoretical one (thin broken line) for a small bearing clearance but it falls down as the clearance increases, which is the same tendency as observed for the circular thrust gas-bearing in Chapter 3. It can be explained by the consideration of the compressibility of the fluid and the pressure fall at the supply holes.

Figs. 1.4.14 are the experimental results of the load capacity with various bearing parameters. In these figures, the theoretical curves are shown by thick lines with consideration of both effects. They are taken into account quite the

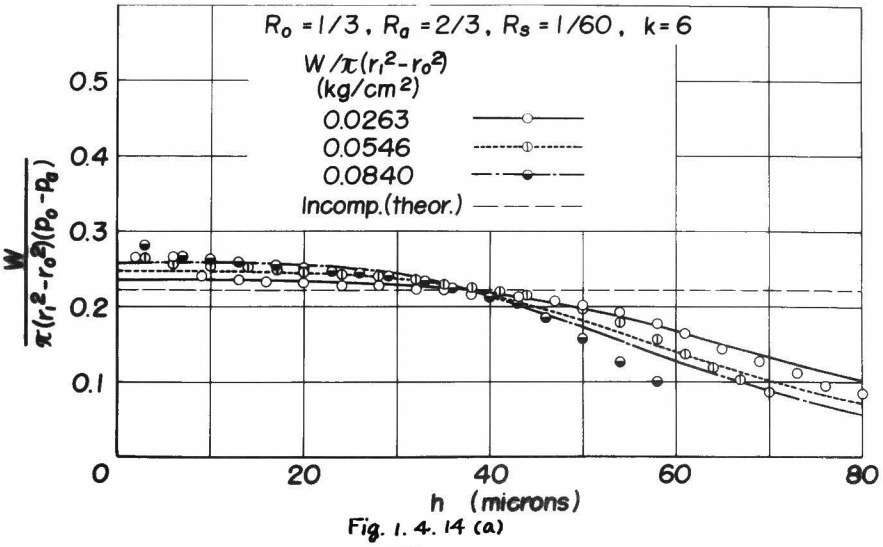

Fig. 1. 4. 14 (a)

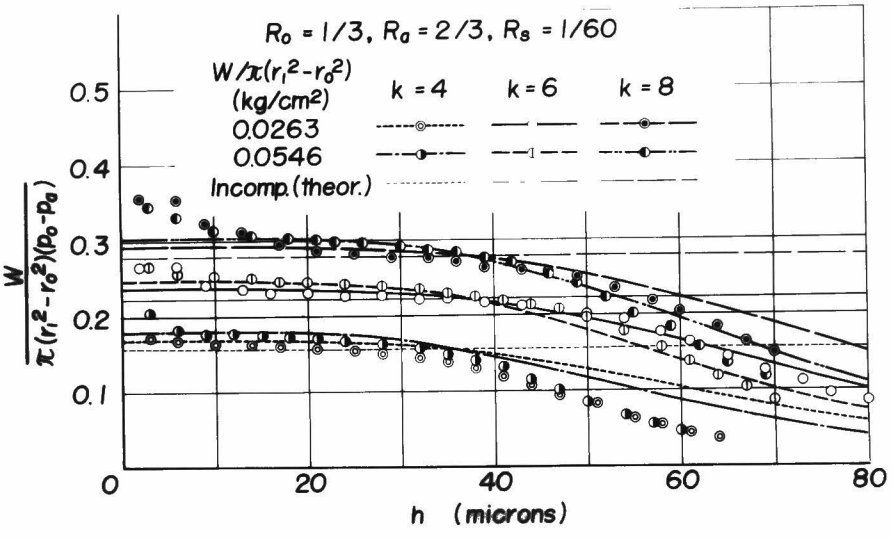
$R_o = 1/3,\ R_a = 2/3,\ R_s = 1/60$
$W/\pi(r_1^2 - r_o^2)$ (kg/cm²)
0.0263
0.0546
Incomp. (theor.)
k = 4
k = 6
k = 8
$\frac{W}{\pi(r_1^2 - r_o^2)(p_o - p_a)}$
0.5
0.4
0.3
0.2
0.1
0
20
40
60
80
h (microns)

(b)

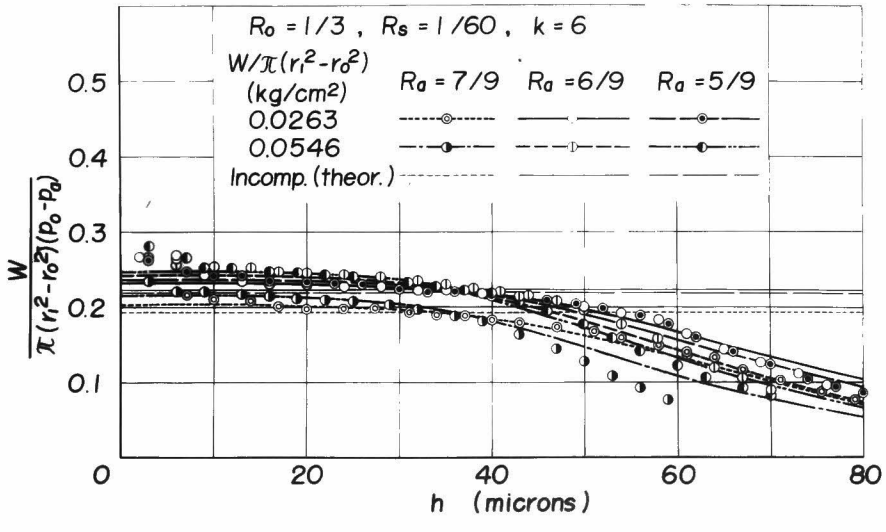
$R_o = 1/3,\ R_s = 1/60,\ k = 6$
$W/\pi(r_1^2 - r_o^2)$ (kg/cm²)
0.0263
0.0546
Incomp. (theor.)
$R_a = 7/9$
$R_a = 6/9$
$R_a = 5/9$
$\frac{W}{\pi(r_1^2 - r_o^2)(p_o - p_a)}$
0.5
0.4
0.3
0.2
0.1
0
20
40
60
80
h (microns)

(c)

Fig. 1.4.14

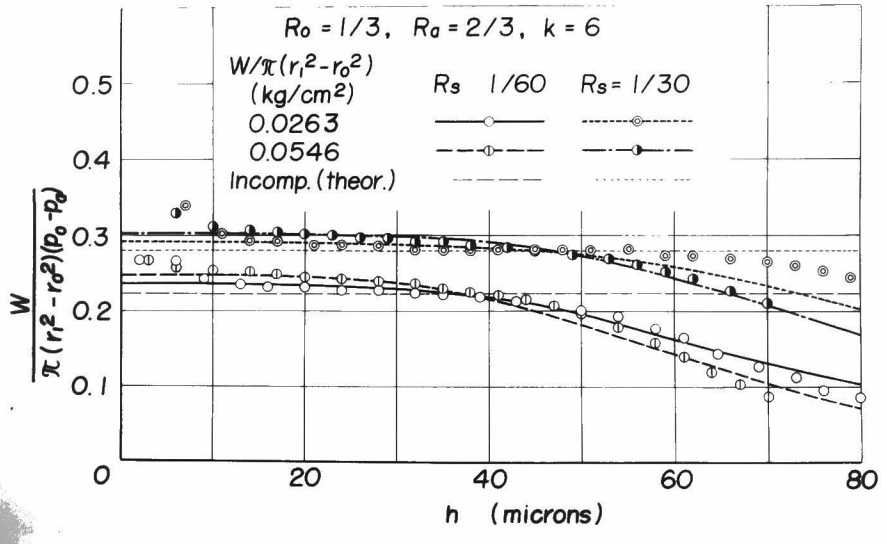

(d)

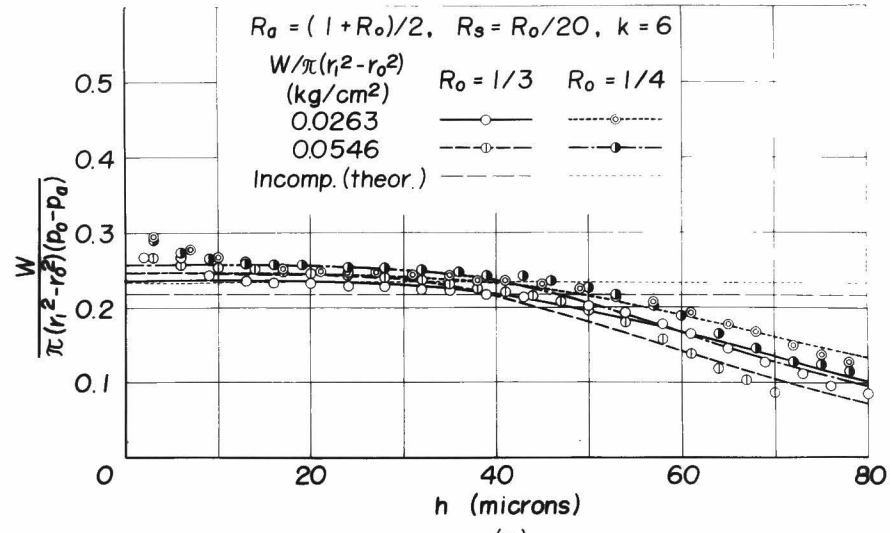

(e)

Fig. 1.4.14 Results of load capacity for various bearing parameters

same way as mentioned in Chapter 3 . Thin lines are for the incompressible solution without the inertia effect of the fluid.

Theoretical curves show a good conformity with the experimental ones especially for a small bearing clearance for any bearing configurations.

(c) Volume Rate of Flow

The volume rate of flow is investigated experimentally by using the experimental apparatus I with fixed bearing clearance.

Three types of thrust collar bearings are employed which are with single supply hole, with six supply holes without radial grooves, and with six supply holes with radial grooves. The bearing configurations are the same that are used in the experiments concerning pressure distribution.

Figs. 1.4.15 are the experimental results in which theoretical curves are drawn by thick line. The experiments are made under various values of p_o. The volume rate of flow is arranged in the form of $Q/\frac{p_o^2-p_a^2}{2p_a}$ against the bearing clearance h, because this is independent on p_o or p_a theoretically.

When the pressure fall at supply holes is taken into account, the volume rate of flow decreases as shown by thin

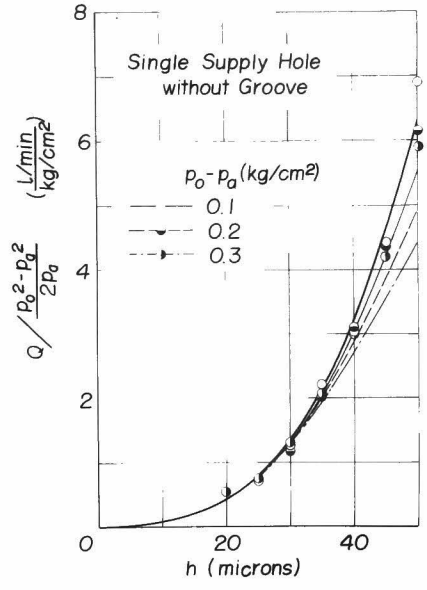
Single Supply Hole
without Groove
$p_o - p_a$ (kg/cm²)
0.1
0.2
0.3
$Q / \frac{p_o^2 - p_a^2}{2p_a}$ $(\frac{L/min}{kg/cm^2})$
8
6
4
2
0
20
40
h (microns)

(a)

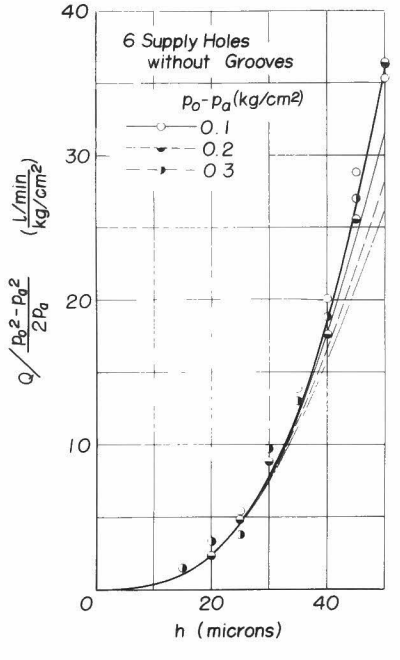
6 Supply Holes
without Grooves
$p_o - p_a$ (kg/cm²)
0.1
0.2
0.3
$Q / \frac{p_o^2 - p_a^2}{2p_a}$ $(\frac{L/min}{kg/cm^2})$
40
30
20
10
0
20
40
h (microns)

(b)

Fig. 1.4.15

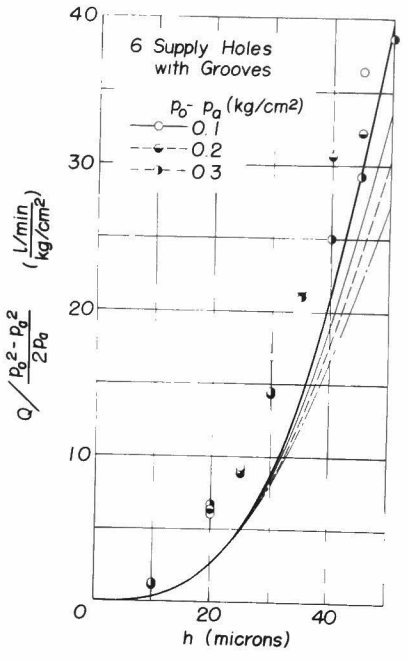

(c)

Fig. 1.4.15 Results of volume rate of flow

lines which are calculated by the same account as mentioned in Chapter 3-7 concerning the circular thrust bearing with multiple supply holes.

The experimental results show a good agreement with the theoretical ones qualitatively and quantitatively. The pressure fall effect at supply holes is, however, not so obvious in the experimental results.

4-7 Application to the Conical Bearing with Multiple Supply Holes

The foregoing theory concerning an externally pressurized thrust collar gas-bearing can be applied to the conical gas-bearing with multiple supply holes as shown in Fig. 1.4.16(a).

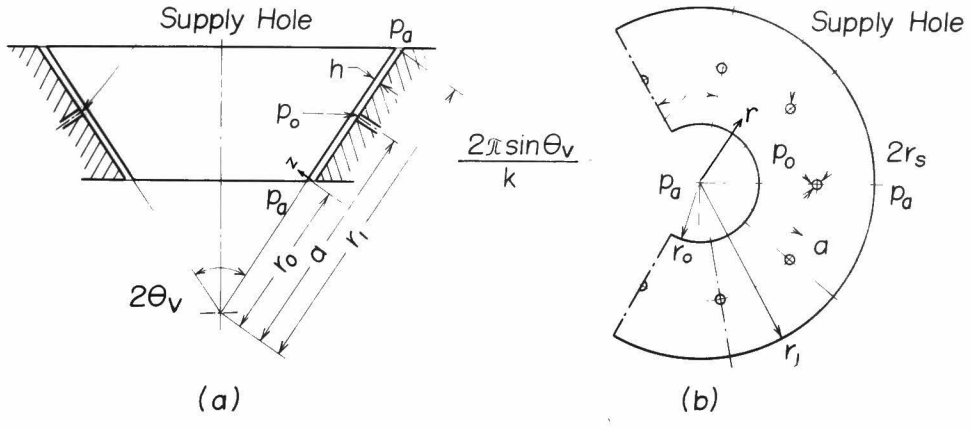

Fig. 1.4.16 Configurations of conical bearing.

Denoting the coordinates (r, z, θ) on the bearing surface as shown in the figure, namely

r : radial ordinate

z : ordinate normal to the bearing surface

θ : ordinate normal to r- and z-axis

and letting h be bearing clearance normal to the bearing surface, then, the bearing surface can be developed in a plane as Fig. 1.4.16(b) on which Reynolds equation as Eq. (1.2.1) is valid. Hence the pressure distribution can be obtained by the same form as Eq. (1.4.12), that is

$$p = K_1 \sum_{j=0}^{k-1} \left\{ \log \left[\sin^2 \frac{\pi \log (ar/r_0^2)}{2 \log (r_0/r_1)} + \sinh^2 \frac{\pi(\theta - j\theta_k)}{2 \log (r_0/r_1)} \right] \right. \tag{1.4.53}$$

$$\left. - \log \left[\sin^2 \frac{\pi \log (r/a)}{2 \log (r_0/r_1)} + \sinh^2 \frac{\pi(\theta - j\theta_k)}{2 \log (r_0/r_1)} \right] \right\} + K_2$$

where the angular spacing of the supply holes is

$$\theta_k = 2\pi \sin \theta_v / k \tag{1.4.54}$$

$2\theta_v$: vertical angle of the conical bearing

and radii r_0 and r_1 are the distances from the top of the conical surface.

The load capacity can be obtained by integrating the axial component of the pressure on the projected bearing area, then

$$\begin{aligned} W_c &= \int_{r_0}^{r_1} \int_0^{2\pi} (p - p_a) \sin\theta_v \, r d\theta \, d(r \sin\theta_v) \\ &= \sin^2 \theta_v \int_{r_0}^{r_1} \int_0^{2\pi} (p - p_a) \, r dr d\theta \\ &= \pi k K_1 \left[(r_1^2 - r_0^2) \frac{\log (a/r_0)}{\log (r_1/r_0)} - (a^2 - r_0^2 + \frac{r_s^2}{2}) \right] \sin^2 \theta_v \end{aligned} \tag{1.4.55}$$

where W_c is load capacity of the conical bearing.

The volume rate of flow can be obtained quite the same equation as Eq. (1.4.49) or Eq. (1.4.51).

Chapter 5 Analysis of Externally Pressurized Rectangular-Pad Type Thrust Bearing

5-1 Complex Potential and Pressure Distribution

The technique of applications of the complex potential theory to externally pressurized thrust bearing with multiple supply holes is also useful to analyze the other thrust-pad type gas-bearings.

In this section, a rectangular-pad type thrust bearing is analyzed theoretically. The bearing has multiple supply holes without recess located anywhere on the bearing surface. This type of thrust bearing is fundamental of rectangular or square thrust-pad, and of externally pressurized journal bearing with multiple supply holes as well when the eccentricity ratio of the journal is small enough to assume that the bearing clearance is constant. For the application to the journal bearing, a transformation has been obtained with consideration of an approximate bearing clearance variation.(1)

Analyses are made on the rectangular thrust pad with multiple supply holes, assuming that the bearing clearance h is constant.

For the first step, rectangular thrust pad with only one supply hole located anywhere on the bearing surface is investigated: an appropriate superposition will give the results of the cases with multiple supply holes.

Denote the bearing surface as the complex plane (Z-plane) with x and y-coordinates parallel to the rectangular bearing edges, and with the origin at the center of the bearing as shown in Fig. 1.5.1. The supply hole locates at $Z = a$ (a is also a complex number), where a source of strength should be put on the complex plane. This single source, however, could not satisfy the boundary conditions which is that the real part of potential function is constant at $x = \pm B/2$ and also $y = \pm L/2$ as well, where B and L are breadth and length of rectangular bearing, respectively.

In order to satisfy this condition, infinite arrays of infinite sources and sinks are put as shown in Fig. 1.5.1 by the principle of inverse point method. In Fig. 1.5.1, the bearing peripheries are shown by the thick solid lines. But now take a group of 4 segments as enclosed by the thick broken lines, then the infinite sources and sinks are equivalent

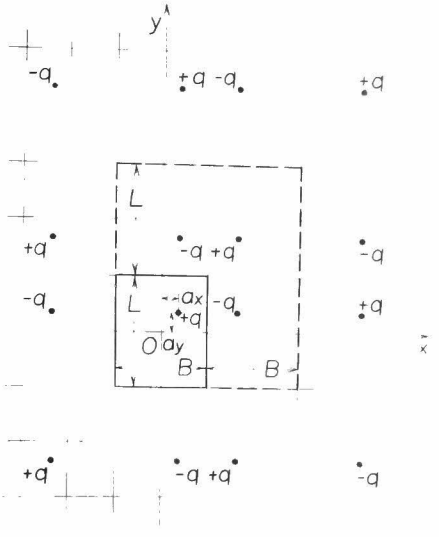

Fig. 1.5.1 Configuration of rectangular-pad thrust bearing and arrangement of sources and sinks

with infinite arrays of inifinite sets of these groups.

The complex potential function of the set is given by

$$w_o(Z) = \frac{q}{2\pi}\log(Z-a) + \frac{q}{2\pi}\log[Z-(B+iL)+a]$$

$$-\frac{q}{2\pi}\log[Z-iL-\tilde{a}] - \frac{q}{2\pi}\log[Z-B-\tilde{a}] \qquad (1.5.1)$$

where $\tilde{a}$ is the conjugate complex number of a. Then the complex potential of infinite sets with spacings of 2B and 2L in x and y-direction, respectively, which satisfies the boundary conditions at the bearing peripheries, is

$$w(Z)=\sum_{\alpha=-\infty}^{\infty}\sum_{\beta=-\infty}^{\infty} w_0(Z-2\alpha B-2i\beta L) \tag{1.5.2}$$

$$=\frac{g}{2\pi}\sum_{\alpha=-\infty}^{\infty}\left\{\log\sinh\frac{\pi[Z-2\alpha B-a]}{2L}-\log\sinh\frac{\pi[Z-(2\alpha+1)B+\tilde{a}]}{2L}\right.$$

$$\left.+\log\cosh\frac{\pi[Z-(2\alpha+1)B+a]}{2L}-\log\cosh\frac{\pi[Z-2\alpha B-\tilde{a}]}{2L}\right\} \tag{1.5.3}$$

The deduction is shown in Appendix XI.

The pressure distribution p for an incompressible fluid can be obtained from the real part of the complex potential function of Eq. (1.5.3), that is

$$p=K_1\sum_{\alpha=-\infty}^{\infty}\log\left[\frac{\sinh^2\frac{\pi[x-a_x-2\alpha B]}{2L}+\sin^2\frac{\pi[y-a_y]}{2L}}{\sinh^2\frac{\pi[x+a_x-(2\alpha+1)B]}{2L}+\sin^2\frac{\pi[y-a_y]}{2L}}\right.$$

$$\left.\times\frac{\sinh^2\frac{\pi[x+a_x-(2\alpha+1)B]}{2L}+\sin^2\frac{\pi[y+a_y-L]}{2L}}{\sinh^2\frac{\pi[x-a_x-2\alpha B]}{2L}+\sin^2\frac{\pi[y+a_y-L]}{2L}}\right]+K_2 \tag{1.5.4}$$

where a_x and a_y are x and y-components of a, respectively, that is

$$a=a_x+ia_y \tag{1.5.5}$$

K_1 and K_2 are constants determined by the boundary conditions which are

$$\left.\begin{aligned} &p=p_o \quad \text{at} \quad Z=a-r_s \\ &p=p_a \quad \text{at the bearing peripheries} \\ &\qquad Z=\pm\frac{B}{2} \quad \text{and} \quad Z=\pm\frac{iL}{2} \end{aligned}\right\} \tag{1.5.6}$$

where r_s is the radius of supply hole.

The pressure distribution for the case of multiple supply holes can be obtained by the superposition of the forms of Eq. (1.5.4) for each supply hole. For the case with k supply holes, k K_1's and K_2 can be obtained by the conditions of

$$\left.\begin{aligned} &p = p_o \quad \text{at} \quad Z = a_j - r_{sj} \quad (j = 1, 2, \ldots, k) \\ &p = p_a \quad \text{at the bearing peripheries} \end{aligned}\right\} \tag{1.5.7}$$

where a_j represents the position of each supply hole.

5-2 Load Capacity with Incompressible Fluid

For the first step, a potential is fundamentally considered in which a point source of strength $+q$ locates at $x = \bar{a}_x$ and $y = \bar{a}_y$, that is

$$\bar{w}(Z) = \frac{q}{2\pi} \log\left(1 - \frac{Z}{\bar{a}}\right) \tag{1.5.8}$$

whose real part $\bar{p}$ is

$$\bar{p} = \frac{q}{4\pi} \log\left[\frac{(x - \bar{a}_x)^2 + (y - \bar{a}_y)^2}{\bar{a}_x^2 + \bar{a}_y^2}\right] \tag{1.5.9}$$

Now consider a double integration of $\bar{p}$ with respect to x and y within the rectangular region bounded by

$$-\frac{B}{2} \leqq x \leqq \frac{B}{2} \quad , \quad -\frac{L}{2} \leqq y \leqq \frac{L}{2} \tag{1.5.10}$$

as shown in Fig. 1.5.2; namely

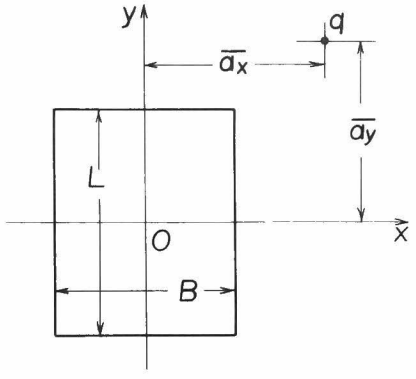

Fig. 1.5.2. Arrangement of source at obtaining load capacity

$$\overline{W}(\bar{a}_x, \bar{a}_y) = \int_{-\frac{B}{2}}^{\frac{B}{2}} \int_{-\frac{L}{2}}^{\frac{L}{2}} \bar{p}\, dx dy$$

$$= \frac{q}{4\pi}\left[\left(\frac{B}{2} - \bar{a}_x\right)^2 \left\{ \mathrm{Tan}^{-1} \frac{\frac{L}{2} - \bar{a}_y}{\frac{B}{2} - \bar{a}_x} + \mathrm{Tan}^{-1} \frac{\frac{L}{2} + \bar{a}_y}{\frac{B}{2} - \bar{a}_x} \right\}\right.$$

$$+ \left(\frac{B}{2} + a_x\right)^2 \left\{ \mathrm{Tan}^{-1} \frac{\frac{L}{2} - \bar{a}_y}{\frac{B}{2} + \bar{a}_x} + \mathrm{Tan}^{-1} \frac{\frac{L}{2} + \bar{a}_y}{\frac{B}{2} + \bar{a}_x} \right\}$$

$$+ \left(\frac{L}{2} - \bar{a}_y\right)^2 \left\{ \mathrm{Tan}^{-1} \frac{\frac{B}{2} - \bar{a}_x}{\frac{L}{2} - \bar{a}_y} + \mathrm{Tan}^{-1} \frac{\frac{B}{2} + \bar{a}_x}{\frac{L}{2} - \bar{a}_y} \right\}$$

$$\left. + \left(\frac{L}{2} + \bar{a}_y\right)^2 \left\{ \mathrm{Tan}^{-1} \frac{\frac{B}{2} - \bar{a}_x}{\frac{L}{2} + \bar{a}_y} + \mathrm{Tan}^{-1} \frac{\frac{B}{2} + \bar{a}_x}{\frac{L}{2} + \bar{a}_y} \right\} \right]$$

$$
\left.
\begin{aligned}
&+\left(\frac{B}{2}-\bar{a}_x\right)\left(\frac{L}{2}-\bar{a}_y\right)\log\left[\left(\frac{B}{2}-\bar{a}_x\right)^2+\left(\frac{L}{2}-\bar{a}_y\right)^2\right] \\
&+\left(\frac{B}{2}-\bar{a}_x\right)\left(\frac{L}{2}+\bar{a}_y\right)\log\left[\left(\frac{B}{2}-\bar{a}_x\right)^2+\left(\frac{L}{2}+\bar{a}_y\right)^2\right] \\
&+\left(\frac{B}{2}+\bar{a}_x\right)\left(\frac{L}{2}-\bar{a}_y\right)\log\left[\left(\frac{B}{2}+\bar{a}_x\right)^2+\left(\frac{L}{2}-\bar{a}_y\right)^2\right] \\
&+\left(\frac{B}{2}+\bar{a}_x\right)\left(\frac{L}{2}+\bar{a}_y\right)\log\left[\left(\frac{B}{2}+\bar{a}_x\right)^2+\left(\frac{L}{2}+\bar{a}_y\right)^2\right] \\
&-3BL-BL\log\left(\bar{a}_x^2+\bar{a}_y^2\right)
\end{aligned}
\right\} \quad (1.5.11)
$$

in which Tan^{-1} represents the principal value of arctangent for the arguments. The deduction of this result is shown in Appendix XII.

In order to satisfy the boundary conditions at bearing peripheries, infinite sources and sinks are put according to the potential function of Eq. (1.5.2). Hence the load capacity supported by a rectangular pad can be obtained by summation of the values $\overline{W}$, the positions of whose sources and sinks are those of each term of the potential function. Then, load capacity for an incompressible fluid is given by the following equations for single supply hole case by using the results of Eq. (1.5.11);

$$W = K_1 \sum_{\alpha=-\infty}^{\infty} \sum_{\beta=-\infty}^{\infty} \{ \overline{W}(a_x + 2\alpha B,\ a_y + 2\beta L) - \overline{W}[-a_x + (2\alpha+1)B,\ a_y + 2\beta L] - \overline{W}[a_x + 2\alpha B,\ -a_y + (2\beta+1)L] + \overline{W}[-a_x + (2\alpha+1)B,\ -a_y + (2\beta+1)L] \} \qquad (1.5.12)$$

For the case with multiple supply holes, the load capacity can be obtained by summing up the load capacities shared by each of supply holes.

5-3 Volume Rate of Flow

The volume rate of flow can be obtained by the out-flow from the bearing peripheries, which is also obtained from the strength of the source, that is for an incompressible fluid

$$Q_{incomp.} = \frac{\pi h^3 K_1}{3\mu} \qquad (1.5.13)$$

This is for the case with single supply hole: for the case with k supply holes located symmetrically, volume rate of

flow, $Q_{incomp.}$, can be obtained by multiplication by k though the value of K_i must be rewritten to satisfy the boundary conditions at supply holes.

For a compressible fluid case, the volume rate of flow corresponding to the ambient pressure is

$$Q_{comp.} = \frac{p_o^{\frac{1+n}{n}} - p_a^{\frac{1+n}{n}}}{p_o - p_a} \cdot \frac{n}{1+n} \cdot p_a^{-\frac{1}{n}} \times Q_{incomp.} \qquad (1.5.14)$$

which can be obtained with consideration of the transformation of Eq. (1.2.6).

5-4 Experimental Investigations

Some experiments are made to investigate the theory concerning the pressure distribution. This is fundamental for the load capacity and volume rate of flow because they may be derived from the integration or the gradient of it.

The configurations of the bearings employed are the square-pad type with only one, two or four supply holes located symmetrically as shown in Fig. 1.5.3.

Figs. 1.5.4 are the typical results of experiments for the pressure distribution measured along to x-direction (parallelly to the bearing edge) at some y-positions. The theoretical curves are shown by thick lines which are calculated under the isothermal condition (n=1.0).

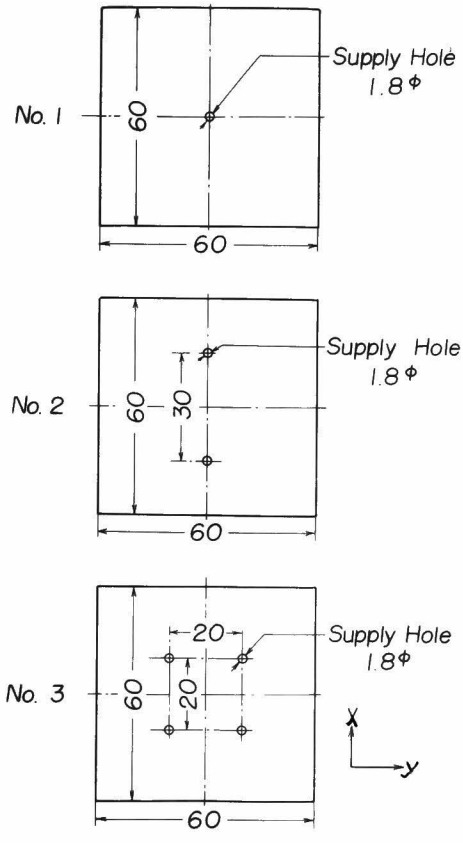

Fig. 1.5.3 Bearings employed in experiments for pressure distributions

For all cases, a good conformity is observed between experimental and theoretical results. The pressure fall, however, may occur at supply holes for the case with higher

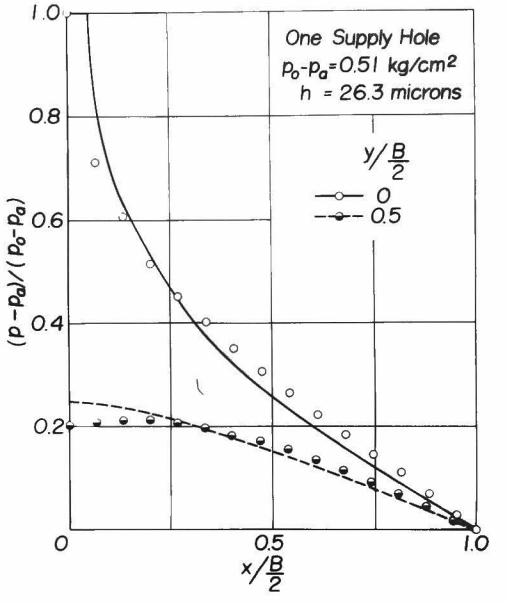
One Supply Hole
$p_o - p_a = 0.51$ kg/cm²
h = 26.3 microns
y/B/2
0
0.5
(p - pa)/(po - pa)
x/B/2
0
0.5
1.0
0.2
0.4
0.6
0.8
1.0

(a)

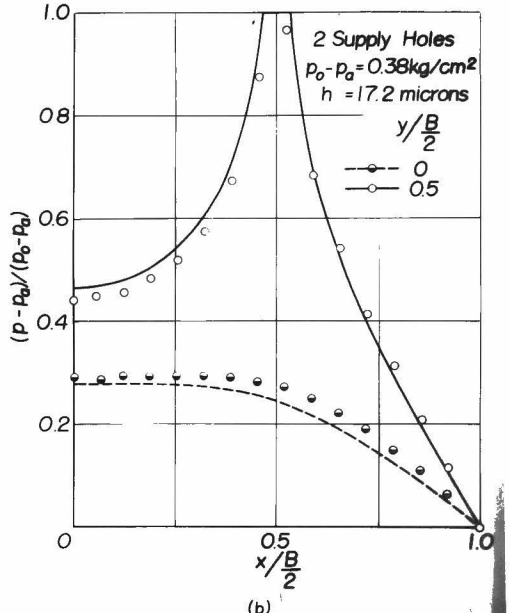
2 Supply Holes
$p_o - p_a = 0.38$kg/cm²
h = 17.2 microns
y/B/2
0
0.5
(p - pa)/(po - pa)
x/B/2
0
0.5
1.0
0.2
0.4
0.6
0.8
1.0

(b)

Fig. 1.5.4

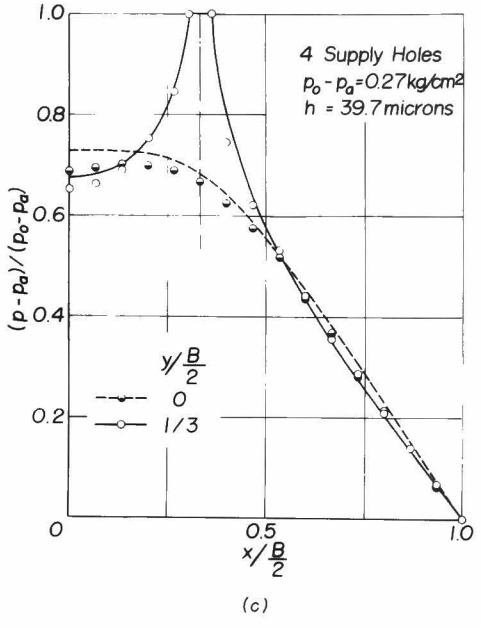

Fig. 1.5.4 Results of pressure distributions

supply pressure or larger bearing clearance. But under the practical condition as experimented here, the complex potential theory can be justified to be applicable with good accuracy for the rectangular-pad type thrust bearings with multiple supply holes as well.

Chapter 6 Conclusion

In Part I, the complex potential theory is introduced to analyze theoretically the externally pressurized thrust gas-berrings for some bearing configurations such as circular thrust bearings, thrust collar bearings, and rectangular pad-type thrust bearings with multiple supply holes, which has no recess to increase the bearing stability.

The appropriate complex potential functions can be found for each case, which satisfy the boundary conditions of the bearings. Then, the pressure distributions and volume rates of flow can be obtained for both of an incompressible fluid and a compressible one. The load capacity is calculated by particular method to each bearing for an incompressible fluid case. The bearing characteristics of volume rate of flow and load capacity, then, are shown in theoretical charts for the bearing designs.

The experiments are made to investigate the theoretical results,yielding good agreements between the results of them both qualitatively and quantitatively with the consideration of secondary effects owing to the compressibility of the fluid and pressure loss at supply holes. Pressure loss takes place at supply holes especially for the case with higher supply pressure and larger bearing clearance,

because of the energy loss for acceleration of the fluid after the supply holes, and the change of the flow velocity profiles, whose effects are estimated by assuming a flow pattern.

The good conformity of the results verifies the theory, and it is found that the complex potential theory may be applicable conveniently to the analyses of various bearing configurations with multiple supply holes.

Part II Analysis of Externally Pressurized Thrust Collar Gas-Bearings with Slit-Supplies

Chapter 1. Introduction

There are many useful applications of the thrust collar bearings because of their configurations of the devices. In these thrust collar bearings, the lubricant is fed either through some supply holes arranged circumferentially on the thrust surface or through the annular slit-supply.

The recesses after the supplies are useful for the load capacity but they often cause the instability of the bearing performance for the case with the compressible fluid lubricant.

The thrust collar bearing with slit-supply is considered as a limit case of the bearing with innumerable supply holes arranged circumferentially, and has rather large load capacity, and they need not have the recesses especially for the double slit-supply case which means their stable performance.

In the followings, the thrust collar bearing with single or double slit-supply is analyzed and the volume rate of flow and load capacity can be obtained as the functions of the radial positions of the slits.

In the analysis, it is assumed that the lubricant is incompressible; one can apply the results for the compressible fluid case if the supply pressure is not so high.

Chapter 2 Single Slit-Supply Case

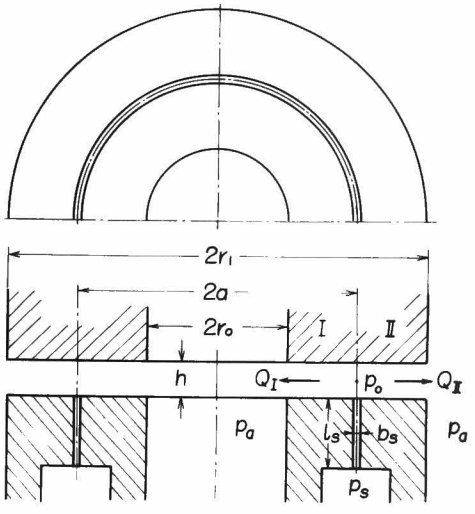

Fig. 2.2.1 Configuration of thrust collar bearing with single slit-supply

Fig. 2.2.1 illustrates a thrust collar bearing with single slit-supply. The lubricant is fed under the supply pressure p_s, and restricted by the slit into the bearing clearance, where the pressure is p_o. Then it flows out

towards inner and outer bearing peripheries. p_a is the ambient pressure. The slit locates at radius a and is assumed that its width is negligible compared with the inner bearing diameter $2r_o$ or outer diameter $2r_i$.

The flow is symmetrical, hence it can be reduced to one-dimensional case. When the bearing clearance h and coefficient of viscosity μ are constant, and if the effect of bearing rotation can be neglected, the following equations can be obtained,

$$\frac{1}{r}\frac{\partial(r\bar{u})}{\partial r} = 0 \qquad (2.2.1)$$

$$\bar{u} = -\frac{h^2}{12\mu}\frac{\partial p}{\partial r} \qquad (2.2.2)$$

where $\bar{u}$ is mean velocity in radial direction.

Then the pressure distribution is given by

$$p = C_1 \log r + C_2 \qquad (2.2.3)$$

By using the boundary conditions to determine the constants C_1 and C_2, it becomes

$$\text{Region I} : \quad p = \frac{\log r/r_o}{\log a/r_o}(p_o - p_a) + p_a \qquad (2.2.4)$$

$$\text{Region II} : \quad p = \frac{\log r_i/r}{\log r_i/a}(p_o - p_a) + p_a \qquad (2.2.5)$$

The volume rate of flow is

$$\text{Region I} : Q_I = 2\pi r h(-\bar{u}) = \frac{\pi h^3}{6\mu}\cdot\frac{p_o - p_a}{\log a/r_o} \qquad (2.2.6)$$

$$\text{Region II} : Q_{II} = 2\pi r h(\bar{u}) = \frac{\pi h^3}{6\mu}\cdot\frac{p_o - p_a}{\log r_i/a} \qquad (2.2.7)$$

The flow through the slit is considered as that between two parallel surfaces, hence

$$Q_s = \frac{\pi a b_s^3}{6\mu}\cdot\frac{p_s - p_a}{l_s} \qquad (2.2.8)$$

where b_s : width of slit

l_s : length of slit

By the condition of continuity, $Q_I + Q_{II} = Q_s$, Eqs. (2.2.6), (2.2.7) and (2.2.8) reduce to be

$$p_o - p_a = \frac{p_s - p_a}{1 + \left(\frac{h}{b_s}\right)^3\left(\frac{l_s}{a}\right)\left(\frac{1}{\log a/r_o} + \frac{1}{\log r_i/a}\right)} \qquad (2.2.9)$$

The load capacity W is

$$W = \int_{r_o}^{r_i} 2\pi r(p - p_a)\,dr$$

$$= \frac{\pi}{2}(p_o - p_a)\left(\frac{r_i^2 - a^2}{\log r_i/a} - \frac{a^2 - r_o^2}{\log a/r_o}\right) \qquad (2.2.10)$$

$$= \frac{\pi}{2}\left(\frac{r_i^2 - a^2}{\log r_i/a} - \frac{a^2 - r_o^2}{\log a/r_o}\right)\frac{p_s - p_a}{1 + \left(\frac{h}{b_s}\right)^3\left(\frac{l_s}{a}\right)\left(\frac{1}{\log a/r_o} + \frac{1}{\log r_i/a}\right)} \qquad (2.2.10)'$$

The condition to maximize the bearing stiffness is

$$\frac{\partial^2 W}{\partial \hat{h}^2} = 0$$

Then from Eq. (2.2.10)'

$$\frac{b_s^3}{l_s} = \frac{2\hat{h}^3}{a}\left(\frac{1}{\log a/r_o} + \frac{1}{\log r_i/a}\right) \tag{2.2.11}$$

This gives the condition of optimum slit dimensions. Then Eq. (2.2.9) becomes

$$p_o - p_a = \frac{2}{3}(p_s - p_a) \tag{2.2.12}$$

The load capacity can be obtained from Eq. (2.2.10) with this condition as

$$W = \frac{\pi}{3}(p_s - p_a)\left(\frac{r_i^2 - a^2}{\log r_i/a} - \frac{a^2 - r_o^2}{\log a/r_o}\right) \tag{2.2.13}$$

$$= \pi (r_i^2 - r_o^2)(p_s - p_a) \cdot F_W$$

where F_W is dimensionless load capacity factor with respect to $p_s - p_a$ given by

$$F_W \equiv \frac{W}{\pi(r_i^2 - r_o^2)(p_s - p_a)} \tag{2.2.13}'$$

$$= \frac{1}{3}\left(\frac{r_i^2 - a^2}{\log r_i/a} - \frac{a^2 - r_o^2}{\log a/r_o}\right)\frac{1}{r_i^2 - r_o^2}$$

$$= \frac{1}{3}\left(-\frac{1 - R_a^2}{\log R_a} - \frac{R_a^2 - R_o^2}{\log R_a/R_o}\right)\frac{1}{1 - R_o^2}$$

where

$$R_a = a/r_i, \quad R_o = r_o/r_i$$

While, the volume rate of flow is given by

$$\left.\begin{aligned} Q &= Q_{I} + Q_{II} \\ &= \frac{\pi h^3}{9\mu}\left(\frac{1}{\log a/r_0} + \frac{1}{\log r_i/a}\right)(p_s - p_a) \\ &= \frac{\pi h^3}{9\mu}(p_s - p_a)\cdot F_Q \end{aligned}\right\} \qquad (2.2.14)$$

where F_Q is dimensionless flow rate factor with respect to $(p_s - p_a)$ given by

$$\left.\begin{aligned} F_Q &\equiv \frac{1}{\log a/r_0} + \frac{1}{\log r_i/a} \\ &= \frac{1}{\log R_a/R_0} - \frac{1}{\log R_a} \end{aligned}\right\} \qquad (2.2.14)'$$

The minimum value of flow rate is acheived for the following radial position of slit a_M given by the condition of $\partial Q/\partial a = 0$;

$$a_M = \sqrt{r_0 r_i} \qquad (2.2.15)$$

These dimensionless factors are shown in Fig. 2.2.2 against the radial position of slit for various ratios of $R_0 (= r_0/r_i)$. In this figure, the curve of $r_0/r_i = 0$ corresponds to the case of the circular thrust bearing with recess of radius a.

The single-dotted chain line shows the minimum flow rate condition $(a = a_M)$ and the double-dotted chain line shows the limit where the slit is arranged imaginarily at the inner

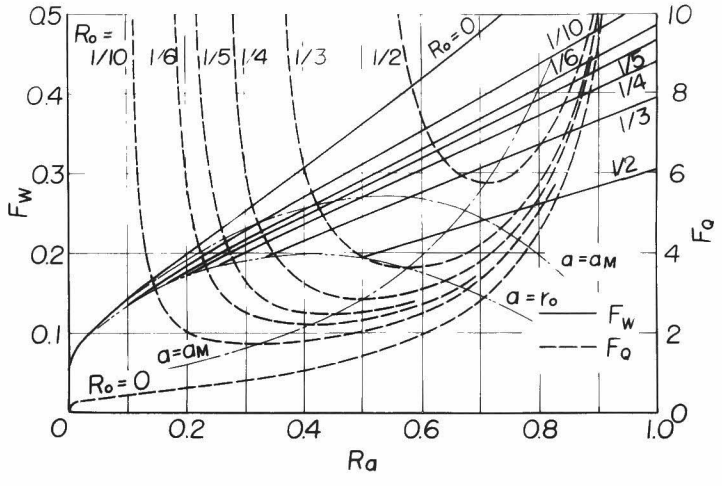

Fig. 2.2.2. Bearing characteristics with single slit-supply

periphery of the bearing ($a = r_o$).

Then the following conclusions can be obtained theoretically for the load capacity and the volume rate of flow concerning the design of thrust collar bearing with single slit-supply:

(i) The maximum bearing stiffness is obtained by the condition of Eq. (2.2.12).

(ii) The load capacity increases when slit position a approaches to the outer bearing periphery r_1, so the optimum value of a can not be determined from the load capacity condition.

(iii) The volume rate of flow increases when the slit approaches either of bearing peripheries.

(iv) Then the slit position must be recommended with considering the working condition of load and flow rate.

(v) The minimum flow rate condition is given by Eq. (2.2.15)

(vi) It is meaningless to design the slit position inner than a_M, because, for this case, the flow rate increases while the load capacity decreases than for the case with $a = a_M$.

Chapter 3. Double Slit-Supply Case

Fig. 2.3.1 is the schematic figure of the thrust collar bearing with double slit-supplies. The lubricant is fed under the supply pressure p_s, and flows through the slits into bearing clearance, then to the bearing peripheries. The slits are arranged at a_0 and a_1.

Denoting the pressure just after the slits as p_{00} and p_{01}, then the pressure distribution can be obtained as

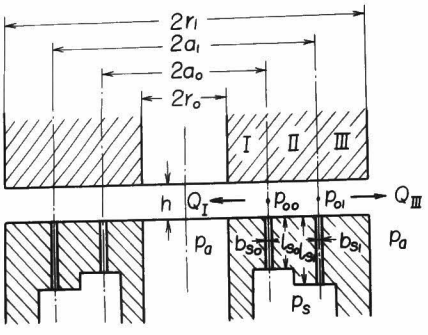

Fig. 2.3.1. Configuration of thrust collar bearing with double slit-supplies

follows similarly as the single slit-supply case:

$$\text{Region I}: \quad p = \frac{\log r/r_0}{\log a_0/r_0}(p_{00} - p_a) + p_a \qquad (2.3.1)$$

$$\text{Region II}: \quad p = \frac{\log r}{\log a_1/a_0}(p_{01} - p_{00}) + \frac{p_{00}\log a_1 - p_{01}\log a_0}{\log a_1/a_0} \qquad (2.3.2)$$

$$\text{Region III}: \quad p = \frac{\log r_1/r}{\log r_1/a}(p_{01} - p_a) + p_a \qquad (2.3.3)$$

These pressure distributions can be considered as the result of superposition of two bearings with single slit-supply which are;

one having a slit at $r = a_0$ with an inlet pressure

$$p_0 = \frac{\log r_1/a_0}{\log(a_1/a_0)\log(r_1/r_0)}(p_{00}\log a_1/r_0 - p_{01}\log a_0/r_0) + p_a \qquad (2.3.4)$$

the other having a slit at r= a_1 with an inlet pressure

$$p_o = \frac{\log a_1/r_o}{\log(a_1/a_o)\log(r_1/r_o)}(p_{o1}\log r_1/a_o - p_{oo}\log r_1/a_1) + p_a \qquad (2.3.5)$$

Considering that these imaginary bearings may be analyzed individually, the pressures p_{oo} and p_{o1} must have the following relation using the maximum bearing stiffness condition similarly as the single slit-supply case.

$$p_{oo} - p_a = p_{o1} - p_a = \frac{2}{3}(p_s - p_a) \qquad (2.3.6)$$

It mearns that the pressures p_{oo} and p_{o1} must be equal to each other. Then denoting p_o as

$$p_o \equiv p_{oo} = p_{o1}$$

the pressure distributions are

Region I : $p = \frac{\log r/r_o}{\log a_o/r_o}(p_o - p_a) + p_a \qquad (2.3.1)'$

Region II : $p = p_o \qquad (2.3.2)'$

Region III : $p = \frac{\log r_1/r}{\log r_1/a_1}(p_o - p_a) + p_a \qquad (2.3.3)'$

The volume rates of flow are

Region I : $Q_I = \frac{\pi h^3}{6\mu}\frac{p_o - p_a}{\log a_o/r_o} \qquad (2.3.7)$

Region II : $Q_{II} = 0 \qquad (2.3.8)$

Region III : $$Q_{III} = \frac{\pi h^3}{6\mu} \frac{p_o - p_a}{\log r_i/a_i} \tag{2.3.9}$$

The volume rates of flow through the slits are

$$Q_{so} = \frac{\pi a_o b_{so}^3}{6\mu \ell_{so}} (p_s - p_o) \tag{2.3.10}$$

$$Q_{si} = \frac{\pi a_i b_{si}^3}{6\mu \ell_{si}} (p_s - p_o) \tag{2.3.11}$$

The slit dimensions must have the following relationships by the condition (2.3.6):

$$\frac{b_{so}^3}{\ell_{so}} = \frac{h^3}{2a_o} \frac{1}{\log a_o/r_o} \tag{2.3.12}$$

$$\frac{b_{si}^3}{\ell_{si}} = \frac{h^3}{2a_i} \frac{1}{\log r_i/a_i} \tag{2.3.13}$$

The load capacity W is

$$\begin{aligned} W &= \frac{\pi}{2}\left(\frac{r_i^2 - a_i}{\log r_i/a_i} - \frac{a_o^2 - r_o^2}{\log a_o/r_o}\right)(p_o - p_a) \\ &= \frac{\pi}{3}\left(\frac{r_i^2 - a_i^2}{\log r_i/a_i} - \frac{a_o^2 - r_o^2}{\log a_o/r_o}\right)(p_s - p_a) \\ &\equiv \pi (r_i^2 - r_o^2)(p_s - p_a) F_W \end{aligned} \tag{2.3.14}$$

where F_W is the dimensionless load capacity factor given by

$$F_W \equiv \frac{1}{3}\left(\frac{r_i^2 - a_i^2}{\log r_i/a_i} - \frac{a_o^2 - r_o^2}{\log a_o/r_o}\right)\frac{1}{r_i^2 - r_o^2} = \frac{1}{3}\left(\frac{R_{ai}^2 - 1}{\log R_{ai}} - \frac{R_{ao}^2 - R_o^2}{\log R_{ao}/R_o}\right)\frac{1}{1 - R_o^2} \tag{2.2.15}$$

where $R_{ai} = a_i/r_i$, $R_{ao} = a_o/r_i$

The total volume rate of flow is

$$
\begin{aligned}
Q &= Q_{\mathrm{I}} + Q_{\mathrm{III}} \\
&= \frac{\pi h^3}{6\mu}\left(\frac{1}{\log a_0/r_0} + \frac{1}{\log r_1/a_1}\right)(p_0 - p_a) \\
&= \frac{\pi h^3}{9\mu}\left(\frac{1}{\log a_0/r_0} + \frac{1}{\log r_1/a_1}\right)(p_s - p_a) \\
&\equiv \frac{\pi h^3}{9\mu}(p_s - p_a)\cdot F_Q
\end{aligned}
\qquad (2.2.16)
$$

where F_Q is the dimensionless flow rate factor given by

$$
\left.
\begin{aligned}
F_Q &\equiv \frac{1}{\log a_0/r_0} + \frac{1}{\log r_1/a_1} \\
&= \frac{1}{\log R_{a_0}/R_0} - \frac{1}{\log R_{a_1}}
\end{aligned}
\right\} \qquad (2.2.17)
$$

Fig. 2.3.2 shows these factors for the case $R_0 = r_0/r_1 = 1/2$; the solid lines correspond to the constant F_W values and the dotted lines to the constant F_Q values.

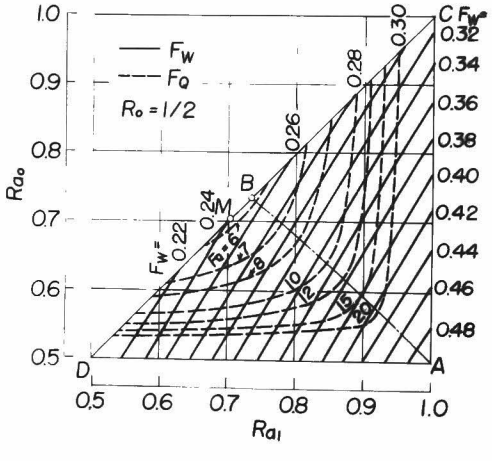

Fig. 2.3.2 Bearing characteristics with double slit-supplies

The bearing is desired to have larger load capacity under a certain volume rate of flow or to give the maximum value of F_w under the condition of F_Q =constant. The optimum positions a_0 and a_1 can be obtained from the condition

$$\frac{\partial \Phi}{\partial a_0} = \frac{\partial \Phi}{\partial a_1} = 0$$

where $\Phi \equiv F_w + \xi F_Q$

$$= \frac{1}{3}\left(\frac{r_1^2 - a_1^2}{\log r_1/a_1} - \frac{a_0^2 - r_0^2}{\log a_0/r_0}\right)\frac{1}{r_1^2 - r_0^2} + \xi\left(\frac{1}{\log a_0/r_0} + \frac{1}{\log r_1/a_1}\right) \quad (2.3.18)$$

The above conditions are

$$\frac{\partial \Phi}{\partial a_0} \equiv \frac{1}{3}\frac{2(a_0/r_0)\log(a_0/r_0) + [1-(a_0/r_0)^2]/(a_0/r_0)}{r_0[\log(a_0/r_0)]^2}\left(\frac{r_0}{r_1}\right)^2 - \frac{\xi}{a_0[\log(a_0/r_0)]^2} = 0 \quad (2.3.19)$$

$$\frac{\partial \Phi}{\partial a_1} \equiv \frac{1}{3}\frac{2(a_1/r_1)\log(a_1/r_1) - [1-(a_1/r_1)^2]/(a_1/r_1)}{r_1[\log(a_1/r_1)]^2} + \frac{\xi}{a_1[\log(a_1/r_1)]^2} = 0 \quad (2.3.20)$$

Eliminating ξ from these equations, one obtains

$$\left.\begin{aligned} &\left[\left(\frac{a_0}{r_0}\right)^2\left\{\log\left(\frac{a_0}{r_0}\right)^2 - 1\right\} - 1\right]\left(\frac{r_0}{r_1}\right)^2 = \left(\frac{a_1}{r_1}\right)^2\left\{\log\left(\frac{a_1}{r_1}\right)^2 - 1\right\} + 1 \\ \text{or}\quad &\left[\left(\frac{R_{a0}}{R_0}\right)^2\left\{\log\left(\frac{R_{a0}}{R_0}\right)^2 - 1\right\}\right]R_0^2 = R_{a_1}^2\left\{\log R_{a_1}^2 - 1\right\} + 1 \end{aligned}\right\} \quad (2.3.21)$$

This gives the optimum relation between the radial positions of the slits.

This is drawn by the chain line (AB) in Fig. 2.3.2 on which the sets of curves of F_w =constant and F_Q= constant contact tangentially with each other.

In Fig. 2.3.2, the straight line CD means that $a_o = a_i$ or two slits approach each other and make a single slit-supply. Then cross point B is a limit of design of double slit-supply because the point B is on the curve AB, which shows the optimum relation between two slits positions, and also on this line CD. In the other hand, the minimum flow rate can be obtained on the point M according to the analysis of single slit-supply bearing. The radial position a_M locates inner than a_B which corresponds to the point B. Hence, one should design the slit-supply bearing with the dimensions on the line A-B-M. (B-M corresponds to the single slit-supply bearing).

a_B can be calculated by substituting $a_o = a_i = a_B$ into Eq. (2.3.21) resulting

$$\frac{a_B}{r_i} = \sqrt{\frac{1-(r_o/r_i)^2}{2\log(r_i/r_o)}} \qquad (2.3.22)$$

or

$$R_{aB} = \sqrt{\frac{R_o^2 - 1}{2\log R_o}} \qquad (2.3.22)'$$

Fig. 2.3.3 illustrates the optimum relations between $a_i/r_i\,(=R_{a_i})$ and $a_o/r_i\,(=R_a)$ with parameter $r_o/r_i\,(=R_o)$, in which the chain line shows the limit case to the single slit-supply.

Fig. 2.3.4 shows F_w and F_Q with parameter r_o/r_i, in which a_o/r_i takes the value calculated in Fig. 2.3.3.

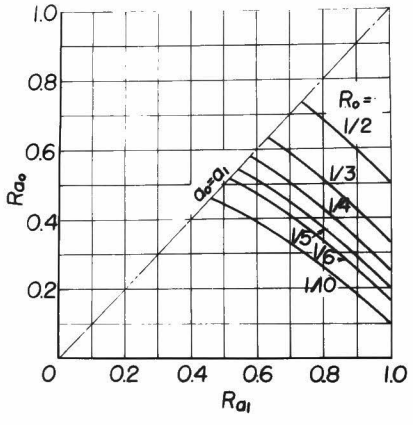

Fig. 2.3.3 Optimum positions of slit-supplies

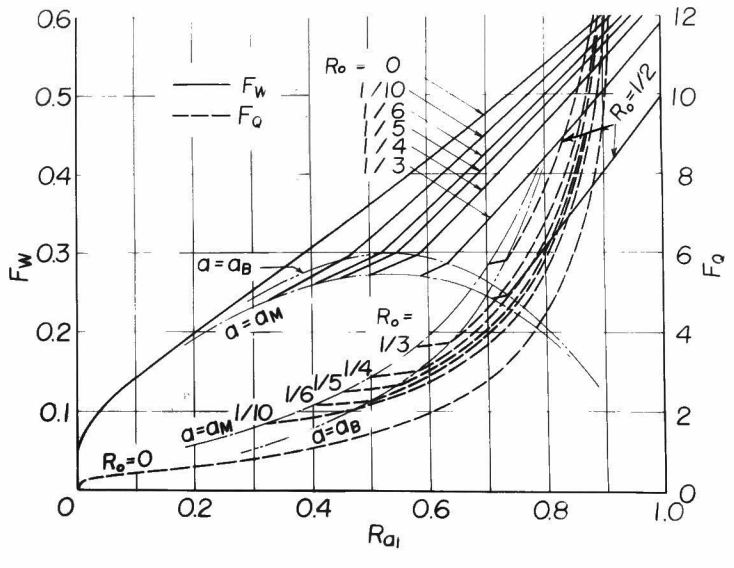

Fig. 2.3.4. Bearing characteristics with double slit-supplies (with optimum radial positions of slits)

The double-dotted lines are for the case of limiting single slit-supply (B), and the results of the single slit-supply case of Chapter 2 are added for inner region than this point ($a_M < a < a_B$).

Then the followings are concluded concerning the design of the double slit-supply bearing.

(i) In order to get the maximum bearing stiffness, the pressure just after the slits satisfies Eq. (2.3.6), and then the bearing should be designed as Eq. (2.3.12) and (2.3.13) are satisfied.

(ii) Both of the load capacity and the volume rate of flow increase as the slits position become nearer to the bearing peripheries. Then the bearing should be designed with considering the working condition of these bearing factors.

(iii) To maximize the load capacity under a constant flow rate, slits positions should be determined by Eq. (2.3.21) or Fig. 2.3.3.

(iv) Eq. (2.3.22) or Eq. (2.3.22)' shows the limiting case of the double slit-supply to the single one. In order to lessen the flow rate than this case, the single slit-supply bearing must be used.

(v) In the above analysis, the pressure is constant to be p_o in region II, which means that the results of it can be applied to the single slit-supply bearing with an annular recess by substituting $a_o = r_{p_o}$ and $a_1 = r_{p_1}$ where r_{p_o} and r_{p_1} are the radii to the inner and outer edges of the annular recess respectively.

Chapter 4 Experimental Investigations

Experiments are made to investigate the foregoing theory for the fundamental single slit-supply case concerning the pressure distribution, load capacity and volume rate of flow by using the compressed air as the fluid.

(a) Pressure Distribution

The pressure distributions in the bearing clearance are investigated experimentally by using the same experimental apparatus (I) as in Chapter 3-7 in Part I.

Configurations of the employed slit-supply thrust collar bearings are shown in Fig. 2.4.1. In these experiments, pressure distribution is measured to compare with theoretical one assuming that the bearing stiffness is considered to be secondary so that the restriction by the slit need not be taken into account.

Fig. 2.4.2 are the experimental results of the

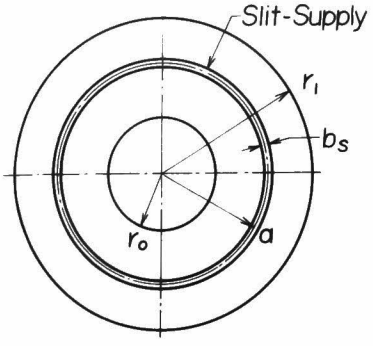

No.	$2r_i$ (mm)	$2r_o$ (mm)	$2a$ (mm)	b_s (mm)
1	90	30	60	1.5
2	90	30	50	1.5
3	90	30	70	1.5
4	60	30	45	1 5

Fig. 2.4.1 Bearings employed in experiments

thrust collar bearing with slit supply with various bearing parameters such as supply pressure, bearing clearance, radial position of slit-supply and ratio of inner and outer bearing radii, respectively. In these figures, the thick lines are theoretical ones calculated with polytropic index n=1.0 (isothermal condition) by using Eqs. (2.3.1)'-(2.3.3)' which are for the double slit-supply case, substituting a_o to be inner radius of slit, and a_i to be outer one. This is because the width of slit is fairly large to be neglected compared with the other bearing dimensions.

The experimental results conform very well with theoretical ones even for comparatively large bearing

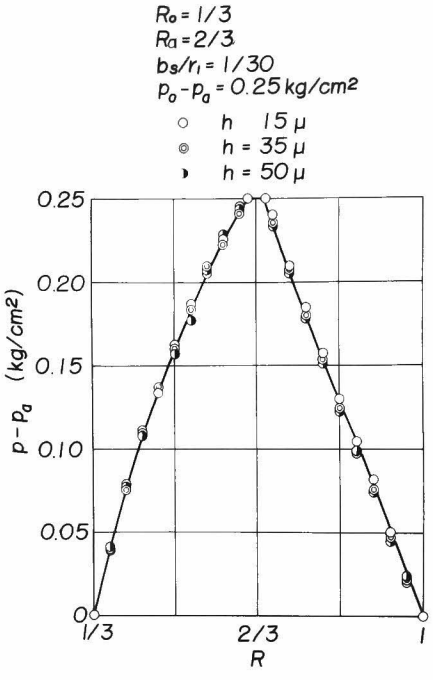

(a)

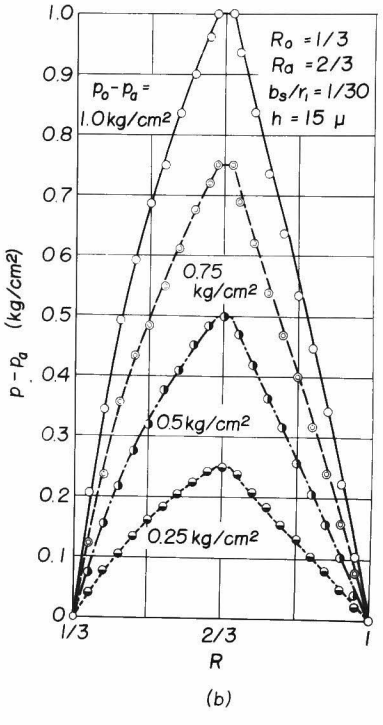

(b)

Fig. 2.4.2 Results of pressure distributions

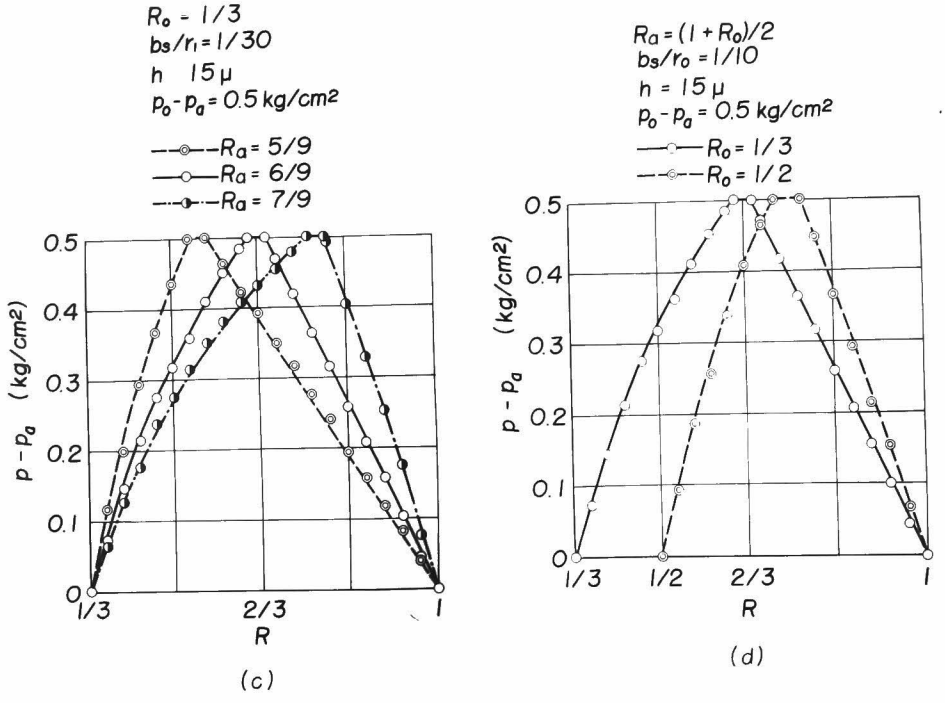

Fig. 2.4.2

clearance and high supply pressure. For the bearing of this type, the lubricant is supplied through a slit into bearing clearance, hence the flow of it just after the slit supply is such as one-dimensional flow between two parallel surfaces rather than a radial flow such as from a point

supply hole. Then, less energy is needed for acceleration of the lubricant after the slit supply, which means the pressure loss is comparatively small even at a large volume rate of flow. These effect is discussed later concerning load capacity.

(b) Load Capacity

Load capacity is experimented by using apparatus II for the same bearings as shown above.

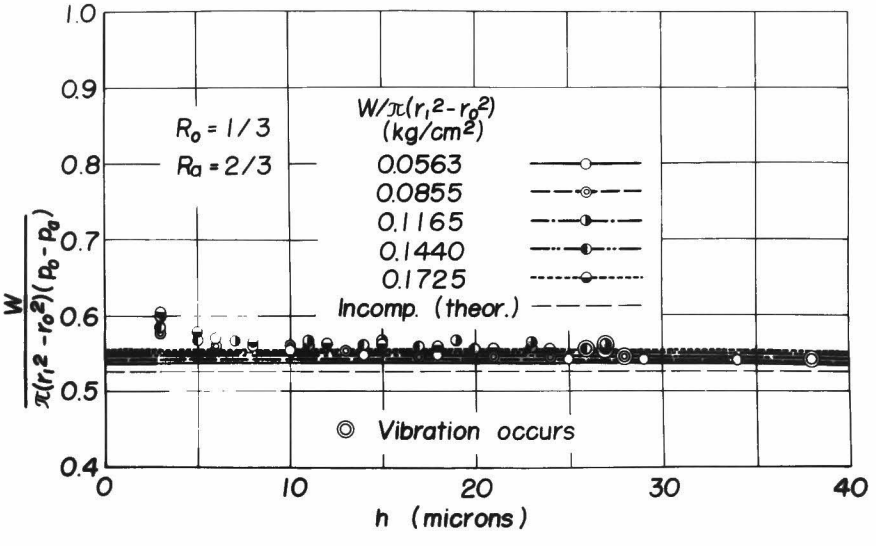

Fig. 2.4.3 Typical results of load capacity

Fig. 2.4.3 is an experimental result for bearing No.1, in which the incompressible theoretical line is drawn by a thin line. The dimensionless load capacity $W/\pi(r_i^2-r_a^2)(p_o-p_a)$ of experimental data is almost independent on the bearing

clearance h, which means that the pressure fall at the slit-supply is not effective. But, the load capacity increases with increase of specific load $W/\pi(r_i^2 - r_o^2)$ (or supply pressure) because of the effect of compressibility of fluid.

The load capacity considering the effect of compressibility can be given by the following approximation for the thrust gas-bearing with slit-supply:

$$W_{comp.} \cong \frac{\sqrt{(p_o + p_a)(p_w - p_a) + p_a^2} - p_a}{p_w - p_a} \times W_{incomp.} \qquad (2.4.1)$$

where W_{comp}: load capacity with compressible fluid

$W_{incomp.}$: load capacity with incompressible fluid

p_w : specific load $W/\pi(r_i^2 - r_o^2)$

This equation is reduced and studied in detail in Appendix XIII.

When the pressure fall at supply hole is taken into account, p_o in the above relation must be substituted by p_o'' where p_o'' is the modified pressure just after supply hole as mentioned in the below.

The thick curves in the figures are theoretical ones considering of both effects of this and pressure fall at slit supply;

$$p_o - p_o'' = \lambda \frac{1}{2} \rho_o u_m^2$$

$$= \lambda \frac{1}{2} \rho_0 \left(\frac{Q_0}{4\pi a R} \right)^2 \qquad (2.4.2)$$

where Q_0 is volume rate of flow corresponding to pressure p_0''.

They coincide very well with each other as shown, which verify the foregoing theory and presumptions of secondary effects for this type of bearing.

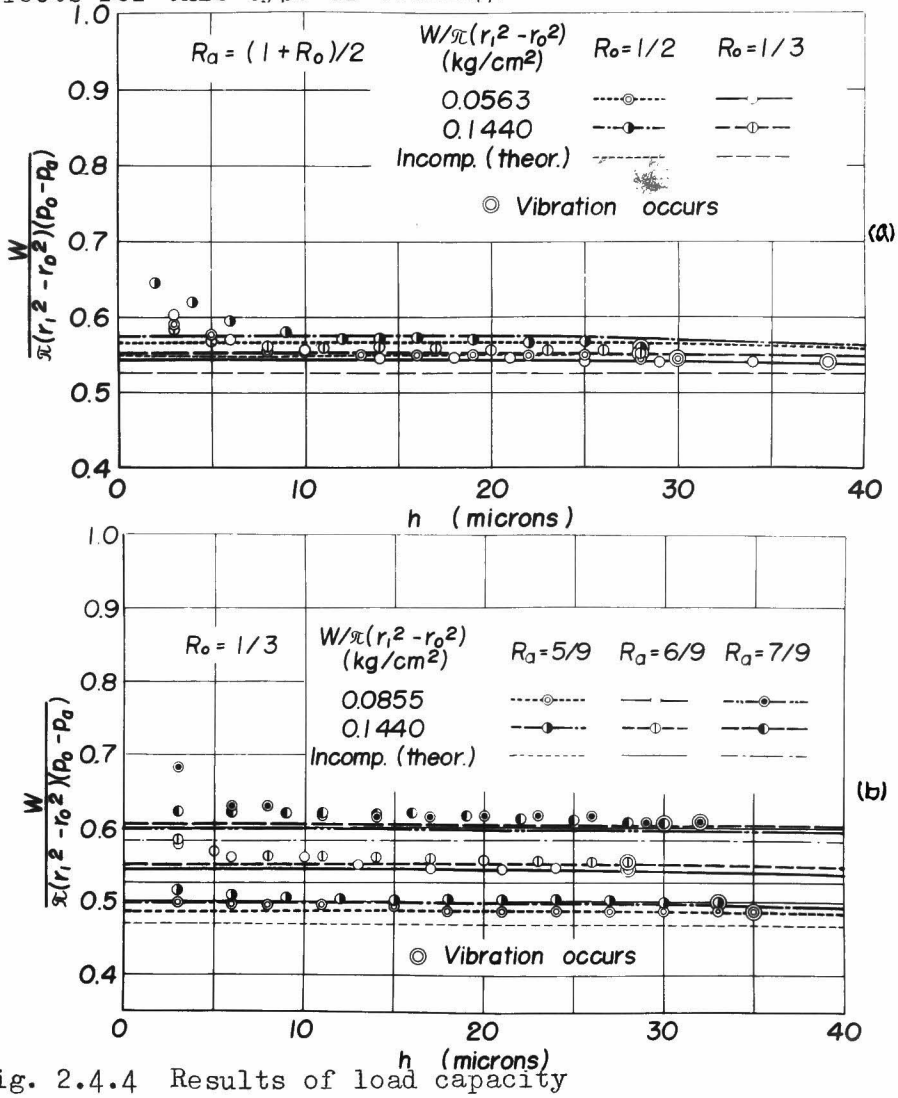

Fig. 2.4.4 Results of load capacity

Fig. 2.3.4 is the experimental results of load capacity for other bearing dimensions such as various slit positions and ratios of inner and outer bearing radii. The theoretical ones are shown by the thick lines which are calculated with consideration of the secondary effects mensioned above.

The results have quite the same property as observed in Fig. 2.3.3. The vibrations are observed for all bearings of this type when the bearing clearance increases more than about 30 microns. The slit for supply may serve as a recess because it is comparatively wide so that the bearing vibrations may be caused.

(c) Volume Rate of Flow

The volume rate of flow is investigated experimentally by using the experimental apparatus I with fixed bearing clearance.

Several bearings are employed with various bearing configurations such as with various values of R_a or R_o.

Fig. 2.4.5 is the experimental results in which theoretical curves are shown in thick line. The volume rate of flow is arranged in the form of $Q \Big/ \frac{p_o^2 - p_a^2}{2p_a}$ against the bearing clearance h, because this is independent theoretically on the values of p_o or p_a.

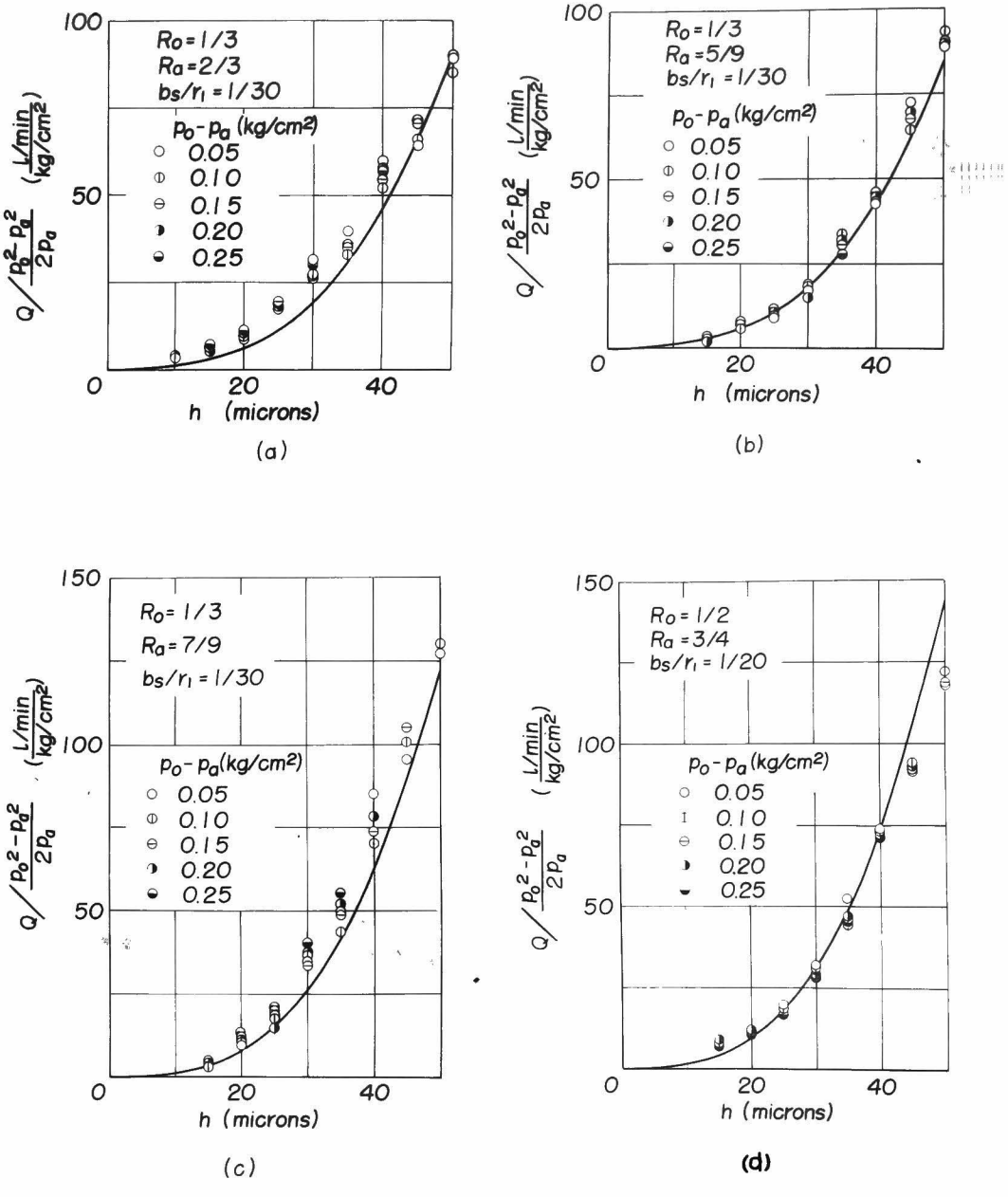

Fig. 2.4.5 Results of volume rate of flow

A good conformity is shown between the experimental results and theoretical ones, which may justify the results of theory very well.

Pressure fall at supply slit is also taken into account but this effect is very small so that the deviation by it may be negligible.

Chapter 5 Conclusion

The externally pressurized thrust collar bearing with single or double slit-supply is analyzed. In both cases of the bearing types, considering the flow as that of two-dimensional one between the parallel surfaces, the pressure distribution is obtained theoretically, and then, the load capacity and volume rate of flow as well from the integration and gradient of it. The condition to maximize the bearing stiffness is applied to yield the optimum dimensions of the supply-slits. The design charts of the bearing with slit supply can be obtained from these theoretical values of bearing characteristics.

Results of experiments agree very well with theoretical ones concerning the pressure distribution, volume rate of flow and load capacity, taking into account the effect of compressibility of fluid. For this type of bearing, the pressure fall after slit-supply seems to be

negligible even for considerably high supply pressure and large bearing clearance, which is because the flow is such that (one-dimensional flow between two parallel plates, rather than a radial) flow from a point supply source which means less energy is needed for the acceleration of the flow.

Part III Analysis of Externally Pressurized Porous Gas-Bearings

Chapter 1 Introduction

Externally pressurized thrust gas-bearings are very advantageous owing to their small static and dynamic friction, and their load capacity can be increased by making a proper recess on the bearing surface. The recess, however, is apt to make the operation less stable because of self-excited vibration(4). If the bearings have a relatively smaller gas-supply hole without recess against high supply pressure or large bearing clearance, the pressure depression takes place in pressure distribution of the bearings and lessens their load capacity greatly.(3) These disadvantages have called forth the recent researches on the externally pressurized thrust porous gas-bearing through which the gas is supplied over the entire bearing surface. The porous bearing can be assumed to consist of a mesh structure incorporating innumerable tubes which serve to restrict gas flow and absorb vibration.

Such a type of externally pressurized porous gas-bearing so far has not been analyzed theoretically, except for some reports in U.S.S.R.,(5) in spite of its application to a number of practical devices. Even in these studies,

analysis were considered only the normal gas flow to the bearing surface in the porous bearing.

In this Part, the externally pressurized porous gas-bearing are analyzed theoretically, considering both axial and radial gas flows in porous bearing with the following assumptions.

When the compressibility of fluid is taken into account, the load capacity cannot be obtained analytically and the calculation of pressure distribution becomes complicated, so the assumption of incompressibility of fluid is applied as mentioned later for the first step of the research on this bearing. The pressure distribution and the load capacity are obtained theoretically and they were compared with the experimental results.

Assumptions

The assumptions made for the analysis are as follows: (1) Porous media are homogeneous with permeability coefficient k. Coefficient k is defined by Darcy's law concerning the flow in porous media as:

$$w = -\frac{k}{\mu}\cdot\frac{\partial p}{\partial z}, \qquad u = -\frac{k}{\mu}\cdot\frac{\partial p}{\partial r} \tag{3.1.1}$$

where u, w : flow velocity in r or z direction

p : pressure

μ : coefficient of viscosity

(2) Porous material can be substituted by an assumed thin layer with so-called equivalent clearance h' so that the characteristics of flow through it can be equivalent to that through the porous material concerning the quantity of flow.

If the quantity of flow parallel to the bearing surface through the porous bearing is equal to that of the flow through the assumed clearance h', h' is to be called the equivalent clearance, thereby

$$h' = \sqrt[3]{12kt} \qquad (3.1.2)$$

t : actual thickness of the porous bearing

(3) The flow of fluid in the porous material consists of two components: one is parallel to the bearing surface and the other vertical to it.

(4) The bearing clearance h and the equivalent clearance h' are so thin that pressure does not change normally in each clearance. But the pressure p in the bearing clearance differs from the pressure p' in porous material.

(5) The flows from porous bearing into bearing clearance and from supply port to porous bearing is proportional to

the pressure difference $(p' - p)$ and $(p_s - p')$, respectively, and permeability coefficient k, and is inversely proportional to t, which is the actual thickness of porous bearing. The assumption is applied as an extension of Darcy's law.

(6) There is no parallel flow on the very surface of bearing.

(7) The fluid is incompressible. This assumption may be appropriate for the flow through the porous media and the bearing clearance with low pressure. When compressibility of the fluid must be taken into consideration, one can obtain the pressure distribution by the following substitution in which absolute pressure P gives the solution for the case of incompressible fluid.(1)

$$P = p^{\frac{1+n}{n}} \qquad (3.1.3)$$

where n is the polytropic index.

(8) The rotating speed of the bearing is so small compared with the gas flow velocity due to the pressure gradient that the static condition can be applied. This static condition may be essential for the study of the externally pressurized gas bearing.

Chapter 2 Analysis of Externally Pressurized Circular Thrust Porous Gas-Bearing

2-1 Theoretical Analysis

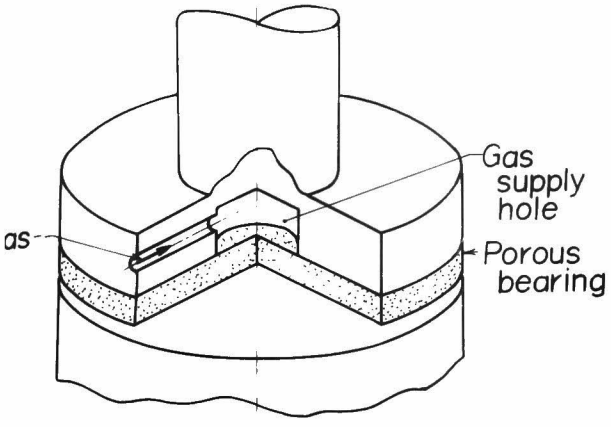

Fig. 3.2.1 Construction of externally pressurized circular thrust porous gas-bearing

Fig. 3.2.1 illustrates the construction of the externally pressurized circular thrust porous gas-bearing to be analyzed. The compressed gas is fed into the gas supply hole and after being restricted through the porous bearing, the gas flows out into the bearing clearance in radial direction. Some part of the gas also flows through the porous bearing in radial direction. Fig. 3.2.2 is the schematic diagram of this bearing.

The average velocities of flow in r-direction in the bearing clearance and the porous bearing are, respectively, as follows:

$$\bar{u} = -\frac{h^2}{12\mu}\cdot\frac{dp}{dr} \tag{3.2.1}$$

$$\bar{u}' = -\frac{k}{\mu}\cdot\frac{dp'}{dr} = -\frac{h'^3}{12\mu t}\cdot\frac{dp'}{dr} \tag{3.2.2}$$

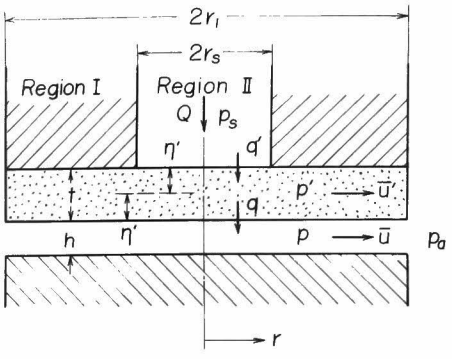

Fig. 3.2.2 Schematic diagram of the bearing

The continuity conditions are

$$2\pi r h \bar{u} = \int_0^r q \cdot 2\pi r\, dr \tag{3.2.3}$$

$$2\pi r t \bar{u}' = Q - \int_0^r q \cdot 2\pi r\, dr \qquad (r_s \leqq r \leqq r_1) \tag{3.2.4}$$

$$= \int_0^r q' \cdot 2\pi r\, dr - \int_0^r q \cdot 2\pi r\, dr \qquad (0 \leqq r \leqq r_s) \tag{3.2.4}'$$

where Q is the volume rate of flow, and q and q' are the velocities of the flow-out from and flow-in to the porous bearing respectively. q and q' are given by the following equations according to the assumption (5).

$$q = \frac{k}{\mu} \cdot \frac{p' - p}{\eta} = \frac{h'^3}{12\mu\eta t}(p' - p) \tag{3.2.5}$$

$$q' = \frac{k}{\mu} \cdot \frac{p_s - p'}{\eta'} = \frac{h'^3}{12\mu\eta' t}(p_s - p') \tag{3.2.6}$$

where η and η' are the effective restricting thickness, and are given by:

$$\eta = ct \qquad \eta' = c't \tag{3.2.7}$$

c and c' should be determined experimentally but they are presumed to be approximately

$$c = c' \cong \frac{1}{2} \tag{3.2.8}$$

Eliminating $\bar{u}$ and q from Eqs. (3.2.1), (3.2.3) and (3.2.5), and differentiating it by r, one obtains

$$\frac{1}{r}\frac{d}{dr}\left(r\frac{dp}{dr}\right) = -\frac{h'^3}{h^3\eta t}(p' - p) \tag{3.2.9}$$

(a) Region I ($r_s \leqq r \leqq r_e$)

From Eqs. (3.2.3) and (3.2.4)

$$2\pi r(h\bar{u} + t\bar{u}') = Q \tag{3.2.10}$$

Eliminating $\bar{u}$ and $\bar{u}'$ by substitution of Eqs. (3.2.1) and (3.2.2) into Eq. (3.2.10), and integrating it with r, one obtains

$$\left.\begin{aligned} h^3 p + h'^3 p' &= C_1 - \frac{6\mu Q}{\pi}\log r \\ p' &= \frac{1}{h'^3}\left(C_1 - \frac{6\mu Q}{\pi}\log r - h^3 p\right) \end{aligned}\right\} \tag{3.2.11}$$

where C_1 is the constant of integration.

In Eq. (3.2.11), p and p' should satisfy the following boundary condition

$$p = p' = p_a \qquad \text{at} \qquad r = r_1 \tag{3.2.12}$$

Then,

$$C_1 = \frac{6\mu Q}{\pi} \log r_1 + (h^3 + h'^3) p_a \tag{3.2.13}$$

Substituting Eq. (3.2.11) into Eq. (3.2.9)

$$\frac{1}{r} \cdot \frac{d}{dr}\left(r \frac{dp}{dr}\right) = \frac{1}{h^3 \eta t}\left\{(h^3 + h'^3)p + \frac{6\mu Q}{\pi} \log r - C_1\right\} \tag{3.2.14}$$

This equation can be expressed as

$$\frac{1}{r} \cdot \frac{d}{dr}\left(r \frac{dp}{dr}\right) - \alpha_0^2 p = B \log r + C \tag{3.2.16}$$

where

$$\alpha_0 = \sqrt{\frac{h^3 + h'^3}{h^3 \eta t}} \qquad B = \frac{6\mu Q}{\pi h^3 \eta t} \qquad C = \frac{C_1}{h^3 \eta t}$$

The solution of Eq. (3.2.15) is given by

$$p = E I_0(\alpha_0 r) + F K_0(\alpha_0 r) - \frac{6\mu Q}{\pi (h^3 + h'^3)} \log r + \frac{C_1}{h^3 + h'^3} \tag{3.2.16}$$

where I_0 and K_0 are the modified Bessel functions of the first and the second kinds respectively, and E and F are the arbitrary constants which should be determined by boundary conditions.

Substituting Eqs. (3.2.13) and (3.2.16) into Eq. (3.2.11), the pressure distributions p and p' in the region I are obtained as follows.

$$p_I = EI_o(\alpha_o r) + FK_o(\alpha_o r) + \frac{6\mu Q}{\pi(R^3 + R'^3)} \log \frac{r_i}{r} + p_a \qquad (3.2.17)$$

$$p_I' = -\frac{R^3}{R'^3}\left[EI_o(\alpha_o r) + FK_o(\alpha_o r)\right] + \frac{6\mu Q}{\pi(R^3 + R'^3)} \log \frac{r_i}{r} + p_a \qquad (3.2.18)$$

(b) Region II $(0 \leq r \leq r_s)$

From Eqs. (3.2.3) and (3.2.4)',

$$2\pi r(h\bar{u} + t\bar{u}') = \int_0^r g' \cdot 2\pi r\, dr \qquad (3.2.19)$$

Eliminating $\bar{u}$, $\bar{u}'$ and p' from Eqs. (3.2.1), (3.2.2), (3.2.6) and (3.2.19), and differentiating it by r, one obtains,

$$\frac{d^2p}{dr^2} + \frac{1}{r}\frac{dp'}{dr} - \frac{1}{\eta t}(p' - p) + \frac{1}{\eta' t}(p_s - p') = 0 \qquad (3.2.20)$$

Eqs. (3.2.9) and (3.2.20) can be rewritten as follows.

$$\left.\begin{aligned} \frac{1}{r}\frac{d}{dr}\left(r\frac{dp'}{dr}\right) &= A'^2 p' - B'^2 p - C' \\ \frac{1}{r}\frac{d}{dr}\left(r\frac{dp}{dr}\right) &= D'^2(p - p') \end{aligned}\right\} \qquad (3.2.21)$$

where

$$A'^2 = \frac{1}{\eta' t} + \frac{1}{\eta t} \qquad B'^2 = \frac{1}{\eta t} \qquad C' = \frac{p_s}{\eta' t} \qquad D'^2 = \frac{R'^3}{R^3 \eta t}$$

The solution of Eqs. (3.2.21) are

$$p = M_1 I_o(\alpha_1 r) + M_2 I_o(\alpha_2 r) + M_3 K_o(\alpha_1 r) + M_4 K_o(\alpha_2 r) + p_s \qquad (3.2.22)$$

$$p' = N_1 I_o(\alpha_1 r) + N_2 I_o(\alpha_2 r) + N_3 K_o(\alpha_1 r) + N_4 K_o(\alpha_2 r) + p_s \qquad (3.2.23)$$

where

$$\alpha_i = \sqrt{\frac{A'^2 - D'^2 \pm \sqrt{(A'^2 - D'^2)^2 + 4(B'^2 - A'^2)D'^2}}{2}} \qquad (3.2.24)$$

The signs in the right-hand side of Eq. (3.2.24) are to be taken as follows

\+ for subscript $i = 1$

\- for subscript $i = 2$

M_j and N_j ($j = 1, 2, 3, 4$) are constants of integration and they should satisfy the following relation;

$$\frac{M_j}{N_j} = \frac{A'^2 - \alpha_i^2}{B'^2} \qquad (3.2.25)$$

where $j = 1$ or 3 when $i = 1$, and $j = 2$ or 4 when $i = 2$. These deductions are shown in Appendix XIV.

Using the following boundary condition

$$\frac{dp}{dr} = \frac{dp'}{dr} = 0 \qquad \text{at} \qquad r = 0 \qquad (3.2.26)$$

then

$$N_3 = N_4 = M_3 = M_4 = 0 \qquad (3.2.27)$$

The pressure distributions in the region II are obtained as follows.

$$p_{II} = M_1 I_0(\alpha_1 r) + M_2 I_0(\alpha_2 r) + p_s \qquad (3.2.28)$$

$$p'_{II} = N_1 I_0(\alpha_1 r) + N_2 I_0(\alpha_2 r) + p_s \qquad (3.2.29)$$

The volume rate of flow is

$$\left.\begin{aligned} Q &= \int_0^{r_s} q' \cdot 2\pi r\,dr = \int_0^{r_s} \frac{h'^3}{12\mu\eta' t} \cdot 2\pi r (p_s - p')\,dr \\ &= -\frac{h^3}{6\mu\eta' t}\left\{\frac{N_1 r_s}{\alpha_1} I_1(\alpha_1 r_s) + \frac{N_2 r_s}{\alpha_2} I_1(\alpha_2 r_s)\right\} \end{aligned}\right\} \quad (3.2.30)$$

The boundary conditions to determine the constants N_1, N_2, (or M_1, M_2) E and F are:

$$\left.\begin{aligned} &\text{(i)} && p_I = p_I' = p_a && \text{at} && r = r_1 \\ &\text{(ii)} && p_I = p_{II} && \text{at} && r = r_s \\ &\text{(iii)} && p_I' = p_{II}' && \text{at} && r = r_s \\ &\text{(iv)} && \frac{dp_I}{dr} = \frac{dp_{II}}{dr} && \text{at} && r = r_s \\ &\text{(v)} && \frac{dp_I'}{dr} = \frac{dp_{II}'}{dr} && \text{at} && r = r_s \end{aligned}\right\} \quad (3.2.31)$$

Among them, conditions (iv) and (v) are not mutually independent, so the unknown constants are determined by the conditions (i), (ii), (iii), and (iv) or (v). The pressure distributions p and p' are given by putting these constants into Eqs. (3.2.17) and (3.2.18) and (3.2.28) and (3.2.29) in each region.

The load capacity for the case of an incompressible fluid is obtained by integrating the pressure in each area.

$$\left.\begin{aligned} W &= \int_0^{r_1} (p - p_a)\,2\pi r\,dr \\ &= \int_0^{r_s} \left\{M_1 I_0(\alpha_1 r) + M_2 I_0(\alpha_2 r) + (p_s - p_a)\right\} 2\pi r\,dr \\ &\quad + \int_{r_s}^{r_1} \left\{E I_0(\alpha_0 r) + F K_0(\alpha_0 r) + \frac{6\mu Q}{\pi(h^3 + h'^3)} \log\frac{r_1}{r}\right\} 2\pi r\,dr \end{aligned}\right|$$

$$= 2\pi r_s \left\{ \frac{M_1}{\alpha_1} I_1(\alpha_1 r_s) + \frac{M_2}{\alpha_2} I_0(\alpha_2 r_s) \right\} + \pi r_s^2 (p_s - p_a)$$

$$+ \frac{2\pi E}{\alpha_0} \left\{ r_i I_1(\alpha_0 r_i) - r_s I_1(\alpha_0 r_s) \right\} - \frac{2\pi F}{\alpha_0} \left\{ r_i K_1(\alpha_0 r_i) - r_s K_1(\alpha_0 r_s) \right\} \qquad (3.2.32)$$

$$+ \frac{12\mu Q}{h^3 + h'^3} \left\{ \frac{r_i^2}{4} - \frac{r_s^2}{2} \log \frac{r_i}{r_s} - \frac{r_s^2}{4} \right\}$$

Since it is difficult to obtain analytically the load capacity with considering the compressibility, the load capacity obtained by Eq. (3.2.32), which is approximate for compressible fluid, will be used to compare with experimental results.

2-2 Permeability Coefficient of the Porous Material

It has been reported that the permeability coefficient of porous media is not constant as the authors assumed in the analysis above.

Gross[6] describes in his book that Robinson and Sterry[7] observed that the permeability coefficient is a function of both bearing clearance pressure and Reynolds number. Fig. 3.2.3 illustrates this variation after them.

Because of this variability, the permeability coefficient to be used for the calculation in the above analysis, should be determined based on the conditions of pressure, Reynolds number, etc. under which bearing will actually

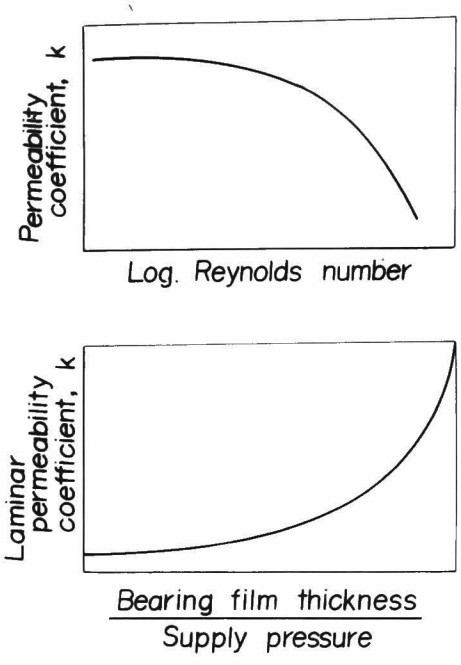

Fig. 3.2.3 Variation of permeability coefficient (after Robinson and Sterry(7))

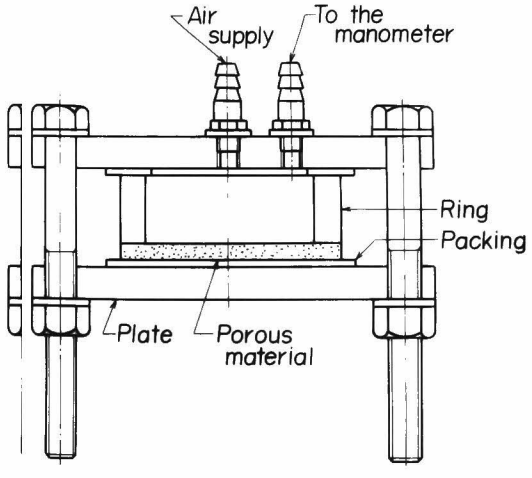

Fig. 3.2.4 Apparatus for measuring the permeability coefficient

work.

Fig. 3.2.4 shows the apparatus for measuring the permeability. The compressed gas is supplied into the space formed with the porous material and the side wall as shown in illustration. The undersurface of the porous material is covered with the packing of synthetic elastic sheet so that the gas is forced to flow through the porous material in the radial direction.

The permeability coefficient can be calculated from the pressure in the space and the volume rate of flow. In this case, the volume rate of flow can be obtained by considering the bearing clearance h to be zero in the above analysis, so that the following equation is obtained

$$k = \frac{\left\{1 + \frac{1}{\eta' t} \cdot \frac{r_s}{\alpha} \cdot \frac{I_1(\alpha r_s)}{I_0(\alpha r_s)} \cdot \log \frac{r_i}{r_s}\right\} Q}{\frac{2\pi}{\mu \eta'} \cdot \frac{r_s}{\alpha} \cdot \frac{I_1(\alpha r_s)}{I_0(\alpha r_s)} (p_s - p_a)} \qquad (3.2.33)$$

where

$$\alpha = \frac{1}{\sqrt{\eta' t}}$$

Fig. 3.2.5 shows a few examples of the permeability coefficient determined for some porous materials by this method.

2-3 Comparison with the Experimental Results

The dimensions of the bearing used for the experiments are as follows.

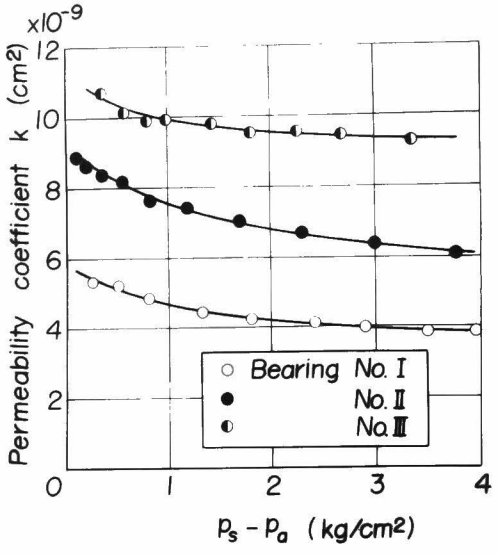

Fig. 3.2.5 Results of measurement of the permeability coefficient

Diameter of the bearing $2r_1 = 60.0$mm

Diameter of the gas supply hole $2r_s = 10.0$mm

Thickness of the porous bearing $t \cong 5.0$mm

The porous bearings employed are shown in Table 3.2.1 The surfaces of them should not be machined because minor maching causes non-homogenety on the porous surfaces so that their characteristics of flow may be varied. So the porous plates are made carefully to hold their flatness of the surfaces. The permeability coefficient is the average of the values shown in Fig. 3.2.5.

Table 3.2.1 Porous materials employed in experiments

Bearing no.	Material	Dia. of grain (microns)	Permeability coefficient (cm^2)	Equivalent clearance (microns)
I	Sintered powder brass	5	4.35×10^{-9}	30
II		10	7.09×10^{-9}	35
III		20	9.73×10^{-9}	39

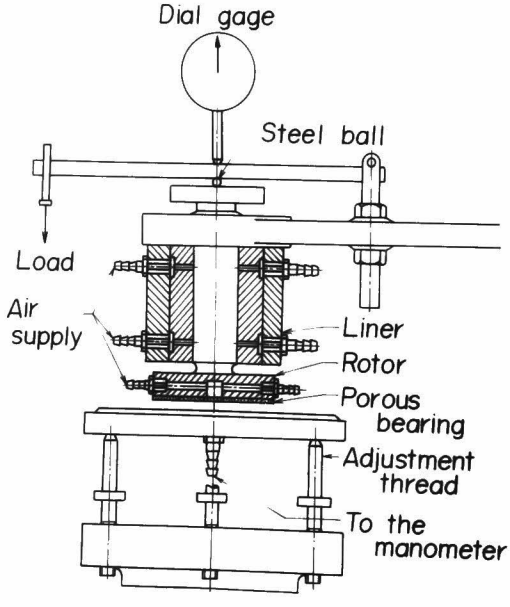

Fig. 3.2.6 Apparatus for measuring the pressure distribution

Fig. 3.2.6 shows the apparatus for measuring the pressure distribution and the load capacity. The rotor has a porous bearing of 60mm diameter on its undersurface through which air is supplied into the bearing clearance. The pressure in the bearing clearance is measured by U-tube mercury

manometer connected with the small hole of 0.2mm diameter drilled in the stator which can be slided to desired positions by operating a fine screw.

The rotor is guided in the liner by an externally pressurized journal air bearing in order to prevent their contact.

The load is put on the top of the rotor by the lever and the load weights.

The pressure p' in the porous material is not measured but the analysis is verified by comparing the pressure distribution p in the bearing clearance, though it would be better to investigate the pressure p'.

Now, let β be a parameter to be defined by

$$\beta = \frac{h'}{h} = \frac{\sqrt[3]{12kt}}{h} \qquad (3.2.34)$$

Then the pressure distribution and the load capacity are, for an incompressible fluid, identified by only the value of β, so that they do not depend directly upon h or h'. Fig. 3.2.7 shows the pressure distributions measured by keeping the value of β constant for some porous bearings. In this figure, the solid line is the theoretical curve for an incompressible fluid obtained for the case of $\eta = \eta' = 0.5t$.

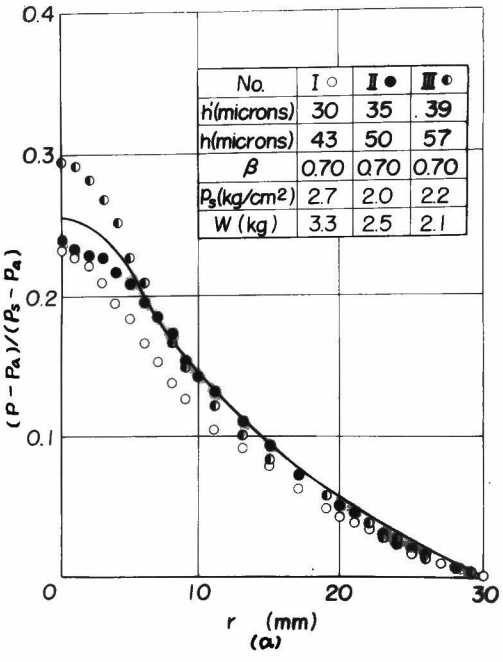

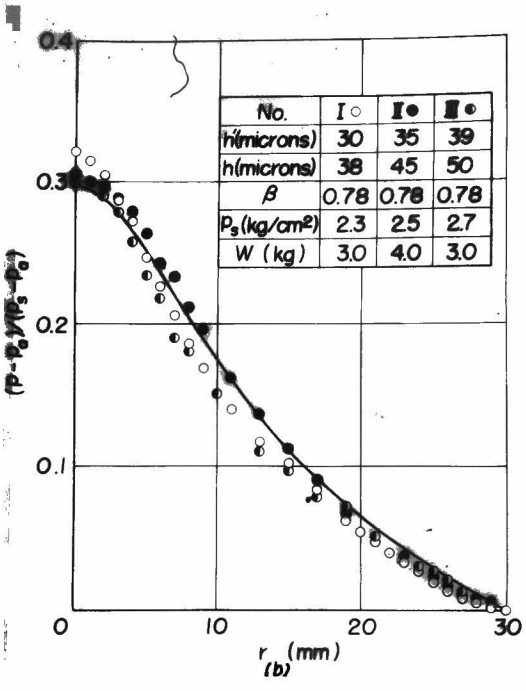

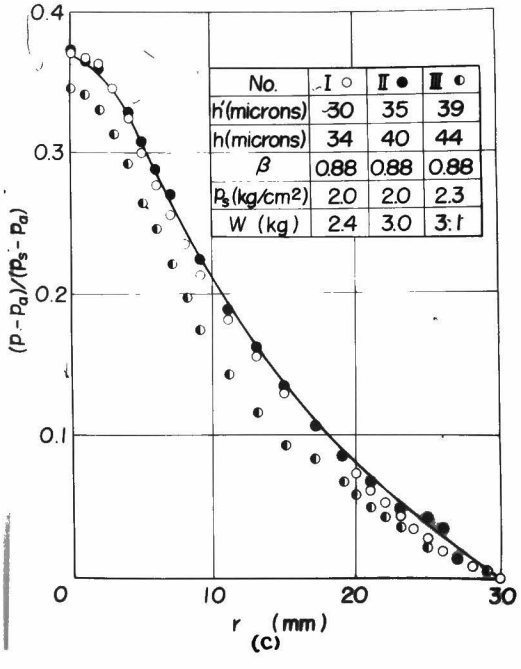

Fig. 3.2.7 Pressure distributions in the bearing clearance

The assumption of incompressibility of fluid is appropriate for the flow through the porous media and the bearing clearance under low supply pressure. When the compressibility of fluid is taken into account, the theoretical line varies with the values of supply pressure when ambient pressure is fixed. While the experimental data are put in order fairly well in the form of $(p-p_a)/(p_s-p_a)$ as shown in figures, which may certify the assumption within the range of supply pressures of the experiments.

The experimental results showed a good agreement with the theoretical values both qualitatively and quantitatively. When β takes smaller values, in case of Fig. 3.2.7 (a), for example, some difference is observed, which is considered to be due to the deviation of the effective restricting thicknesses (η and η') from 0.5t. This deviation may be caused by the variety of the permeability in it.

Fig. 3.2.8 shows the relation between the supply pressure and the air film thickness (bearing clearance) under the constant load. In this figure, the dotted line shows the limits against the vibration when the bearing encounters some disturbance. But in the experiments the bearing worked without any vibration when it was not disturbed. The values of the film thickness are measured statically before the

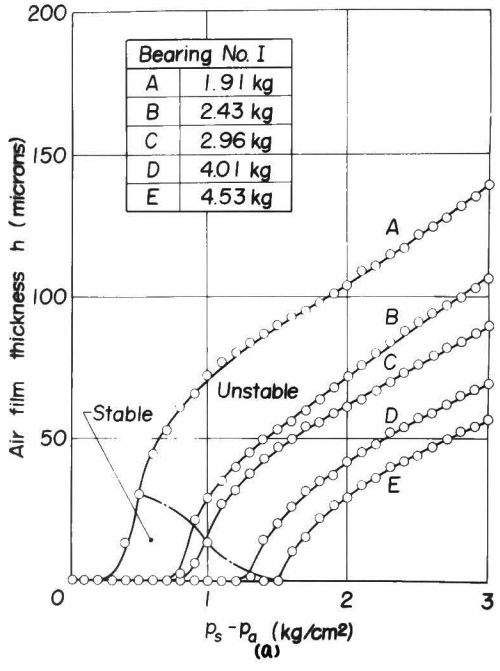

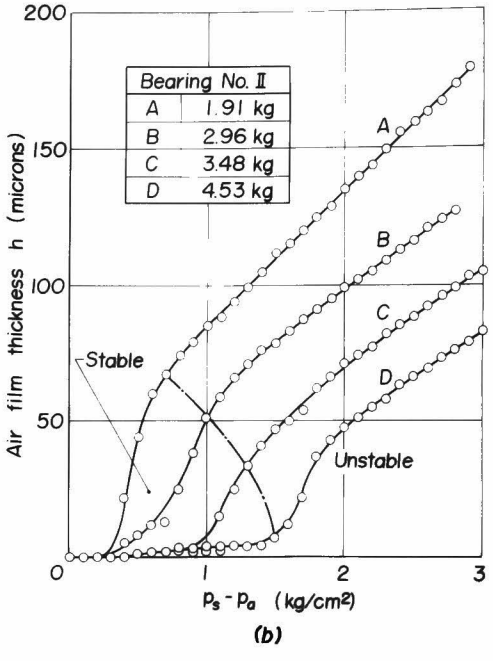

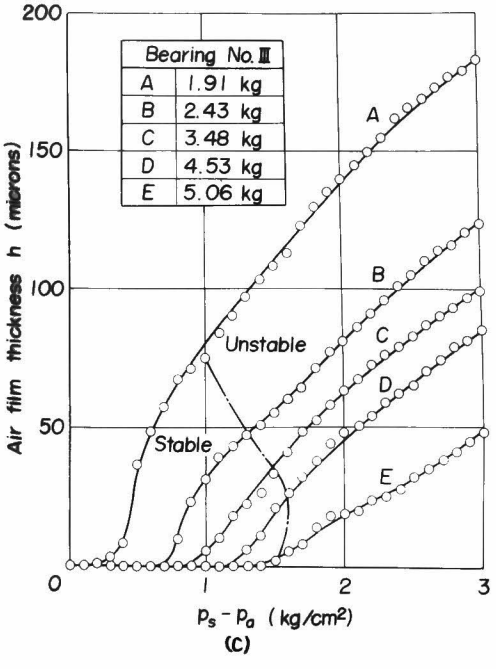

Fig. 3.2.8 Relation between supply pressure and bearing clearance under constant loads

bearing is disturbed. The stable working region extends with the increase of the permeability coefficient. Moreover it has been observed that the stable working region extends much when the diameter of gas supply hole is made larger though the effects of the diameter is not discussed here. The stable work of the porous bearing is considered to be due to its structure. Porous material can be assumed to consist of the meshy structure of innumerable tubes which serve to dissipate the energy of vibrations.

Fig. 3.2.9 shows the relation between the load and the air film thickness (bearing clearance) under the constant supply pressure.

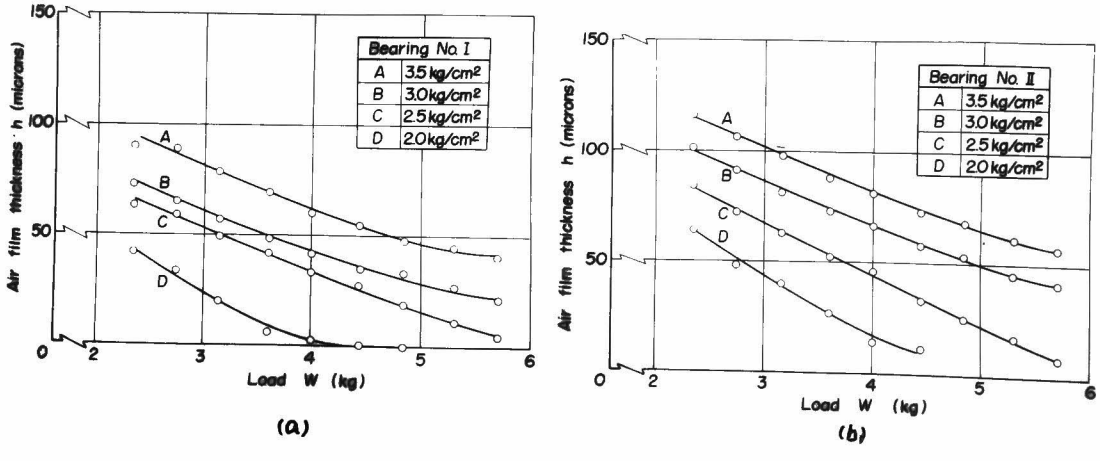

Fig. 3.2.9

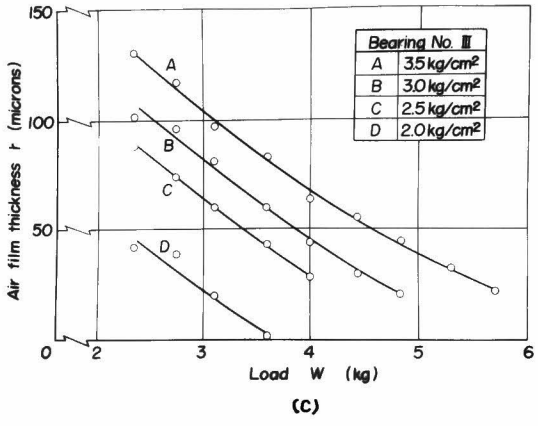

Fig. 3.2.9 Relation between load and bearing clearance under constant supply pressures

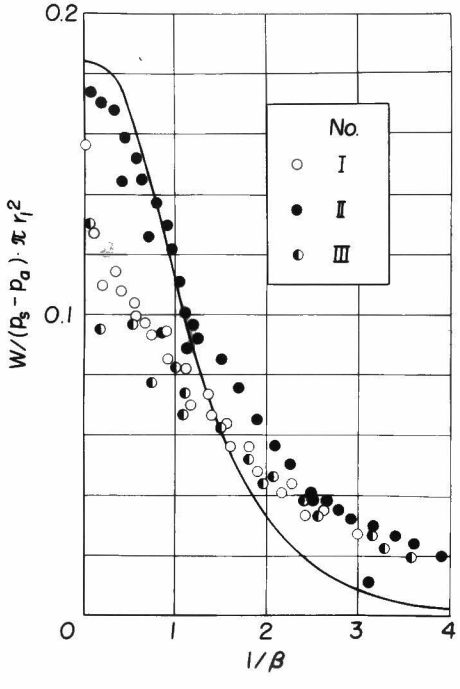

Fig. 3.2.10 Relation between load capacity and $1/\beta$

The load capacity is shown in Fig. 3.2.10 with respect to the value of $1/\beta$ which corresponds to the air film thickness. The solid line shows the theoretical curve obtained from Eq. (3.2.32). The experimental results coincide with the theoretical curve except when $1/\beta$ is so very large or small. The variability of the effective restricting thickness is considered to cause these differences.

2-4 Boundary conditions at the Periphery of Porous Bearing

In the above sections such a porous thrust gas-bearing is analyzed that the gas flows out from the bearing clearance and also from the periphery of the porous bearing, because of the simplicity of the theoretical calculation. For the practical usage of this bearing, however, it is naturally desirable that the bearing needs less rate of compressed gas-flow. This leads to the idea to close the outer periphery of the porous bearing so that the pressurized gas may be kept in the bearing clearance without escaping from porous edge.

Theoretical analysis for this closed-edge type of porous circular thrust bearing is mentioned in this section.

The pressure in the bearing is obviously governed also in this case by the same equations (3.2.1)-(3.2.6) yielding the pressure distributions of Eqs. (3.2.16) and (3.2.11),

and Eqs. (3.2.28) and (3.2.29) in Region I and II, respectively.

But the boundary condition to determine the value of C_1 in these equations should be as follows instead of condition (3.2.12); namely

$$p = p_a \qquad at \qquad r = r_1 \tag{3.2.35}$$

and

$$\int_0^{r_1} q \cdot 2\pi r\, dr = Q \tag{3.2.36}$$

By using Eq. (3.2.4), Eq. (3.2.36) becomes

$$\left(\frac{dp'}{dr}\right)_{r=r_1} = 0 \tag{3.2.36}'$$

Then the unknown constants N_1, N_2, E, F, and C_1 must be determined by the conditions of (3.2.35) and (3.2.36)' instead of codition (3.2.31)-(i).

The load capacity and volume rate of flow can be obtained easily by the same reductions as used for Eq. (3.2.32) and Eq. (3.2.30), respectively.

Fig. 3.2.11 shows an example of the difference of theoretical pressure distributions between open- and closed-boundary conditions. The boundary-closed bearing has higher pressure distribution of p so that the load

capacity may increase fiarly well than the otherwise case.

For the practical design, closed-type bearing is recommended on account of its better bearing static characteristics.

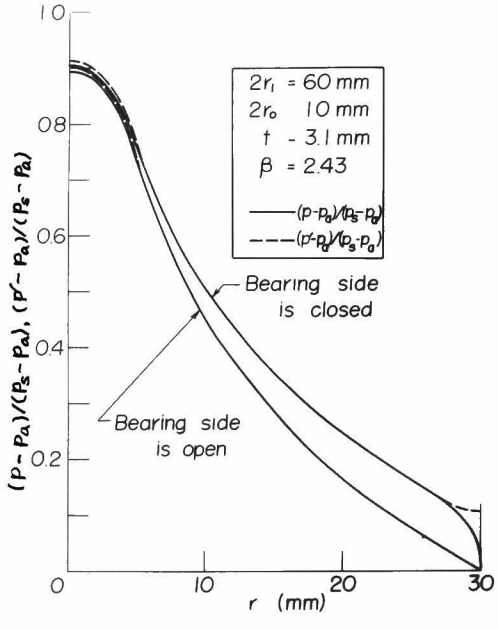

Fig. 3.2.11 Theoretical pressure distributions under open- and closed-boundary conditions

Chapter 3 Applications to the Other Configurations of Externally Pressurized Thrust Porous Gas-Bearing

3-1 Introduction

In Chapter 2, the externally pressurized porous thrust

gas-bearing is analyzed theoretically for such type of bearing that has a circular porous material all over its bearing surface. Hence, the bearing performance depends very much upon the roughness and flatness of the porous surface at the time of its manufacture. For example, it has been reported[5] that the roughness of 2 or 3 microns on the porous surface makes the bearing clearance not to be uniform, which lessens the load capacity very much.

In order to avoid this disadvantages, investigations are made for the porous thrust gas-bearing with flat and solid ring part, so-called 'flange', around the porous part in Section 3-2.

In the practical applications, the thrust collar-type gas-bearing with porous bearing is also used because of the bearing configuration. Some of them are analyzed in this Chapter as well.

The above theory is applied under the same assumption as made in Section 3-1 to these of the porous thrust gas-bearing to obtain theoretical pressure distribution, volume rate of flow and load capacity.

3-2 Externally Pressurized Porous Thrust Gas-Bearing with Flat and Solid Ring Surface

3-2-1 Theoretical Analysis

Fig. 3.3.1 illustrates the construction of the externally pressurized porous thrust gas-bearing with flat and solid ring surface to be analyzed. The gas is supplied from the supply port, and restricted through the porous material, then it is fed into brearing recess (H), and then flows out through the 'flange' part with clearance h.

Fig. 3.3.2 is a schematic figure of this bearing, where

r, z : cylindrical coordinates

r_f : radius of porous material

r_i : radius of bearing

The other notations are the same as defined in Chapter 2.

(a) Region I ($0 \leq r \leq r_i$)

In this region, the previous theory obtained in Chapter 2 can be easily applied. Using the fundamental equations

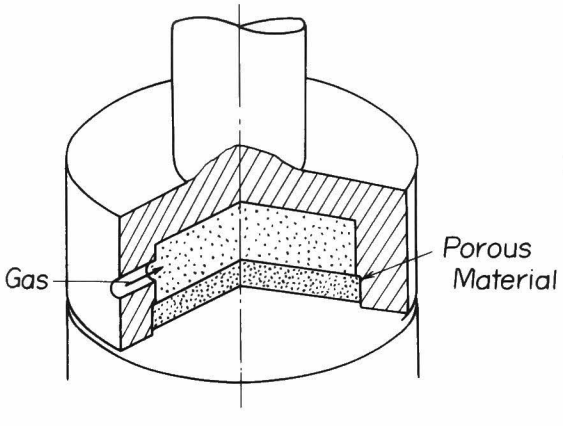

Fig. 3.3.1 Construction of externally pressurized porous thrust gas-bearing with flat and ring surface

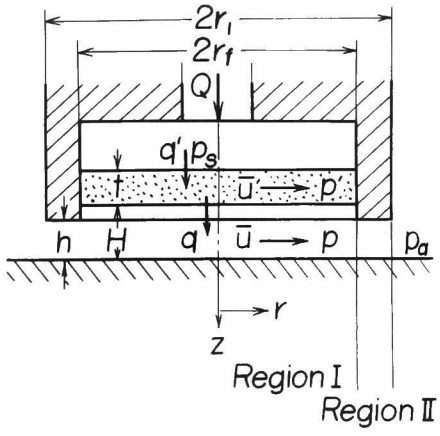

Fig. 3.3.2 Schematic figure of the bearing

(3.2.1), (3.2.2), (3.2.3), (3.2.4)', (3.2.5) and (3.2.6), the pressure distributions p and p' in the bearing clearance and in the porous bearing, respectively, are governed by the following differential equations:

$$\left.\begin{aligned} \frac{1}{r}\frac{d}{dr}\left(r\frac{dp'}{dr}\right) &= A'^2p' - B'^2p - C' \\ \frac{1}{r}\frac{d}{dr}\left(r\frac{dp}{dr}\right) &= D'^2(p - p') \end{aligned}\right\} \qquad (3.3.1)$$

where

$$A'^2 = \frac{1}{\eta t} + \frac{1}{\eta' t}\ ,\quad B'^2 = \frac{1}{\eta t}\ ,\quad C' = \frac{p_s}{\eta' t}\ ,\quad D'^2 = \frac{h^3}{H^3\eta t} \qquad (3.3.2)$$

Solving these equations under the condition

$$\frac{dp}{dr} = \frac{dp'}{dr} = 0 \quad \text{at} \quad r = 0 \qquad (3.3.3)$$

yielding

$$P_I = M_1 I_0(\alpha_1 r) + M_2 I_0(\alpha_2 r) + P_s \tag{3.3.4}$$

$$P_I' = N_1 I_0(\alpha_1 r) + N_2 I_0(\alpha_2 r) + P_s \tag{3.3.5}$$

where N_1 , N_2, M_1 and M_2 are integral constants, and I_0 is a modified Bessel function. α_1 and α_2 are constants determined by design parameters as

$$\left.\begin{aligned} \alpha_1 &= \sqrt{\frac{A'^2 - D'^2 + \sqrt{(A'^2 - D'^2)^2 + 4(B'^2 - A'^2)D'^2}}{2}} \\ \alpha_2 &= \sqrt{\frac{A'^2 - D'^2 - \sqrt{(A'^2 - D'^2)^2 - 4(B'^2 - A'^2)D'^2}}{2}} \end{aligned}\right\} \tag{3.3.6}$$

The volume rate of flow is given by

$$Q_I = \int_0^{r_f} q' \cdot 2\pi r dr = -\frac{\pi h'^3}{6\mu\gamma' t}\left\{\frac{N_1 r_f}{\alpha_1} I_1(\alpha_1 r_f) + \frac{N_2 r_f}{\alpha_2} I_1(\alpha_2 r_f)\right\} \tag{3.3.7}$$

The symbols in these equations are the same that defined in Chapter 2.

(b) Region II ($r_f \leqq r \leqq r_1$)

In this region, the flow can be considered as that between two parallel surfaces. Then the following equations can be obtained from equations of motion and equation of flow continuity,

$$u = -\frac{1}{2\mu}\frac{dp}{dr} z(h - z) \tag{3.3.8}$$

$$p = C_0 \log r + C_0' \tag{3.3.9}$$

In order to determine the constants C_0 and C_0' , the boundary condition is used as

$$\left.\begin{aligned} p &= p_f \qquad at \qquad r = r_f \\ p &= p_a \qquad at \qquad r = r_i \end{aligned}\right\} \tag{3.3.10}$$

then,

$$p_{II} = p_f \left(\frac{\log r_i/r}{\log r_i/r_f}\right) + p_a \tag{3.3.11}$$

The volume rate of flow out of bearing periphery is

$$Q_{II} = 2\pi r_i h \bar{u}\big|_{r=r_i} = \frac{h^3(p_f - p_a)}{6\mu \log r_i/r_f} \tag{3.3.12}$$

(c) Connection of Regions I and II

The unknown constants N_1, N_2, M_1, M_2 and p_f in Eqs. (3.3.4), (3.3.5) and (3.3.11) are determined by the following boundary conditions:

$$\left.\begin{aligned} &(i) \quad p_I = p_f \qquad at \qquad r = r_f \\ &(ii) \quad \frac{dp_I}{dr} = 0 \qquad at \qquad r = r_f \\ &(iii) \quad Q_I = Q_{II} \end{aligned}\right\} \tag{3.3.13}$$

N_1, N_2, M_1, and M_2 must satisfy the following relations:

$$\frac{M_1}{N_1} = \frac{A'^2 - \alpha_1^2}{B'^2}, \qquad \frac{M_2}{N_2} = \frac{A'^2 - \alpha_2^2}{B'^2} \tag{3.3.14}$$

The unknown constants can be determined by conditions (3.3.13) and (3.3.14). Then, the pressure distributions are obtained from Eqs. (3.3.4), (3.3.5) and (3.3.11) with these contants.

(d) Load Capacity

The load capacity W_I in region I is

$$W_I = \int_0^{r_f} (p_I - p_a) 2\pi r dr$$

$$= \frac{2\pi M_1 r_f}{\alpha_1} I_1(\alpha_1 r_f) + \frac{2\pi M_2 r_f}{\alpha_2} I_1(\alpha_2 r_f) + \pi r_f^2 (p_s - p_a) \quad (3.3.15)$$

The load capacity W_{II} in region II is

$$W_{II} = \int_{r_f}^{r_i} (p_{II} - p_a) 2\pi r dr$$

$$= \frac{\pi (p_f - p_a)}{2} \left(\frac{r_i^2 - r_f^2}{\log r_i / r_f} - 2r_f^2 \right) \quad (3.3.16)$$

The total load capacity W is given by

$$W = W_I + W_{II} \quad (3.3.17)$$

3-2-2 Experimental Apparatus

(a) Measurement of Permeability Coefficient

Fig. 3.3.3 shows experimental apparatus for measuring the permeability coefficient. It consists of two plates, a ring and the measured porous material, and they compose a closed space into which the compressed air is supplied to flow through the porous material in axial direction. The pressure in that space is measured by a manometer.

The permeability coefficient can be calculated from the supply pressure and the volume rate of flow by using the following equation:

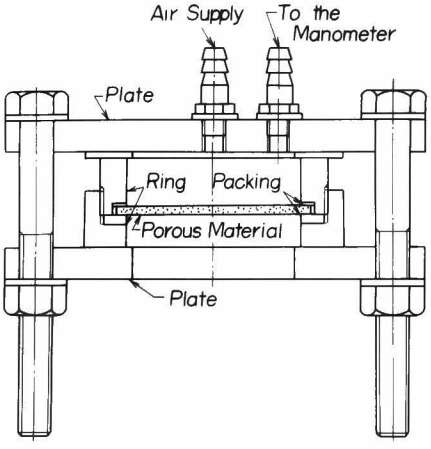

Fig. 3.3.3 Experimental apparatus for measuring the permeability coefficient

$$\left.\begin{aligned} Q &= \pi r_f^2 \frac{k}{\mu}\frac{p_s - p_a}{\eta+\eta'} = \pi r_f^2 \frac{k}{\mu}\frac{p_s - p_a}{t} \\ k &= \frac{kt}{\pi r_f^2 (p_s - p_a)} \end{aligned}\right\} \qquad (3.3.18)$$

It should be noted that the permeability coefficient of porous media is not constant as assumed in the analysis above. Gross[6] states that the permeability coefficient is a function of both bearing clearance pressure and Reynolds number. Because of this variability, the permeability coefficient to be used for the calculation in the above analysis should be determined on the condition of pressure, Reynolds number, and so forth, under which the bearing will actually work.

(b) Measurement of Pressure Distribution

The experimental apparatus for measuring the pressure

distribution and load capacity is quite the same that used in Chapter 2 as shown in Fig. 3.2.6. The method of experiments is also the same. They are made under the static condition.

The dimensions of the bearing used for the experiments are as follows:

Diameter of bearing $2r_1 = 80.0\text{mm}$

Diameter of porous material $2r_f = 60.0\text{mm}$

Thickness of porous material $t \cong 5.0\text{mm}$

3-2-3 Experimental Results

The porous materials used in experiments are listed in Table 3.3.1.

Table 3.3.1 Porous materials employed in experiments

Bearing No.	Material	Dia. of Grain (microns)	Permeability Coefficient (cm^2)	Equivalent Clearance (microns)
I	Sintered Powder Brass	10	8.39×10^{-8}	79.6
II		5	4.27×10^{-8}	67.5

Now, let β a parameter to be defined by

$$\beta = \frac{h'}{H} = \frac{\sqrt[3]{12kt}}{H} \qquad (3.3.19)$$

Then, the pressure distribution and the load capacity are identified by only the value of β, so that they do not

depend directly upon H or h'.

Fig. 3.3.4 shows the pressure distributions for these bearings. The solid line shows the theoretical one. The experimental results coincide well with the theoretical pressure distribution for a large value of β or a small bearing clearance; but for the contrary case (a large bearing clearance), there are some differences between them. The reason for this difference seems to be that the flow in the recess may not be fully viscous when the depth of recess becomes larger.

Fig. 3.3.5 shows the relations between the supply

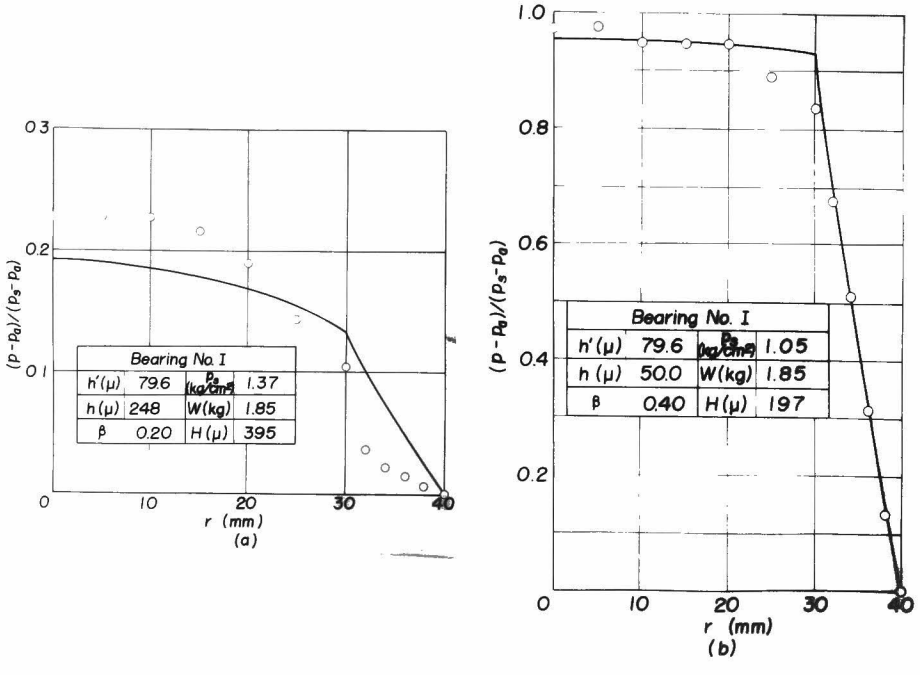

Fig. 3.3.4

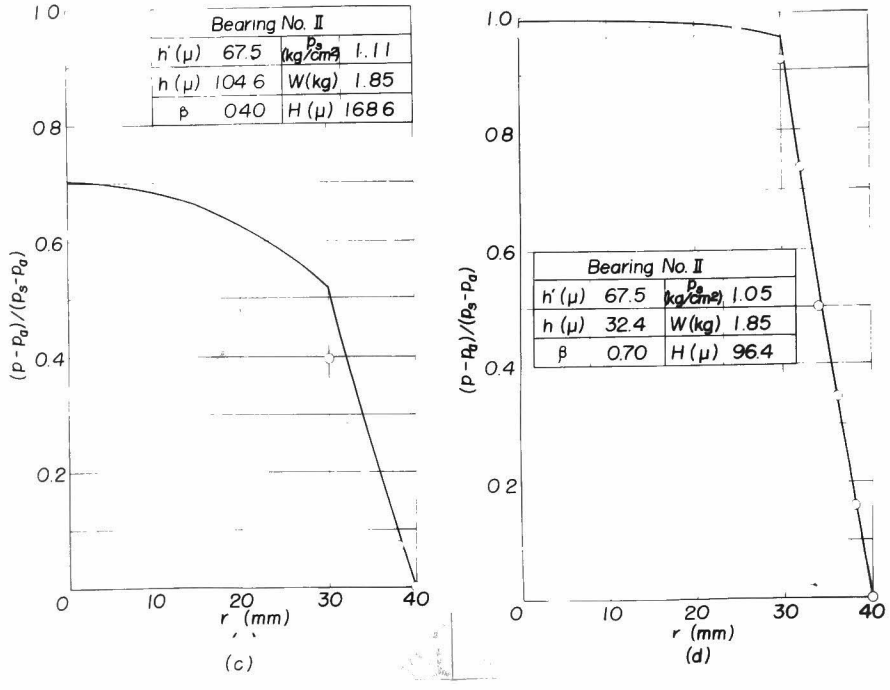

Fig. 3.3.4 Results of pressure distributions

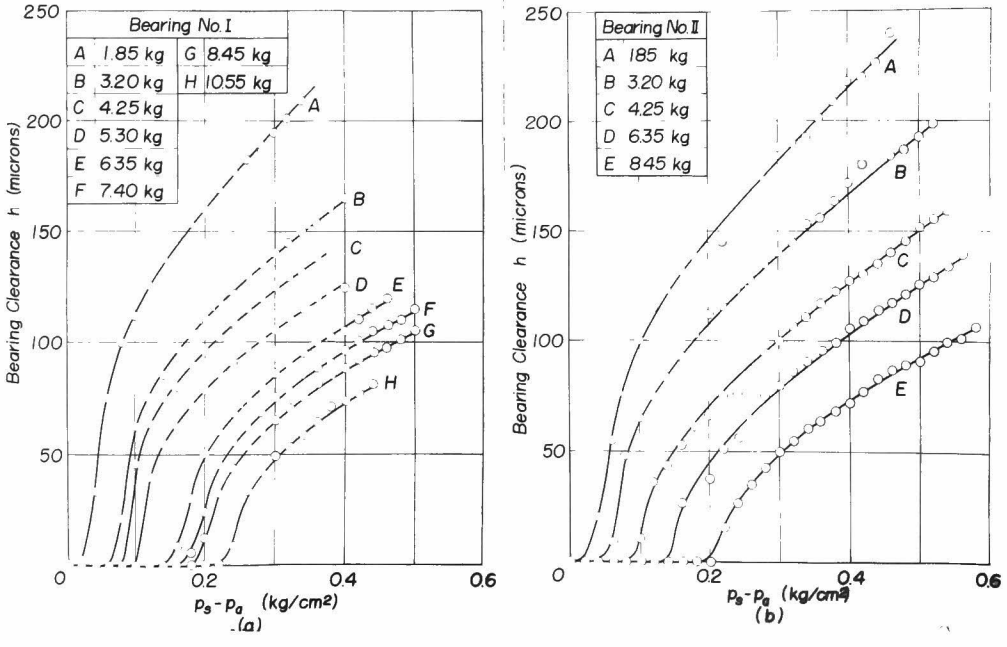

Fig. 3.3.5 Relation between supply pressure and bearing clearance under constant loads

pressure and the bearing clearance h under the constant loads. Fig. 3.3.6 shows those between the load and the bearing clearance h under constant supply pressure.

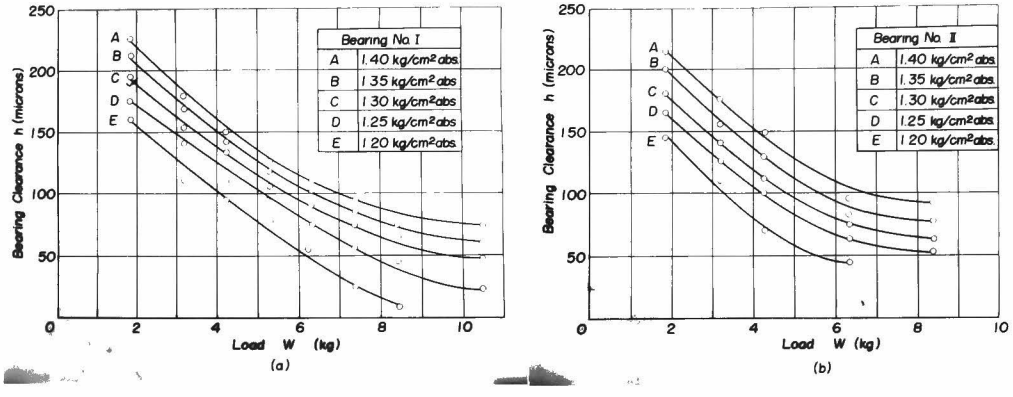

Fig. 3.3.6 Relation between load and bearing clearance under constant supply pressure

The dimensionless load capacities $W/\pi r_1^2(p_s - p_a)$ are shown in Fig. 3.3.7. with respect to $1/\beta$ which corresponds to the bearing clearance. The experimental results coincide with the theoretical curve (solid line) very well qualitatively and fiarly well quantitatively with a small value of load capacity. The deviation of experimental results at a small value of $1/\beta$ is considered to be due to the errors in measurements of the bearing clearances.

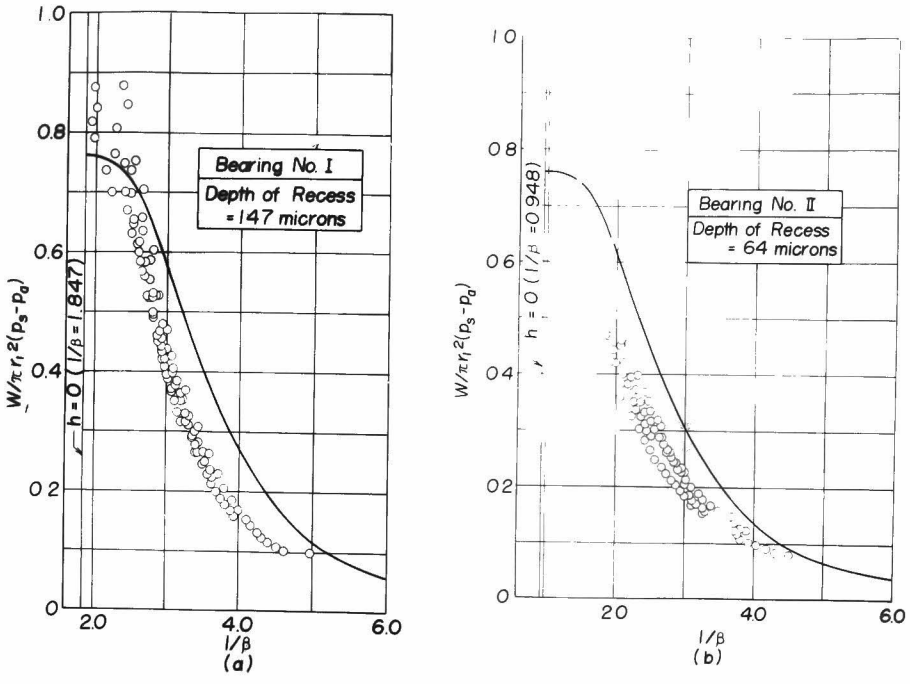

Fig. 3.3.7 Relation between load capacity and $1/\beta$

3-3 Other Applications

Investigations are made for the externally pressurized porous gas-bearings of the thrust collar type, which are also applicable to the practical devices because of their configurations.

(i) Thrust Collar Gas-Bearing with Full Porous Surface

The thrust collar gas-bearing with full porous surface is analyzed: the bearing configuration is such as shown in Fig. 3.3.8 where r_0 and r_1 are inner and outer bearing radii respectively. The gas is fed under pressure p_s through

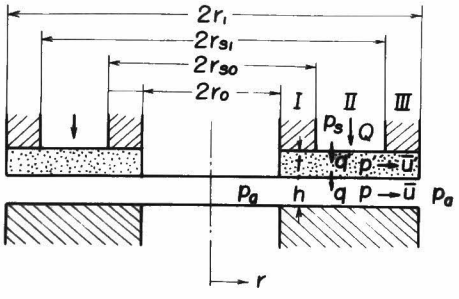

Fig. 3.3.8 Schematic diagram of thrust collar gas-bearing with full porous surface

the annular supply slit, inner and outer radii of which are r_{so} and r_{si} , respectively.

Dividing the bearing surface into three regions (Region I, II and III), the pressure p and p' in the bearing clearance and in the porous material may be obtained in each region from the following differential equations, which are reduced as Eqs. (3.2.9), and (3.2.21) in Chapter 2:

Region I ($r_o \leqq r \leqq r_{so}$) and Region III ($r_{si} \leqq r \leqq r_1$)

$$\left.\begin{aligned} \frac{1}{r}\frac{d}{dr}\left(r\frac{dp'}{dr}\right) &= B'^2(p'-p) \\ \frac{1}{r}\frac{d}{dr}\left(r\frac{dp}{dr}\right) &= D'^2(p-p') \end{aligned}\right\} \qquad (3.3.20)$$

Region II ($r_{so} \leqq r \leqq r_{si}$)

$$\left.\begin{aligned} \frac{1}{r}\frac{d}{dr}\left(r\frac{dp'}{dr}\right) &= A'^2p' - B'^2p - C' \\ \frac{1}{r}\frac{d}{dr}\left(r\frac{dp}{dr}\right) &= D'^2(p-p') \end{aligned}\right\} \qquad (3.3.21)$$

$$A'^2 = \frac{1}{\eta t} + \frac{1}{\eta' t}\ ,\quad B'^2 = \frac{1}{\eta t}\ ,\quad C' = \frac{p_s}{\eta t}\ ,\quad D'^2 = \frac{h'^3}{h^3 \eta t} \qquad (3.3.22)$$

where $h' = \sqrt[3]{12kt}$ is equivalent clearance of porous material.

The general solutions of them are

Region I : $$p_I = E_1 I_0(\alpha_0 r) + F_1 K_0(\alpha_0 r) + G_1 \log r + G_2 \qquad (3.3.23)$$

$$p_I' = -\frac{h'^3}{h^3}\left[E_1 I_0(\alpha_0 r) + F_1 K_0(\alpha_0 r)\right] + G_1 \log r + G_2 \qquad (3.3.24)$$

Region II : $$p_{II} = M_1 I_0(\alpha_1 r) + M_2 I_0(\alpha_2 r) + M_3 K_0(\alpha_1 r) + M_4 K_0(\alpha_2 r) + p_s \qquad (3.3.25)$$

$$p_{II}' = N_1 I_0(\alpha_1 r) + N_2 I_0(\alpha_2 r) + N_3 K_0(\alpha_1 r) + N_4 K_0(\alpha_2 r) + p_s \qquad (3.3.26)$$

Region III: $$p_{III} = E_2 I_0(\alpha_0 r) + F_2 K_0(\alpha_0 r) + G_3 \log r + G_4 \qquad (3.3.27)$$

$$p_{III}' = -\frac{h'^3}{h^3}\left[E_2 I_0(\alpha_0 r) + F_2 K_0(\alpha_0 r)\right] + G_3 \log r + G_4 \qquad (3.3.28)$$

where I_0 and K_0 are modified Bessel functions, and α_0, α_1, and α_2 are constants determined by design parameters as

$$\left.\begin{aligned} \alpha_0 &= \sqrt{B'^2 + D'^2} \\ \alpha_1 &= \sqrt{\frac{A'^2 - D'^2 + \sqrt{(A'^2 - D'^2)^2 + 4(B'^2 - A'^2)D'^2}}{2}} \\ \alpha_2 &= \sqrt{\frac{A'^2 - D'^2 - \sqrt{(A'^2 - D'^2)^2 + 4(B'^2 - A'^2)D'^2}}{2}} \end{aligned}\right\} \qquad (3.3.29)$$

E's, F's, G's, M's and N's are integral constants which have the following relations between themselves,

$$\left.\begin{aligned} \frac{M_1}{N_1} &= \frac{M_3}{N_3} = \frac{A'^2 - \alpha_1^2}{B'^2} \\ \frac{M_2}{N_2} &= \frac{M_4}{N_4} = \frac{A'^2 - \alpha_2^2}{B'^2} \end{aligned}\right\} \qquad (3.3.30)$$

The volume rate of flow can be given by

$$
\left.
\begin{aligned}
Q &= \int_{r_{s0}}^{r_{s1}} g' \cdot 2\pi r dr = \int_{r_{s0}}^{r_{s1}} \frac{p'^3}{12\mu\eta' t} \cdot 2\pi r (p_s - p') dr \\
&= -\frac{p'^3}{6\mu\eta' t}\left\{\frac{N_1}{\alpha_1}\left[r_{s1} I_1(\alpha_1 r_{s1}) - r_{s0} I_1(\alpha_1 r_{s0})\right] + \frac{N_2}{\alpha_2}\left[r_{s1} I_1(\alpha_2 r_{s1}) - r_{s0} I_1(\alpha_2 r_{s0})\right]\right. \\
&\quad \left. - \frac{N_3}{\alpha_1}\left[r_{s1} K_1(\alpha_1 r_{s1}) - r_{s0} K_1(\alpha_1 r_{s0})\right] - \frac{N_4}{\alpha_2}\left[r_{s1} K_1(\alpha_2 r_{s1}) - r_{s0} K_1(\alpha_2 r_{s0})\right]\right\}
\end{aligned}
\right\} \quad (3.3.31)
$$

The boundary conditions to determine the constants are

$$
\left.
\begin{aligned}
&p_I = p_a \ , \quad p'_I = p_a && \text{at} \quad r = r_o \\
&p_I = p_{II} \ , \quad p'_I = p'_{II} && \text{at} \quad r = r_{so} \\
&\frac{dp_I}{dr} = \frac{dp_{II}}{dr} \ , \quad \frac{dp'_I}{dr} = \frac{dp'_{II}}{dr} && \text{at} \quad r = r_{so} \\
&p_{II} = p_{III} \ , \quad p'_{II} = p'_{III} && \text{at} \quad r = r_{s1} \\
&\frac{dp_{II}}{dr} = \frac{dp_{III}}{dr} \ , \quad \frac{dp'_{II}}{dr} = \frac{dp'_{III}}{dr} && \text{at} \quad r = r_{s1} \\
&p_{III} = p_a \ , \quad p_{III} = p_a && \text{at} \quad r = r_i
\end{aligned}
\right\} \quad (3.3.32)
$$

The pressure distributions and volume rate of flow can be obtained from the above equations with using the determined constants.

The load capacity is

$$
\left.
\begin{aligned}
W &= \int_{r_o}^{r_i} (p - p_a) 2\pi r dr \\
&= 2\pi\left\{\frac{E_1}{\alpha_0}\left[r_{s0} I_1(\alpha_0 r_{s0}) - r_o I_1(\alpha_0 r_o)\right] - \frac{F_1}{\alpha_0}\left[r_{s0} K_1(\alpha_0 r_{s0}) - r_o K_1(\alpha_0 r_o)\right]\right. \\
&\quad + \frac{G_1}{2}\left[r_{s0}^2 \log r_{s0} - r_o^2 \log r_o - \frac{r_{s0}^2 - r_o^2}{2}\right] + \frac{G_2}{2}(r_{s0}^2 - r_o^2) \\
&\quad \left. + \frac{M_1}{\alpha_1}\left[r_{s1} I_1(\alpha_1 r_{s1}) - r_{s0} I_1(\alpha_1 r_{s0})\right] + \frac{M_2}{\alpha_2}\left[r_{s1} I_1(\alpha_2 r_{s1}) - r_{s0} I_1(\alpha_2 r_{s0})\right]\right.
\end{aligned}
\right\}
$$

$$
\left.
\begin{aligned}
&-\frac{M_3}{\alpha_1}\left[r_{s1}K_1(\alpha_1 r_{s1})-r_{s0}K_1(\alpha_1 r_{s0})\right]-\frac{M_4}{\alpha_2}\left[r_{s1}K_1(\alpha_2 r_{s1})-r_{s0}K_1(\alpha_2 r_{s0})\right]\\
&+\frac{p_s}{2}\left(r_{s1}^2-r_{s0}^2\right)\\
&+\frac{E_2}{\alpha_0}\left[r_1 I_1(\alpha_0 r_1)-r_{s1}I_1(\alpha_0 r_{s1})\right]-\frac{F_2}{\alpha_0}\left[r_1 K_1(\alpha_0 r_1)-r_{s1}K_1(\alpha_0 r_1)\right]\\
&+\frac{G_4}{2}\left[r_1^2\log r_1-r_{s1}^2\log r_{s1}-\frac{r_1^2-r_{s1}^2}{2}\right]+\frac{G_4}{2}\left(r_1^2-r_{s1}^2\right)\\
&-\frac{p_a}{2}\left(r_1^2-r_0^2\right)\Big\}
\end{aligned}
\right\} \quad (3.3.33)
$$

(ii) Thrust Collar Porous Gas-Bearing with Solid and Flat Ring Part

In order to avoid the disadvantages due to roughness and waviness of the porous bearing surface, thrust collar porous gas-bearing with solid and flat ring part is introduced here to be analyzed.

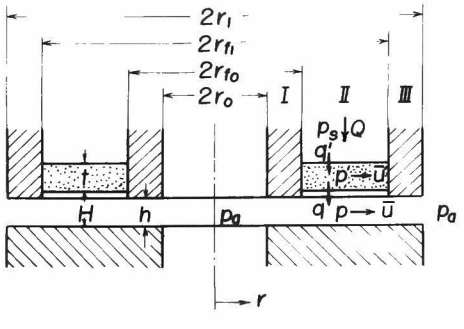

Fig. 3.3.9 Schematic diagram of thrust collar porous gas-bearing with solid falt ring part

Fig. 3.3.9 shows the schematic configuration of the bearing, in which r_0 and r_1 are inner and outer bearing radii, respectively, and r_{f0} and r_{f1} are those of porous bearing. h is the bearing clearance and H is the depth of the recess of porous bearing part. The compressed gas is supplied through porous bearing into recess and flows out to atmosphere through bearing clearance with the solid bearing part so-called 'flange'.

The solutions of pressure distributions can be obtained from the following equations for each region in the figure by the same reduction as in Section 3-2.

In region I ($r_0 \leqq r \leqq r_{f0}$), and region III ($r_{f1} \leqq r \leqq r_1$), the flow is considered as that of between two parallel solid surface, then, the pressure distributions can be obtained as follows:

In region I, from the continuity equation,

$$2\pi r h \bar{u} = 2\pi r_{f0} H \bar{u}\Big|_{r=r_{f0}}$$

or

$$2\pi r \frac{h^3}{12\mu}\frac{dp}{dr} = 2\pi r_{f0} \frac{H^3}{12\mu}\frac{dp_{II}}{dr}\Big|_{r=r_{f0}} \tag{3.3.34}$$

where $\bar{u}$ is the mean flow velocity.

Integrating this equation under the condition of

$$p = p_a \qquad \text{at} \qquad r = r_0 \tag{3.3.35}$$

resulting

$$p_I = r_{f_0} \frac{H^3}{h^3} \frac{dp_{II}}{dr}\bigg|_{r=r_{f_0}} \log \frac{r}{r_0} + p_a \tag{3.3.36}$$

Similarly in region III,

$$p_{III} = r_{f_1} \frac{H^3}{h^3} \frac{dp_{II}}{dr}\bigg|_{r=r_{f_1}} \log \frac{r}{r_1} + p_a \tag{3.3.37}$$

where the boundary condition used is

$$p = p_a \quad \text{at} \quad r = r_1 \tag{3.3.38}$$

In region II ($r_{f_0} \leqq r \leqq r_{f_1}$), the pressure distribution is governed by the following differential equations for the fundamental equations (3.2.1)~(3.2.6) are valid for this region;

$$\left.\begin{aligned} \frac{1}{r}\frac{d}{dr}\left(r\frac{dp'}{dr}\right) &= A'^2 p' - B'^2 p - C' \\ \frac{1}{r}\frac{d}{dr}\left(r\frac{dp}{dr}\right) &= D'^2 (p - p') \end{aligned}\right\} \tag{3.3.39}$$

$$A'^2 = \frac{1}{\eta t} + \frac{1}{\eta' t}\ , \quad B'^2 = \frac{1}{\eta t}\ , \quad C' = \frac{p_s}{\eta' t}\ , \quad D'^2 = \frac{h'^3}{H^3 \eta t} \tag{3.3.40}$$

where h' is the equivalent clearance of porous material.

Solving Eq. (3.3.39),

$$p_{II} = M_1 I_0(\alpha_1 r) + M_2 I_0(\alpha_2 r) + M_3 K_0(\alpha_1 r) + M_4 K_0(\alpha_2 r) + p_s \tag{3.3.41}$$

$$p'_{II} = N_1 I_0(\alpha_1 r) + N_2 I_0(\alpha_2 r) + N_3 K_0(\alpha_1 r) + N_4 K_0(\alpha_2 r) + p_s \tag{3.3.42}$$

where I_0 and K_0 are modified Bessel functions. α_1 and α_2

are defined by Eq. (3.3.29) in which A'^2, B'^2, and D'^2 are given by Eq. (3.3.40). Integral constants M_j and N_j $(j=1,2,3,4)$ have the relationships of Eq. (3.3.30) between themselves.

The volume rate of flow is given by

$$Q_{II} = \int_{r_{fo}}^{r_{f1}} \frac{h^3}{12\mu\eta' t} \cdot 2\pi r (p_s - p')\, dr$$

$$= -\frac{h'^3}{6\mu\eta' t}\left\{ \frac{N_1}{\alpha_1}\left[r_{f1} I_1(\alpha_1 r_{f1}) - r_{fo} I_1(\alpha_1 r_{fo})\right] + \frac{N_2}{\alpha_2}\left[r_{f1} I_1(\alpha_2 r_{f1}) - r_{fo} I_1(\alpha_2 r_{fo})\right] \right.$$

$$\left. - \frac{N_3}{\alpha_1}\left[r_{f1} K_1(\alpha_1 r_{f1}) - r_{fo} K_1(\alpha_1 r_{fo})\right] - \frac{N_4}{\alpha_2}\left[r_{f1} K_1(\alpha_2 r_{f1}) - r_{fo} K_1(\alpha_2 r_{fo})\right] \right\} \quad (3.3.43)$$

The load capacity can be obtained by the integration of pressure p with respect to the bearing area, resulting

$$W = W_I + W_{II} + W_{III} \quad (3.3.44)$$

where

$$W_I = \int_{r_o}^{r_{fo}} 2\pi r (p_I - p_a)\, dr$$

$$= 2\pi r_{fo} \frac{H^3}{h^3} \left.\frac{dp_{II}}{dr}\right|_{r=r_{fo}} \left\{ \frac{r_{fo}^2}{2} \log \frac{r_{fo}}{r_o} - \frac{1}{4}(r_{fo}^2 - r_o^2) \right\} \quad (3.3.45)$$

$$W_{II} = \int_{r_{fo}}^{r_{f1}} 2\pi r (p_{II} - p_a)\, dr$$

$$= 2\pi \left\{ \frac{M_1}{\alpha_1}\left[r_{f1} I_1(\alpha_1 r_{f1}) - r_{fo} I_1(\alpha_1 r_{fo})\right] + \frac{M_2}{\alpha_2}\left[r_{f1} I_1(\alpha_2 r_{f1}) - r_{fo} I_1(\alpha_2 r_{fo})\right] \right.$$

$$- \frac{M_3}{\alpha_1}\left[r_{f1} K_1(\alpha_1 r_{f1}) - r_{fo} K_1(\alpha_1 r_{fo})\right] - \frac{M_4}{\alpha_2}\left[r_{f1} K(\alpha_2 r_{f1}) - r_{fo} K_1(\alpha_2 r_{fo})\right]$$

$$\left. + \frac{1}{2}(p_s - p_a)(r_{f1}^2 - r_{fo}^2) \right\} \quad (3.3.46)$$

$$W_{III} = \int_{r_{f1}}^{r_1} 2\pi r (p_{III} - p_a)\, dr$$
$$= 2\pi r_{f1} \frac{H^3}{R^3} \frac{dp_{II}}{dr}\bigg|_{r=r_{f1}} \left\{ \frac{r_{f1}^2}{2} \log \frac{r_{f1}}{r_1} - \frac{1}{4}(r_{f1}^2 - r_1^2) \right\} \qquad (3.3.47)$$

Chapter 4 Analysis of Externally Pressurized Porous Journal Gas-Bearing

4-1 Theoretical Analysis

Externally pressurized porous journal gas-bearing is also analyzed here theoretically under the same assumptions as made in Chapter 1.

There could be various bearing configurations of it, but in this chapter, a porous journal gas-bearing with circumferential slit gas-supply as shown in Fig. 3.4.1 is analyzed fundamentally, and later with some varieties of bearing configurations.

In the followings, it is assumed that the eccentricity ratio is comparatively small so that the secondary circumferential gas-flow may be neglected and, hence, the flow of gas may be two-dimensional.

The bearing configuration to be analyzed is shown in Fig. 3.4.2 schematically. The compressed gas is fed from a slit supply of width b under the supply pressure p_s into the porous bushing, then, restricted by it, the gas flows

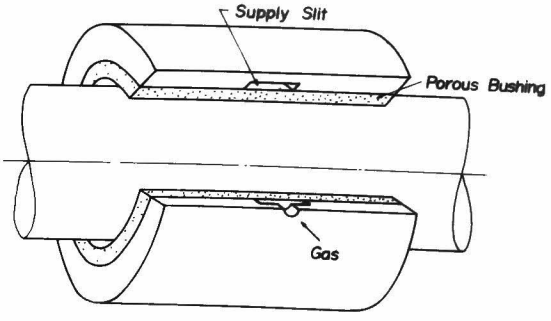

Fig. 3.4.1 Construction of externally pressurized porous journal gas-bearing

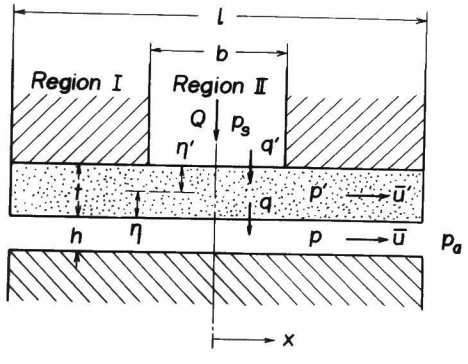

Fig. 3.4.2 Schematic diagram of the bearing

into the bearing clearance in axial direction. Some part of the gas also flows through the porous bushing in axial direction.

The average velocities of flows in the x-direction in

the bearing clearance and the porous bushing are, respectively as follows:

$$\bar{u} = -\frac{h^2}{12\mu}\frac{dp}{dx} \tag{3.4.1}$$

$$\bar{u}' = -\frac{k}{\mu}\frac{dp'}{dx} = -\frac{h'^3}{12\mu t}\frac{dp'}{dx} \tag{3.4.2}$$

The continuity conditions are

$$h\bar{u} = \int_0^x q\,dx \tag{3.4.3}$$

$$t\bar{u}' = \frac{Q}{2} - \int_0^x q\,dx \qquad \left(\frac{b}{2} \leqq x \leqq \frac{l}{2}\right) \tag{3.4.4}$$

$$= \int_0^x q'\,dx - \int_0^x q\,dx \qquad \left(0 \leqq x \leqq \frac{b}{2}\right) \tag{3.4.4}'$$

where Q is the volume rate of flow per unit bearing width, and q and q' are the velocities of the flow-out from and flow-in to the porous bushing, respectively; q and q' are given by the following equations according to the assumption:

$$q = \frac{k}{\mu}\cdot\frac{p'-p}{\eta} = \frac{h'^3}{12\mu\eta t}(p'-p) \tag{3.4.5}$$

$$q' = \frac{k}{\mu}\cdot\frac{p_s-p'}{\eta'} = \frac{h'^3}{12\mu\eta' t}(p_s-p') \tag{3.4.6}$$

where η and η' are the effective restricting thickness, and are given by

$$\eta = ct\,, \qquad \eta' = c't \tag{3.4.7}$$

c and c' should be determined experimentally but they are presumed to be approximately

$$c = c' \cong \frac{1}{2} \tag{3.4.8}$$

Eliminating $\bar{u}$ and q from Eqs. (3.4.1), (3.4.3), and (3.4.5), and differentiating by x, one obtains

$$\frac{d^2p}{dx^2} = -\frac{h'^3}{h^3 \eta t}(p' - p) \tag{3.4.9}$$

Region I $\left(\frac{b}{2} \leqq x \leqq \frac{l}{2}\right)$

From Eqs. (3.4.3) and (3.4.4)

$$h\bar{u} + t\bar{u}' = \frac{Q}{2} \tag{3.4.10}$$

Eliminating $\bar{u}$ and $\bar{u}'$ by substitution of Eqs. (3.4.1) and (3.4.2) into Eq. (3.4.10), and integrating it with x, one obtains

$$p' = \frac{1}{h'^3}(C_1 - 6\mu Q x - h^3 p) \tag{3.4.11}$$

where C_1 is the constant of integration.

In Eq. (3.4.11), p and p' should satisfy the following boundary condition:

$$p = p' = p_a \qquad \text{at} \qquad x = \frac{l}{2} \tag{3.4.12}$$

Then

$$C_1 = 3\mu l Q + (h^3 + h'^3) p_a \tag{3.4.13}$$

Substituting Eq. (3.4.11) into Eq. (3.4.9)

$$\frac{d^2p}{dx^2} - \alpha_0^2 p = \frac{6\mu Q}{h^3\eta t}x - \frac{C_1}{h^3\eta t} \tag{3.4.14}$$

where

$$\alpha_0 = \sqrt{\frac{h^3 + h'^3}{h^3\eta t}} \tag{3.4.15}$$

The solution of Eq. (3.4.14) is given by

$$p = E\sinh\alpha_0 x + F\cosh\alpha_0 x - \frac{6\mu Q}{h^3 + h'^3}x + \frac{C_1}{h^3 + h'^3} \tag{3.4.16}$$

where E and F are the arbitrary constants which should be determined by the boundary conditions.

Substituting Eqs. (3.4.13) and (3.4.11) into Eq. (3.4.16), the pressure distributions p and p' in the region I are obtained as follows.

$$p_I = E\sinh\alpha_0 x + F\cosh\alpha_0 x + \frac{6\mu Q}{h^3 + h'^3}\left(\frac{l}{2} - x\right) + p_a \tag{3.4.17}$$

$$p'_I = -\frac{h^3}{h'^3}\left[E\sinh\alpha_0 x + F\cosh\alpha_0 x\right] + \frac{6\mu Q}{h^3 + h'^3}\left(\frac{l}{2} - x\right) + p_a \tag{3.4.18}$$

(b) Region II $\left(0 \leqq x \leqq \frac{b}{2}\right)$

From Eqs. (3.4.3) and (3.4.4)'

$$h\bar{u} + t\bar{u}' = \int_0^x g' dx \tag{3.4.19}$$

Eliminating $\bar{u}$, $\bar{u}'$; and g' from Eqs. (3.4.1), (3.4.2), (3.4.6) and (3.4.19), and differentiating it by x, one obtains

$$\frac{d^2p'}{dx^2} = \frac{1}{\eta t}(p'-p) - \frac{1}{\eta' t}(p_s - p') \qquad (3.4.20)$$

Eqs. (3.4.9) and (3.4.20) can be rewritten as follows:

$$\left.\begin{aligned} \frac{d^2p'}{dx^2} &= A'^2 p' - B'^2 p - C' \\ \frac{d^2p}{dx^2} &= D'^2 (p - p') \end{aligned}\right\} \qquad (3.4.21)$$

where

$$A'^2 = \frac{1}{\eta t} + \frac{1}{\eta' t}\ , \quad B'^2 = \frac{1}{\eta t}\ , \quad C' = \frac{p_s}{\eta t}\ , \quad D'^2 = \frac{R'^3}{R^3 \eta t} \qquad (3.4.22)$$

The solutions of Eqs. (3.4.21) are

$$p = M_1 \cosh\alpha_1 x + M_2 \cosh\alpha_2 x + M_3 \sinh\alpha_1 x + M_4 \sinh\alpha_2 x + p_s \qquad (3.4.23)$$

$$p' = N_1 \cosh\alpha_1 x + N_2 \cosh\alpha_2 x + N_3 \sinh\alpha_1 x + N_4 \sinh\alpha_2 x + p_s \qquad (3.4.24)$$

where

$$\alpha_i = \sqrt{\frac{A'^2 - D'^2 \pm \sqrt{(A'^2 - D'^2)^2 - 4(B'^2 - A'^2)D'^2}}{2}}\ , \quad (i = 1, 2) \qquad (3.4.25)$$

The signs in the right-hand side of Eq. (3.4.25) are to be taken as follows:

+ for subscript i = 1

- for subscript i = 2

M_j and N_j (j = 1, 2, 3, 4) are constants of integration and they should satisfy the following relation:

$$\frac{M_j}{N_j} = \frac{A'^2 - \alpha_i^2}{B'^2} \qquad (3.4.26)$$

where $j = 1$ or 3 when $i = 1$, and $j = 2$ or 4 when $i = 2$.

These dudections are quite the same as shown in Appendix XIV.

Using the following boundary condition:

$$\frac{dp}{dx} = \frac{dp'}{dx} = 0 \qquad at \qquad x = 0 \tag{3.4.27}$$

then

$$M_3 = M_4 = N_3 = N_4 = 0 \tag{3.4.28}$$

The pressure distribution in the region II are obtained as follows:

$$p_{II} = M_1 \cosh \alpha_1 x + M_2 \cosh \alpha_2 x + p_s \tag{3.4.29}$$

$$p'_{II} = N_1 \cosh \alpha_1 x + N_2 \cosh \alpha_2 x + p_s \tag{3.4.30}$$

The volume rate of flow is

$$\frac{Q}{2} = \int_0^{\frac{b}{2}} q' \, dx$$

$$= -\frac{h'^3}{12\mu\eta' t}\left[\frac{N_1}{\alpha_1}\sinh\frac{\alpha_1 b}{2} + \frac{N_2}{\alpha_2}\sinh\frac{\alpha_2 b}{2}\right] \tag{3.4.31}$$

The boundary conditions to determine the constants N_1, N_2 (or M_1, M_2) E and F are

$$\left.\begin{array}{lllll} \text{(i)} & p_I = p'_I = 0 & at & x = \frac{\ell}{2} & \\ \text{(ii)} & p_I = p_{II} & at & x = \frac{b}{2} & \\ \text{(iii)} & p'_I = p'_{II} & at & x = \frac{b}{2} & \end{array}\right\} \tag{3.4.32}$$

$$\left.\begin{aligned} &\text{(iv)} \quad \frac{dp_I}{dx} = \frac{dp_{II}}{dx} \qquad \text{at} \qquad x = \frac{b}{2} \\ &\text{(v)} \quad \frac{dp'_I}{dx} = \frac{dp'_{II}}{dx} \qquad \text{at} \qquad x = \frac{b}{2} \end{aligned}\right\}$$

Among them, conditions (iv) and (v) are not mutually independent, so the unknown constants are determined by the conditions (i), (ii), (iii) and (iv) or (v). The pressure distributions p and p' are given by putting these constants into Eqs. (3.4.17), (3.4.18), (3.4.29) and (3.4.30) in each region.

The load capacity per unit bearing breadth for the case of an incompressible fluid is obtained by integrating the pressure in each region:

$$\begin{aligned} \Delta W &= 2\int_0^{\frac{l}{2}} (p - p_a)\,dx \\ &= \frac{2M_1}{\alpha_1}\sinh\frac{\alpha_1 b}{2} + \frac{2M_2}{\alpha_2}\sinh\frac{\alpha_2 b}{2} + b(p_s - p_a) + \frac{2E}{\alpha_0}\left[\cosh\frac{\alpha_0 l}{2} - \cosh\frac{\alpha_0 b}{2}\right] \\ &\quad + \frac{2F}{\alpha_0}\left[\sinh\frac{\alpha_0 l}{2} - \sinh\frac{\alpha_0 b}{2}\right] + \frac{6\mu Q}{h^3 + h'^3}\left(\frac{l}{2} - \frac{b}{2}\right)^2 \end{aligned} \tag{3.4.33}$$

The load capacity is obtained by the integration of load-applied direction component of this value of ΔW with consideration of the eccentricity of the journal and hence the bearing clearance variation. As it is very hard to obtain it analytically, an approximate method to calculate the load capacity is discussed later in Section.4-4.

4-2 Experimental Investigations

(a) Experimental Apparatus

The experiments are made for the pressure distribution.

The porous journal bearings and shafts employed in the experiments are shown in Fig. 3.4.3. The dimensions are as follows:

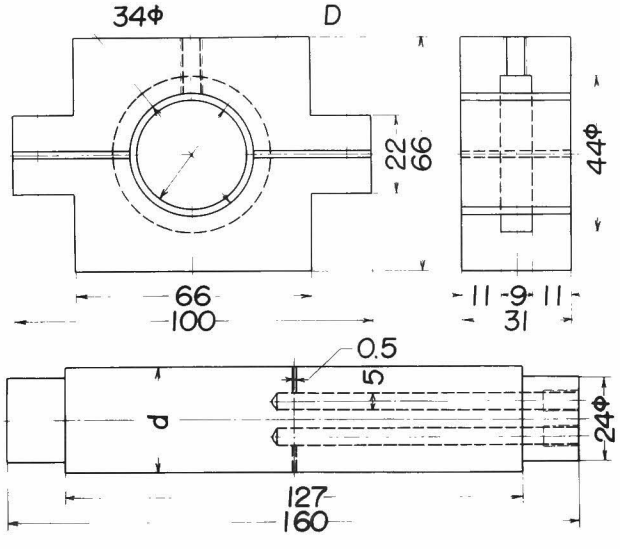

Fig. 3.4.3 Bearings and shafts employed in experiments

Diameter of shafts

Shaft	No. 1	29.940mm
	No. 2	29.951mm
	No. 3	29.770mm

Inner diameter of porous bushings

Bushing No. 1 30.070mm

No. 2 30.074mm

Outer diameter of porous bushings 34.0mm

Length of porous bushing (ℓ) 31.0 mm

Width of air-supply slit (b) 9.0 mm

The pressure in the bearing clearance is measured by a U-tube mercury manometer connected with a small hole of 0.5mm diameter drilled in the shaft.

For the pressure distribution in the axial direction, the bearing is slided axially along the static shaft, while the shaft is rotated for continuous measurement of the circumferential pressure distribution.

(b) Permeability Coefficient and Eccentricity Ratio

Because of the valiability of the permeability coefficient of porous media, it should be determined based on the condition of pressure, Reynolds number, and so on, under which the bearing will actually work.

In the following experimental study, the permeability coefficient k and eccentricity ratio are presumed by another method mentioned in later, because of the difficulty of measuring them experimentally.

Denoting β to be

$$\beta = \frac{h'}{h} = \frac{\sqrt[3]{12kt}}{h} \tag{3.4.35}$$

and the bearing clearance h can be given by

$$h = c_r(1+\varepsilon\cos\theta) \tag{3.4.36}$$

where c_r : radial clearance

ε : eccentricity ratio

θ : angle

then Eq. (3.4.36) becomes

$$\frac{1}{\beta} = \frac{c_r}{\sqrt[3]{12kt}}(1+\varepsilon\cos\theta) \tag{3.4.37}$$

On the other hand, the theoretical curve of $(p_o-p_a)/(p_s-p_a)$ versus $1/\beta$ can be obtained identically when the bearing dimensions are given even if the permeability coefficient is not known, where p_o is the pressure at $x = 0$.

Fig. 3.4.4 shows theoretical relation between $(p_o-p_a)/(p_s-p_a)$ and $1/\beta$ calculated for the porous bearing with the dimensions shown in the above. By using this figure, one can obtain the value of $1/\beta$ which corresponds to the experimental data of p_o. Fig. 3.4.5 shows the values of $1/\beta$ at the circumferential positions of every 30° in the bearing clearance. The permeability coefficient k and eccentricity ratio ε are presumed by the minimum square method to match these experimental data of $1/\beta$ to Eq. (3.4.37). In Fig. 3.4.5 the data of Bushing No.1 at $\theta = 60^\circ$

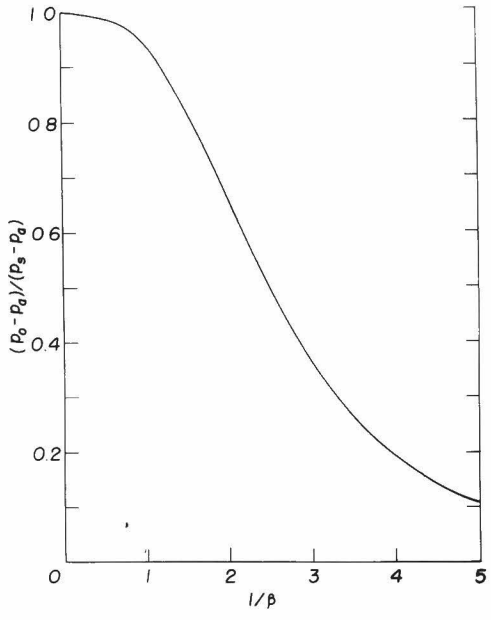

Fig. 3.4.4 Theoretical relation between $(p_o - p_a) \div (p_s - p_a)$ and $1/\beta$

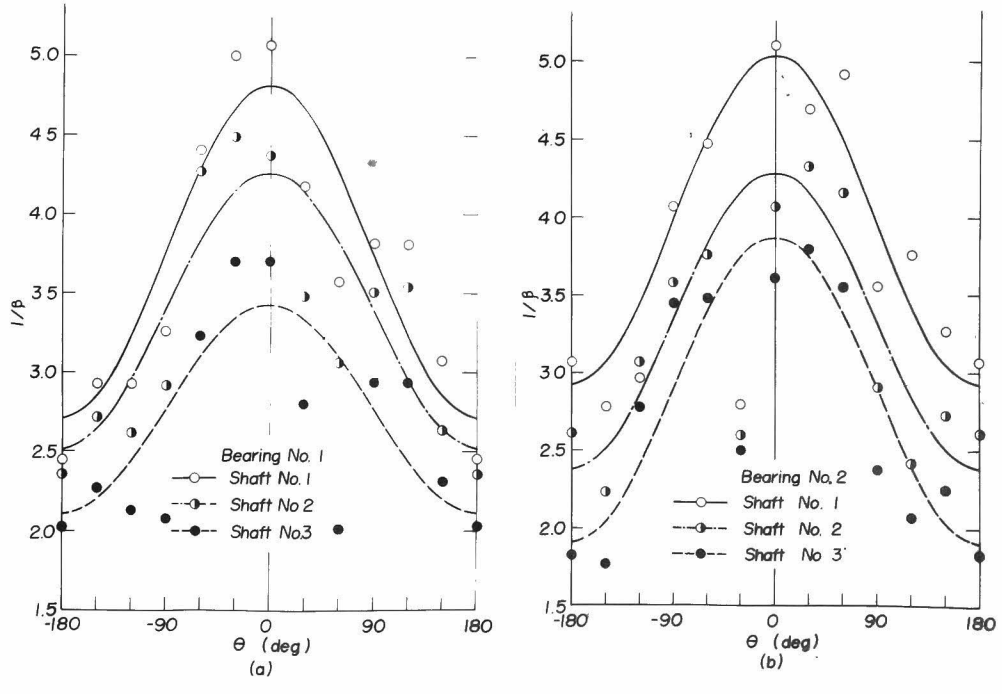

Fig. 3.4.5 The values of $1/\beta$ at circumferential positions

and those of Bushing No.2 at $\theta = -30^{o}$ are excluded because they may be bad due to the fault of manufacture of bushings. The presumed results of them are shown in Table 3.4.1. The permeability coefficients are reasonably constant which may justify this method. The thick lines in the figures are the theoretical ones by using these results.

Table 3.4.1 Presumed results of permeability coefficient and eccentricity ratio

Bearing No.	Shaft No.	Bearing Clearance (microns)	Supply Pressure (kg/cm^2)	Eccentricity Ratio	Permeability Coefficient (cm^2)
1	1	130	1.8	0.281	2.10×10^{-9}
1	2	119	1.8	0.258	2.21×10^{-9}
1	3	100	1.7	0.277	2.42×10^{-9}
2	1	134	2.5	0.266	1.96×10^{-9}
2	2	123	2.0	0.287	2.57×10^{-9}
2	3	104	1.5	0.342	2.34×10^{-9}

Eccentricity ratio could be also obtained directly by measuring the clearance or eccentricity, but the accuracy of the direct measurement seems to be doubtful, hence the above method is applied here to yield these values of k and ε, which are used for the theoretical calculation of pressure distribution for comparison with the experimental one.

(c) Experimental Results of Pressure Distribution

Figs. 3.4.6 and 3.4.7 show the experimental results of pressure distributions in the bearing clearance. In the figures, the theoretical curves are drawn calculated with the values of k and obtained by the above method.

The experimental pressure distributions agree fairly well with theoretical ones qualitatively, but for some cases, they show rather poor quantitative agreement. If one calculates the pressure distribution curves with the value of p_o just at the middle of the bearing clearance, quantitative

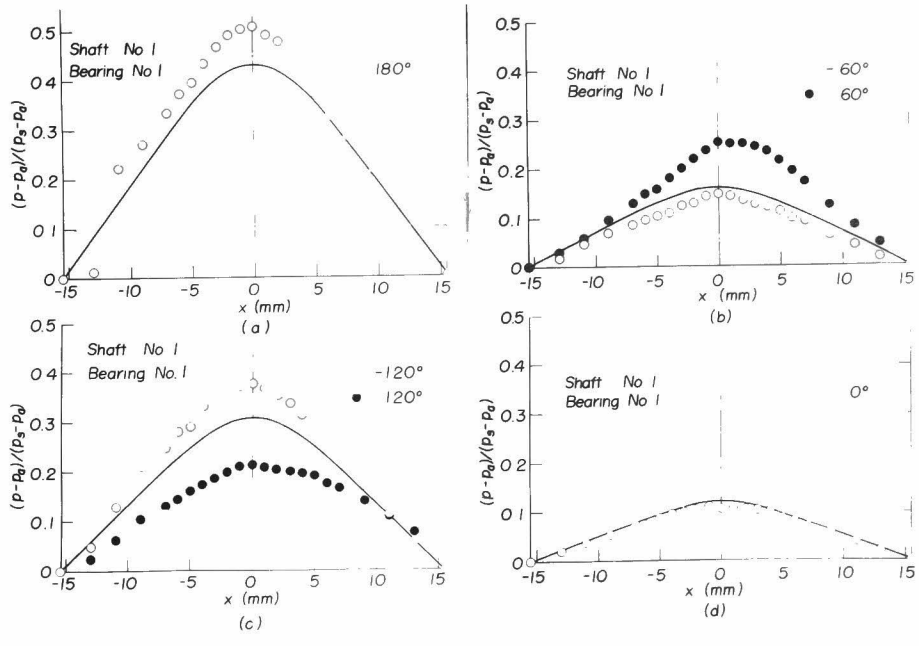

Fig. 3.4.6 Results of pressure distributions (shaft No.1 and bearing No.1)

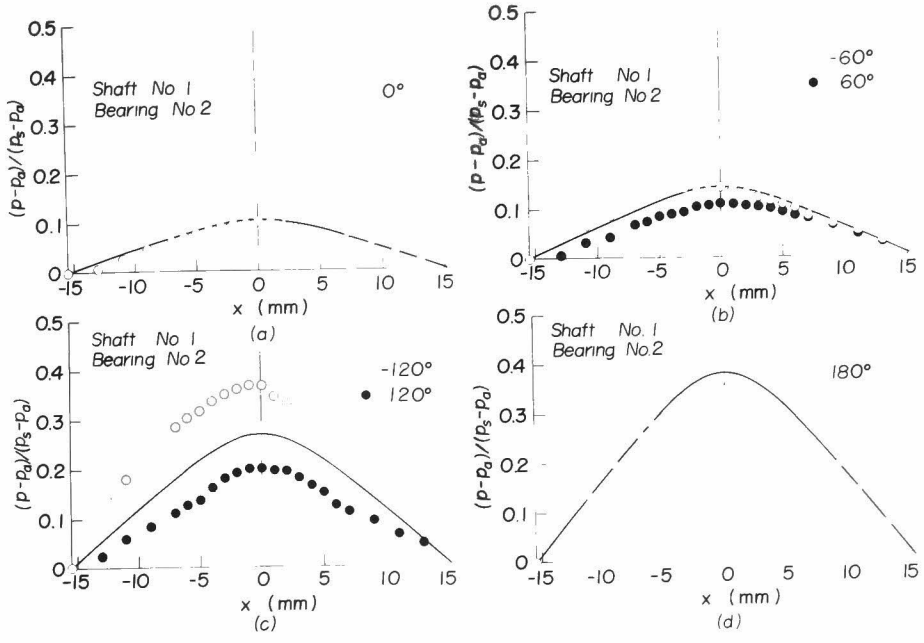

Fig. 3.4.7 Results of pressure distributions (shaft No.1 and bearing No.2)

agreement would be also obtained between theoretical and experimental results. The pressure distributions at the opposite circumferential positions (that is, at $\Theta = 60^{\circ}$ and -60°, and at $\Theta = 120^{\circ}$ and -120°) have some deviations between each other, which seems to be due to the poor roundness of the porous bushings at manufacture.

4-3 Externally Pressurized Porous Journal Gas-Bearing with Solid Sleeve-Part

The externally pressurized porous journal bearing is

very advantageous owing to its large load capacity and good stability of performance, but, in the other hand, disadvantage exists in manufacturing it within tolerable roughness and roundness of porous bearing surface. Several microns of these defects may cause to lose the good performance of the bearing.

In order to avoid this disadvantage without losing the good characteristics of porous wall, the externally pressurized porous journal gas-bearing with solid ring so-called 'sleeve' part is introduced in this section to be analyzed.

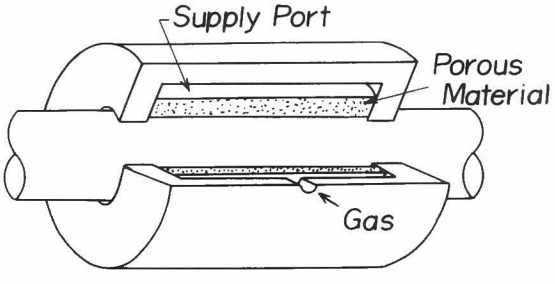

Fig. 3.4.8 Construction of porous journal gas-bearing with 'sleeve' part

Fig. 3.4.8 illustrates schematically this type of porous journal gas-bearing. Assuming that the eccentricity of the journal is so small that two-dimensional flow may be considered with neglecting the circumferential flow, unit

width of the bearing is analyzed fundamentally. Fig. 3.4.9 shows the cross-section of the bearing in which the compressed gas is supplied under pressure p_s from the back of porous bushing of breadth b and thickness t, restricted through it into recess part of clearance H, then flows between 'sleeve' part of clearance h to atmosphere. The pressures in bearing clearance and in porous material are p and p', and average axial velocities are $\bar{u}$ and $\bar{u}'$, respectively. q and q' are the flow velocities from porous material to bearing clearance and from supply port to porous material, respectively.

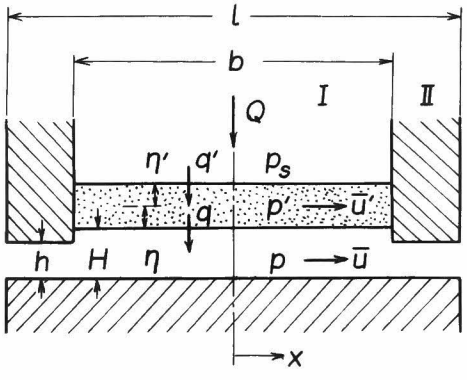

Fig. 3.4.9 Schematic diagram of the bearing

(a) Region I $\left(0 \leqq x \leqq \frac{b}{2}\right)$

In this region, the fundamental equations (3.4.1)-(3.4.6) are valid, hence the pressure distributions p and p' are governed by the following differential equations,

$$\left.\begin{aligned} \frac{d^2p'}{dx^2} &= A'^2p' - B'^2p - C' \\ \frac{d^2p}{dx^2} &= D'^2(p - p') \end{aligned}\right\} \qquad (3.4.38)$$

where

$$A'^2 = \frac{1}{\eta t} + \frac{1}{\eta' t}\ ,\quad B'^2 = \frac{1}{\eta t}\ ,\quad C' = \frac{p_s}{\eta t}\ ,\quad D'^2 = \frac{h'^3}{H^3 \eta t} \qquad (3.4.39)$$

Solving these equations under a boundary condition of

$$\frac{dp}{dx} = \frac{dp'}{dx} = 0 \qquad \text{at} \qquad x = 0 \qquad (3.4.40)$$

resulting

$$p_I = M_1 \cosh \alpha_1 x + M_2 \cosh \alpha_2 x + p_s \qquad (3.4.41)$$

$$p'_I = N_1 \cosh \alpha_1 x + N_2 \cosh \alpha_2 x + p_s \qquad (3.4.42)$$

where α_1 and α_2 are constants determined by design parameters and given by Eq. (3.4.25). M_1, M_2, N_1 and N_2 are integral constants having the relationships of

$$\frac{M_1}{N_1} = \frac{A'^2 - \alpha_1^2}{B'^2}\ ,\qquad \frac{M_2}{N_2} = \frac{A'^2 - \alpha_2^2}{B'^2} \qquad (3.4.43)$$

The volume rate of flow is

$$\frac{Q}{2} = \int_0^{\frac{b}{2}} q'\, dx$$

$$= -\frac{h'^3}{12\mu\eta' t}\left[\frac{N_1}{\alpha_1}\sinh\frac{\alpha_1 b}{2} + \frac{N_2}{\alpha_2}\sinh\frac{\alpha_2 b}{2}\right] \qquad (3.4.44)$$

(b) Region II $\left(\frac{b}{2} \leqq x \leqq \frac{\ell}{2}\right)$

In this region, the flow is considered as that between two-parallel surfaces. Then, from the continuity condition,

$$\frac{Q}{2} = -\frac{h^3}{12\mu}\frac{dp}{dx} \qquad (3.4.45)$$

Integrating this by x,

$$p = \frac{1}{h^3}(C_1 - 6\mu Q x) \qquad (3.4.46)$$

where C_1 is integral constant determined by a boundary condition of

$$p = p_a \quad \text{at} \quad x = \frac{\ell}{2} \qquad (3.4.47)$$

resulting

$$C_1 = 3\mu Q\ell + h^3 p_a \qquad (3.4.48)$$

The pressure distribution p becomes

$$p_{II} = \frac{6\mu Q}{h^3}\left(\frac{\ell}{2} - x\right) + p_a \qquad (3.4.49)$$

(c) Connection of Region I and II

The unknown constants M_1 and M_2 (or N_1 and N_2) can be determined by the following boundary conditions

$$\left.\begin{array}{ll} \text{(i)} & p_I = p_{II} \quad \text{at} \quad x = \frac{b}{2} \\ \text{(ii)} & \frac{dp_I}{dx} = 0 \quad \text{at} \quad x = \frac{b}{2} \end{array}\right\} \qquad (3.4.50)$$

The pressure distributions can be given by Eqs. (3.3.41), (3.4.42) and (3.4.49) for each region with determined constants.

(d) Load Capacity

Load capacity ΔW for unit breadth of the bearing is obtained by the integration of pressure p with respect to the regions, namely

$$\Delta W = \Delta W_{I} + \Delta W_{II} \tag{3.3.51}$$

where

$$\Delta W_{I} = 2\int_{0}^{\frac{b}{2}} (p_{I} - p_{a})dx$$

$$= \frac{2M_{1}}{\alpha_{1}} \sinh\frac{\alpha_{1}b}{2} + \frac{2M_{2}}{\alpha_{2}} \sinh\frac{\alpha_{2}b}{2} + b(p_{s} - p_{a}) \tag{3.3.52}$$

$$\Delta W_{II} = 2\int_{\frac{b}{2}}^{\frac{\ell}{2}} (p_{II} - p_{a})dx$$

$$= \frac{6\mu Q}{h^{3}} \left(\frac{\ell}{2} - \frac{b}{2}\right)^{2} \tag{3.4.53}$$

4-4 Load Capacity

The load capacity supported by an externally pressurized porous journal gas-bearing is obtained by the integration of the vertical component of ΔW of Eq. (3.4.33) or (3.3.51) around the bearing surface assuming that the eccentricity ratio is small so that the circumferential flow may be neglected.

The load capacity for a small breadth of bearing, ΔW, can be given by Eq. (3.3.33) or (3.3.51) which is a function directly of $1/\beta$ and independent on the values of $\hbar$ and $\hbar'$. The calculation of ΔW versus $1/\beta$ is fairly complicated, but it is found that ΔW may be expressed by the following equation approximately,

$$\frac{\Delta W}{P_s - P_a} = \frac{a_1}{b_1 + (1/\beta)^3} + \frac{a_2}{b_2 + (1/\beta)^2} \qquad (3.3.54$$

where a_1, a_2, b_1 and b_2 are constants particular to each bearing configuration obtained from $\Delta W/(P_s - P_a) \sim 1/\beta$ figures. $1/\beta$ is expressed as

$$\frac{1}{\beta} = \frac{1}{\beta_o}(1 + \varepsilon \cos\theta) \qquad (3.4.55$$

where ε is eccentricity ratio and θ is circumferential angle from the position of maximum bearing clearance. β_o shows the value of β at $\varepsilon = 0$ and it corresponds to the radial bearing clearance.

Total load capacity W can be obtained by

$$W = (P_s - P_a)\int_o^{2\pi} \frac{\Delta W}{P_s - P_a}(-\cos\theta) r\, d\theta$$

$$= (P_s - P_a)\int_o^{2\pi} \left[\frac{a_1}{b_1 + (1/\beta)^3} + \frac{a_2}{b_2 + (1/\beta)^2}\right](-\cos\theta) r\, d\theta \qquad (3.4.56$$

where r is journal radius.

By using Eq. (3.3.55),

$$W = (p_s - p_a)(-2r)\left[\frac{a_1 B_1}{b_1}\int_0^{\pi}\frac{\cos\theta\, d\theta}{B_1+(1+\varepsilon\cos\theta)^3} + \frac{a_2 B_2}{b_2}\int_0^{\pi}\frac{\cos\theta\, d\theta}{B_2+(1+\varepsilon\cos\theta)^2}\right] \qquad (3.4.57)$$

where

$$B_1 = b_1\beta_o^3$$
$$B_2 = b_2\beta_o^2 \qquad (3.3.58)$$

(i) Integration of the First Term

By the transformation of variable of

$$\tan\frac{\theta}{2} = t \qquad (3.4.59)$$

and hence

$$\cos\theta = \frac{1-t^2}{1+t^2}, \qquad d\theta = \frac{2}{1+t^2}\,dt$$

then the integration of the first term of Eq. (3.3.57) becomes

$$\int_0^{\pi}\frac{\cos\theta}{B_1+(1+\varepsilon\cos\theta)^3}d\theta = \int_0^{\infty}\frac{2(1-t^2)(1+t^2)}{B_1(1+t^2)^3+[1+t^2+\varepsilon(1-t^2)]^3}\,dt \qquad (3.4.60)$$

The integrand can be separated into the following partial fractions

$$\frac{2(1-t^2)(1+t^2)}{B_1(1+t^2)^3+[1+t^2+\varepsilon(1-t^2)]^3} = \frac{2}{K_1}\left[\frac{P_1}{t^2+L_1} + \frac{S_1 t+T_1}{t^2-Q_1 t+R_1} + \frac{-S_1 t+T_1}{t^2+Q_1 t+R_1}\right] \qquad (3.4.61)$$

where

$$K_1 = B_o^3 + (1-\varepsilon)^3$$
$$L_1 = \frac{B_o+(1+\varepsilon)}{B_o+(1-\varepsilon)}$$
$$P_1 = -\frac{1}{3\varepsilon B_o^2}\left[B_o^3+\varepsilon B_o^2-\varepsilon(1-\varepsilon)B_o+(1-\varepsilon)^2\right] \qquad (3.4.62)$$

$$R_1 = \left[\frac{B_0^2 - (1+\varepsilon)B_0 + (1+\varepsilon)^2}{B_0^2 - (1-\varepsilon)B_0 + (1-\varepsilon)^2}\right]^{\frac{1}{2}}$$

$$Q_1 = \left[2R_1 - \frac{2\{B_0^2 - B_0 + (1-\varepsilon^2)\}}{B_0^2 - (1-\varepsilon)B_0 + (1-\varepsilon)^2}\right]^{\frac{1}{2}}$$

$$S_1 = -\frac{P_1 + T_1 + 1}{2Q_1}$$

$$T_1 = \frac{B_0^3 + (3-\varepsilon)\varepsilon B_0 + (1-\varepsilon^2)}{6\varepsilon B_0 R_1}$$

in which

$$B_0 \equiv B_1^{\frac{1}{3}} = \sqrt[3]{b_1}\beta_0 \tag{3.4.63}$$

The integrations of each term with t are as follows

$$\left.\begin{aligned}
I_0 &= \int_0^\infty \frac{dt}{t^2 + L_1} = \frac{\pi}{2\sqrt{L_1}} \\
I_1 &= \int_0^\infty \frac{t\,dt}{(t - Q_1/2)^2 + R_1 - Q_1^2/4} \\
&= \frac{1}{2}\left[\log(t^2 - Q_1 t + R_1) + \frac{Q_1/2}{\sqrt{R_1 - Q_1^2/4}} \tan^{-1}\frac{t - Q_1/2}{\sqrt{R_1 - Q_1^2/4}}\right]_0^\infty \\
I_2 &= \int_0^\infty \frac{t\,dt}{(t + Q_1/2)^2 + R_1 - Q_1^2/4} \\
&= \frac{1}{2}\left[\log(t^2 + Q_1 t + R_1) + \frac{Q_1/2}{\sqrt{R_1 - Q_1^2/4}} \tan^{-1}\frac{t + Q_1/2}{\sqrt{R_1 - Q_1^2/4}}\right]_0^\infty \\
I_3 &= \int_0^\infty \frac{dt}{(t - Q_1/2)^2 + R_1 - Q_1^2/4} = \frac{1}{\sqrt{R_1 - Q_1^2/4}}\left[\frac{\pi}{2} + \tan^{-1}\frac{Q_1/2}{\sqrt{R_1 - Q_1^2/4}}\right] \\
I_4 &= \int_0^\infty \frac{dt}{(t + Q_1/2)^2 + R_1 - Q_1^2/4} = \frac{1}{\sqrt{R_1 - Q_1^2/4}}\left[\frac{\pi}{2} - \tan^{-1}\frac{Q_1/2}{\sqrt{R_1 - Q_1^2/4}}\right]
\end{aligned}\right\} \tag{3.4.64}$$

Then, the integration of Eq. (3.4.60) is

$$\int_0^\infty \frac{2(1-t^2)(1+t^2)}{B_1(1+t^2)^3 + [1+t^2+\varepsilon(1-t^2)]^3}\,dt$$

$$= \frac{2}{K_1}\left[P_1 I_0 + S_1(I_1 - I_2) + T_1(I_3 + I_4)\right]$$

$$= \frac{\pi}{K_1}\left[\frac{P_1}{\sqrt{L_1}} + \frac{Q_1 S_1 + 2T_1}{\sqrt{R_1 - Q_1^2/4}}\right] \qquad (3.4.65)$$

(ii) Integration of the Second Term

By using the same transformation of variable, $\tan\frac{\theta}{2} = t$, the integration of the second term of Eq. (3.4.57) becomes

$$\int_0^{\pi} \frac{\cos\theta}{B_2 + (1+\varepsilon\cos\theta)^2}\, d\theta = \int_0^{\infty} \frac{2(1-t^2)}{B_2(1+t^2)^2 + [1+t^2+\varepsilon(1-t^2)]^2}\, dt \qquad (3.4.66)$$

The denominator of integrand has no terms of t and t^3, and its characteristic value with respect to t^2 is minus, then the integrand can be separated into the following partial fractions

$$\frac{2(1-t^2)}{B_2(1+t^2)^2 + [1+t^2+\varepsilon(1-t^2)]^2} = \frac{1}{B_2 + (1-\varepsilon)^2}\left[\frac{S_2 t + T_2}{t^2 - Q_2 t + R_2} + \frac{-S_2 t + T_2}{t^2 + Q_2 t + R_2}\right] \qquad (3.3.67)$$

where

$$\left.\begin{aligned} Q_2 &= \left[2R_2 - \frac{2\{\kappa^2 B_0^2 + (1-\varepsilon^2)\}}{\kappa^2 B_0 + (1-\varepsilon)^2}\right]^{\frac{1}{2}} \\ R_2 &= \left[\frac{\kappa^2 B_0^2 + (1+\varepsilon)^2}{\kappa^2 B_0^2 + (1-\varepsilon)^2}\right]^{\frac{1}{2}} \\ S_2 &= -\frac{1}{2Q_2}\left(1 + \frac{1}{R_2}\right) \\ T_2 &= \frac{1}{2R_2} \end{aligned}\right\} \qquad (3.4.68)$$

in which

$$\kappa = \frac{B_2^{\frac{1}{2}}}{B_1^{\frac{1}{3}}} = \frac{b_2^{\frac{1}{2}}}{b_1^{\frac{1}{3}}} \tag{3.3.69}$$

or

$$\kappa B_0 = B_2^{\frac{1}{2}} = \sqrt{b_2}\,\beta_0$$

By using the same integrations of each term of Eqs. (3.4.67), the integral of Eq. (3.4.66) is

$$\int_0^{\pi} \frac{\cos\theta}{B_2+(1+\varepsilon\cos\theta)^2}\,d\theta = \frac{\pi}{B_2+(1-\varepsilon)^2}\left[\frac{S_2Q_2+2T_2}{\sqrt{R_2-Q_2^2/4}}\right] \tag{3.4.70}$$

Then, the total load capacity is obtained as follows;

$$\begin{aligned} W &= (p_s-p_a)\int_0^{2\pi}\left[\frac{a_1}{b_1+(1/\beta)^3}+\frac{a_2}{b_2+(1/\beta)^2}\right](-\cos\theta)\,r\,d\theta \\ &= -2r(p_s-p_a)\left\{\frac{a_1B_0^3}{b_1}\cdot\frac{\pi}{B_0^3+(1-\varepsilon)^3}\left[\frac{P_1}{\sqrt{L_1}}+\frac{S_1Q_1+2T_1}{\sqrt{R_1-Q_1^2/4}}\right]\right. \\ &\qquad \left.+\frac{a_2\kappa^2B_0^2}{b_2}\cdot\frac{\pi}{\kappa^2B_0^2+(1-\varepsilon)^2}\cdot\frac{S_2Q_2+2T_2}{\sqrt{R_2-Q_2^2/4}}\right\} \end{aligned} \tag{3.4.71}$$

The symbols are notated in the above.

The load capacity can be calculated for any eccentricity ratio ε by using the design parameters B_0 and κ .

The load capacity for a small width of bearing ΔW may be generally approximated by Eq. (3.4.54) with two terms. In the followings, two special cases are calculated in which ΔW is approximated by only one term of cubic or square fractional expression of $1/\beta$ as

$$\Delta W_1 = (p_s-p_a)\cdot\frac{a_1}{b_1+(1/\beta)^3}$$

$$\Delta W_2 = (p_s - p_a)\cdot\frac{a_2}{b_2+(1/\beta)^2} \qquad (3.4.72)$$

respectively. Then the load capacities of journal bearing are respectively

$$\left.\begin{aligned} W_1 &= -2\pi r(p_s-p_a)\cdot\frac{a_1}{b_1}\cdot\frac{B_o^3}{B_o^3+(1-\varepsilon)^3}\left[\frac{P_1}{\sqrt{L_1}}+\frac{Q_1S_1+2T_1}{\sqrt{R_1-Q_1^2/4}}\right] \\ W_2 &= -2\pi r(p_s-p_a)\cdot\frac{a_2}{b_2}\cdot\frac{\kappa^2B_o^2}{\kappa^2B_o^2+(1-\varepsilon)^2}\cdot\frac{Q_2T_2-2T_2}{\sqrt{R_2-Q_2^2/4}} \end{aligned}\right\} \qquad (3.4.73)$$

In these equations, the terms of $(p_s-p_a)\cdot a_1/b_1$ and $(p_s-p_a)\cdot a_2/b_2$ are the values of ΔW_1 and ΔW_2 respectively at $1/\beta = 0$ or no radial clearance. The load capacity are calculated in dimensionless forms of load capacity as

$$\left.\begin{aligned} F_{W_1} &= \frac{W_1}{2\pi r(p_s-p_a)\cdot a_1/b_1} \\ F_{W_2} &= \frac{W_2}{2\pi r(p_s-p_a)\cdot a_2/b_1} \end{aligned}\right\} \qquad (3.4.74)$$

in which $2\pi r(p_s-p_a)\cdot a_j/b_j$ are the load by the above ΔW_1 or ΔW_2 at no radial clearance all over the journal.

Figs. (3.4.10) and (3.4.11) shows the theoretical load capacity against the accentircity ratio ε for various values of B_o or κB_o for each case respectively.

The bearing stiffness near non-eccentric state is important at the bearing design. The stiffness is defined by $\partial W/\partial\varepsilon$, hence it can be obtained as the tangent of the curves on W (or F_w)-ε plane. The case of $B_o = 1.0$ or $\kappa B_o = 1.0$ has maximum tangent or maximum stiffness near the origin

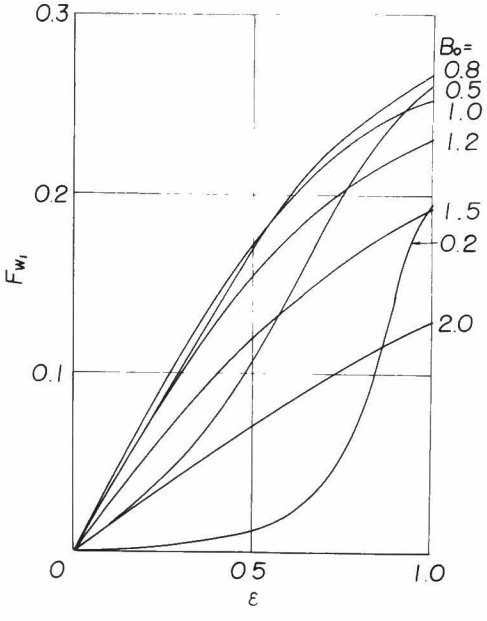

Fig. 3.4.10 Theoretical load capacity by approximation of cubic fractional expression of $1/\beta$

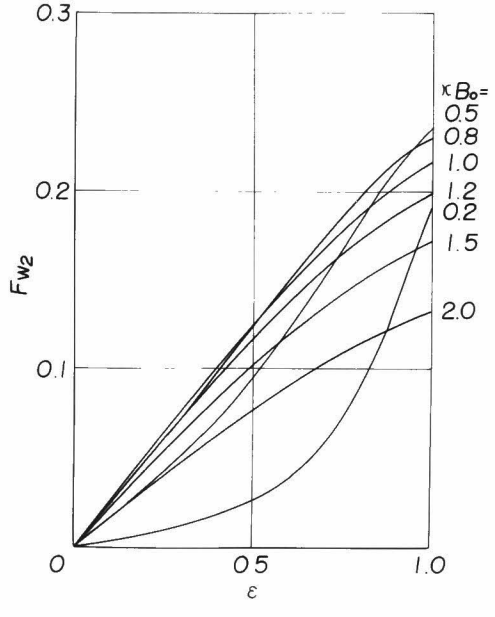

Fig. 3.4.11 Theoretical load capacity by approximatior of square fractional expression of $1/\beta$

in both of the figures. This can be also derived theoretically as shown in Appendix XV.

In the practical porous journal bearings, ΔW can be approximated by Eq. (3.4.54), and hence the characteristics of them may be between of these special cases. At the bearing design, $1/\beta_0$, which corresponds to the radial clearance, should be chosen so that B_0 and κB_0 may be nearly unity.

Chapter 5 Conclusion

In Part III, the externally pressurized porous thrust and journal gas-bearings are analyzed theoretically which may have a good bearing performances of large load capacity and stable working owing to the mesh structure of bearing surface.

The analysis yields theoretical pressure distribution, volume rate of flow and load capacity. The permeability coefficient which identifies the characteristics of the porous material is used assuming that Darcy's law may be applicable to the flow in it. Then the equivalent clearance h' and effective restricting thicknesses η and η' are introduced so that the flow in porous gas-bearing may be considered as two fundamental parallel flows in the

porous material and in the bearing clearance connected with each other.

These results are applied to the investigation of externally pressurized porous thrust and journal gas-bearings with solid part so-called 'flange' or 'sleeve', which are introduced to avoid the disadvantage due to the roughness of the porous wall at the manufacture, without losing their good characteristics of performance.

Experiments are made to investigate theoretical results. The results of experimental pressure distribution have shown very good conformity to the theory not only qualitatively but quantitatively for several gas-bearing configurations. The permeability coefficient used in the calculation of theoretical curve can be measured for the thrust bearing based on the condition of pressure, Reynolds number and so on, under which the bearing will actually work. But, for the journal bearing, the coefficient as well as eccentricity ratio is presumed from the results of circumferential pressure distribution.

Load capacity for the thrust bearing is also experimented resulting good agreement with theoretical one.

These results may verify the theory very well.

It should be noted that the theory with the effective

restricting thicknesses η and η' to be about 0.5t coincide well with ones from an analytical solution on a theoretical standpoint in which the flow condition in the bearing clearance is taken into consideration as a boundary value of the three-dimensional flow in porous media(8)

These factors of η and η', and permeability coefficient, however, may involve several problems yet to be studied.

Conclusions

The externally pressurized gas-bearings of several configurations are investigated theoretically.

The complex potential theory is applied conveniently to analyze the thrust gas bearing with multiple supply holes of circular thrust type, thrust collar type and rectangular thrust pad type. Pressure distributions are obtained from the appropriate complex potential functions which satisfy the boundary conditions for each configuration, then integration and gradient of it result in theoretical load capacity and volume rate of flow. The bearing characteristics are shown in design charts.

Externally pressurized thrust collar bearings with single and double slit-supplies are investigated theoretically yielding the optimum dimensions of slit-supplies, load capacity and volume rate of flow.

A new concept of the flow model is applied to the analysis of externally pressurized porous gas-bearings of thrust and journal types. Equivalent clearance and effective restricting thickness are introduced so that the flow in the porous media may be considered as two parallel flows connected each other. Then the pressure distribution, load capacity and volume rate of flow are obtained theoretically.

Theoretical results are investigated experimentally, and good conformity observed between them verifies the theory

Acknowledgements

The author wishes to express his sincerest appreciation to Dr. H. Mori, Professor of Mechanical Engineering, Kyoto University, Japan, for his valuable guidances and suggestions throughout this entire investigation.

All analyses and experiments were supported by research funds from the Ministry of Education of the Japanese Government, and done at the Lubrication Laboratory in the Department of Mechanical Engineering, Kyoto University, Japan.

The author would like to thank the staff of the Lubrication Labratory, in particular, Messrs. T. Ono, T. Yamamotc, H. Yamada and K. Onishi, who were engineering students at that time, for their great help during the conduct of experiments.

Notation

Part I

A, A' : functions of r defined in the body

A_0, A_1, A_s, A_s' : constants defined in the body

a : position of supply hole

a_x, a_y : x-and y-component of a, respectively

B : breadth of rectangular bearing

B_j : function of Θ defined in the body

f_Q : coefficient of volume rate of flow with respect to $(p_o - p_a)$

f_W : coefficient of load capacity with respect to $(p_o - p_a)$

h : bearing clearance

i : unit of imaginary number

J : momentum of fluid

j : integer

K_1, K_2 : constants

k : number of supply holes

k' : number of supply holes in an array

L : length of rectangular bearing

l_e : entrance length

m : integer

n : polytrotic index

P : modified pressure

p : pressure, absolute

p_a : ambient pressure, absolute

p_o : pressure just after supply hole, absolute

p_o', p_o'' : pressure just after supply hole with consideration of pressure fall

Q : volume rate of flow

q : strength of source and sink

R : dimensionless radius with respect to r_i (r/r_i)

R_a, R_o, R_s : a/r_i, r_o/r_i, r_s/r_i, respectively

R_e : Reynolds number

r : radius

r_o : radius to bearing inner periphery

r_i : radius to bearing outer periphery

r_s : radius of supply hole

S : area enclosed by a constant pressure line

U_x, U_y : sliding velocity in x and y directions

u : flow velocity

u_m : flow velocity from supply hole to bearing clearance

u_o : flow velocity at the middle plane of bearing clearance

$\bar{u}$: average flow velocity

W : load capacity

w : complex potential function

x, y, z : coordinates

Z : complex number

α : integer

β, β' : integer

δ : thickness of boundary layer

Θ : argument

Θ_k : angular spacing

$2\Theta_v$: vertical angle of conical bearing

λ : coefficient of pressure fall at supply hole

μ : coefficient of viscosity

ρ : density

σ $= r/\bar{a}$

τ_b : frictional stress at bearing wall

Φ : function

ϕ : function of p defined in the body

Ψ_0, Ψ_1 : functions

Subscripts

0 : inner edge of thrust collar

1 : outer edge of thrust collar

(k) : k supply holes

s : supply

Superscripts

$*$: modified

$-$: conventional for obtaining load capacity

$\sim$: conjugate

$'$, $''$: with considering secondary effects at supply ho

Part II

a : radius to slit-supply

b_s : width of slit

C_1, C_2 : constants

F_Q, f_Q : dimensionless volume rate of flow with respect to $(p_s - p_a)$ and $(p_o - p_a)$, respectively

F_W, f_W : dimensionless load capacity with respect to $(p_s - p_a)$ and $(p_o - p_a)$, respectively

h : bearing clearance

ℓ_s : length of slit

P : modified pressure

p : pressure, absolute

p_a : ambient pressure, absolute

p_o : pressure just after slit-supply, absolute

p_s : supply pressure, absolute

p_W : specific load

Q : volume rate of flow

R : dimensionless radius with respect to r_i (r/r_i)

R_o, R_a : r_o/r_i , a/r_i , respectively

r : radius

r_o : radius to bearing inner periphery

r_i : radius to bearing outer periphery

S : area enclosed by a constant pressure line

$\bar{u}$: average flow velocity

W : load capacity

λ : coefficient of pressure fall at supply-slit

μ : coefficient of viscosity

ξ : arbitrary constant

ρ : density

Φ : function

Subscripts

I, II, III : at region I, II and III, respectively

0 : inner

1 : outer

$''$: with considering secondary effects at supply-slit

B : corresponding to point B (limiting case of double slits to single one)

M : corresponding to point M (minimum flow rate)

Part III

A' : constant defined in the body

a_1, a_2 : constants

B, B', C, C', D' : constant defined in the body

B_0 : design parameter defined in the body

B_1, B_2 : $b_1\beta_0^3$ and $b_2\beta_0^2$, respectively

b : width of supply slit

b_1, b_2 : constants

C_1 : constant of integration

c, c' : effective restricting thickness coefficients

C_r : radial clearance

E, F
$G_1 \sim G_4$: constants of integration

H : bearing clearance at recess

h : bearing clearance

h' : equivalent clearance

I, K : modified Bessel function

$I_0 \sim I_4$: integration

K_1, K_2 : constants

k : permeability coefficient

L_1, L_2 : constants

l : length of journal bearing

M, N : arbitrary constants

n : polypropic index

P_1, P_2, Q_1
Q_2, R_1, R_2 : constants
S_1, S_2, T_1
T_2

p : pressure in bearing clearance, absolute

p' : pressure in porous bearing, absolute

p_a : ambient pressure, absolute

p_s : supply pressure, absolute

Q : volume rate of flow

q : flow velocity from porous bearing into bearing clearance

q' : flow velocity from supply port into porous bearing

r : radius

r_o : radius to bearing inner periphery

r_i : radius to bearing outer periphery

r_f : radius to flange

r_s : radius to supply port

t : actual thickness of porous bearing

τ : variable (in Section 4-4)

$\bar{u}$: average velocity of radial flow in bearing clearance

$\bar{u}'$: average velocity of radial flow in porous bearing

W : load capacity

ΔW : load capacity for unit breadth of journal bearing

$\alpha_o, \alpha_1, \alpha_2$: constants defined in the body

β : h'/h or h'/H

β_o : value of β corresponding to non-eccentric state

ε : eccentricity ratio

η, η' : effective restricting thicknesses

κ : parameter

μ : coefficient of viscosity

Subscripts

I, II, III : at region I, II, and III, respectively

o : inner

1 : outer

Appendices

Appendix I

By de Moivre's theorem, the following equation can be obtained

$$x^k - y^k e^{-ik\theta} = x^k - (ye^{-i\theta})^k$$

$$= \prod_{j=0}^{k-1} (x - \omega_j y e^{-i\theta}) \qquad \text{(A.1)}$$

where

$$\omega_j = e^{i\frac{2\pi j}{k}} = e^{i\theta_j} \qquad : \text{ roots of } x^k - 1 = 0$$

Square of absolute value of Eq. (A.1) is as follows:

$$|x^k - y^k e^{-ik\theta}|^2 = [x^k - y^k \cos(-k\theta)]^2 + y^{2k} \sin^2(-k\theta)$$

$$= x^{2k} + y^{2k} - 2x^k y^k \cos k\theta$$

$$|x - \omega_j y e^{-i\theta}|^2 = |x - y^{i(\theta_j - \theta)}|^2$$

$$= x^2 + y^2 - 2xy\cos(\theta_j - \theta)$$

$$= x^2 + y^2 - 2xy\cos(\theta - \theta_j)$$

Thus

$$\log[x^{2k} + y^{2k} - 2x^k y^k \cos k\theta] = \sum_{j=0}^{k-1} \log[x^2 + y^2 - 2xy\cos(\theta - \theta_j)] \qquad \text{(A.2)}$$

Substituting $x = R_a R$ and $y = 1$, or $x = R$ and $y = R_a$, then Eq. (1.3.6) can be obtained.

Appendix II

From Eq. (1.3.9)

$$d\phi = \frac{1}{K_1}\exp\left(\frac{p-K_2}{K_1}\right)dp = \frac{\phi}{K_1}dp \qquad (A.3)$$

Then, letting $\phi_o = \exp\left(\frac{p_o - K_2}{K_1}\right) = \left[\frac{1-R_s(R_a-R_s)}{R_s}\right]^2$, the load capacity is

$$\begin{aligned} W_{(1)} &= \pi r_i^2 (1-R_a^2)^2 \int_{p_a}^{p_o} \frac{\phi\, dp}{(\phi - R_a^2)^2} \\ &= \pi r_i^2 K_1 (1-R_a^2)^2 \int_{p=p_a}^{p=p_o} \frac{d\phi}{(\phi - R_a^2)^2} \\ &= -\pi r_i^2 K_1 (1-R_a^2)^2 \left[\frac{1}{\phi - R_a^2}\right]_{\phi=1}^{\phi=\phi_o} \\ &= \pi r_i^2 K_1 (1-R_a^2)(\phi_o - 1)/(\phi_o - R_a^2) \\ &= \pi r_i^2 K_1 (1-R_a^2)\{1-(R_a-R_s)^2\}/\{1-R_a(R_a-2R_s)\} \end{aligned} \qquad (A.4)$$

Appendix III

From Eqs. (1.3.2), 1.3.12), and (1.3.14)

$$\begin{aligned} W_{(1)} &= \int_0^{r_1}\int_0^{2\pi} (p-p_a)\, r\, dr\, d\theta \\ &= \int_{R=0}^{R=1}\int_{\theta=0}^{\theta=2\pi} K_1 \log\frac{R_a^2R^2 + 1 - 2R_aR\cos\theta}{R^2 + R_a^2 - 2R_aR\cos\theta}\, r_i dR \cdot r_i R\, d\theta \\ &= \pi r_i^2 K_1 (1-R_a^2)[1-(R_a-R_s)^2]/[1-R_a(R_a-2R_s)] \end{aligned} \qquad (A.5)$$

The load capacity for the case with multiple supply holes is obtained by using the relation of Eq. (A.5)

$$W_{(k)} = \int_{R=0}^{R=1} \int_{\theta=0}^{\theta=2\pi} K_{1(k)} \sum_{j=0}^{k-1} \log \frac{R_a^2 R^2 + 1 - 2R_a R\cos(\theta-\theta_j)}{R^2 + R_a^2 - 2R_a R\cos(\theta-\theta_j)} r_i dR \cdot r_i R d\theta$$

$$= \frac{K_{1(k)}}{K_1} \sum_{j=0}^{k-1} \int_{R=0}^{R=1} \int_{\theta=\theta_j}^{\theta=2\pi+\theta_j} K_1 \log \frac{R_a^2 R^2 + 1 - 2R_a R\cos(\theta-\theta_j)}{R^2 + R_a^2 - 2R_a R\cos(\theta-\theta_j)} r_i dR \cdot r_i R d\theta$$

$$= \frac{k K_{1(k)}}{K_1} \int_{R=0}^{R=1} \int_{\theta=0}^{\theta=2\pi} K_1 \log \frac{R_a^2 R^2 + 1 - 2R_a R\cos\theta}{R^2 + R_a^2 - 2R_a R\cos\theta} r_i dR \cdot r_i R d\theta$$

$$= \pi r_i^2 k K_{1(k)} (1 - R_a^2)[1 - (R_a - R_s)^2] / [1 - R_a(R_a - 2R_s)] \qquad (A.6)$$

Appendix IV

In order to satisfy the condition described in the body, the pressure at $R = R_a - R_s$, $\theta = 0$ must be equal to that at $R = R_a + R_s$, $\theta = 0$. Using these conditions in Eq. (1.3.19), R_a^* must satisfy the following equation,

$$K_{1(k)}^* \log \frac{R_a^{*2k}(R_a - R_s)^{2k} - 2R_a^{*k}(R_a - R_s)^k + 1}{R_a^{*2k} - 2R_a^{*k}(R_a - R_s)^k + (R_a - R_s)^{2k}} + K_{2(k)}^*$$

$$= K_{1(k)}^* \log \frac{R_a^{*2k}(R_a + R_s)^{2k} - 2R_a^{*k}(R_a + R_s)^k + 1}{(R_a + R_s)^{2k} - 2R_a^{*k}(R_a + R_s)^k + R_a^{*2k}} + K_{2(k)}^* \qquad (A.7)$$

Let $\alpha^* = (R_a - R_s)^k$, $\beta^* = (R_a + R_s)^k$

$$\frac{1 - \alpha^* R_a^{*k}}{R_a^* - \alpha^*} = \frac{1 - \beta^* R_a^{*k}}{\beta^* - R_a^{*k}}$$

or

$$(R_a^{*k})^2 - \frac{2(1 + \alpha^*\beta^*)}{\alpha^* + \beta^*} R_a^{*k} + 1 = 0 \qquad (A.8)$$

Solving this equation with respect to R_a^{*k} under $R_a^* < 1$, we can obtain Eq. (1.3.20).

Appendix V

Assuming the isothermal expansion of gas in the bearing clearance ($n=1$), the relations of Eqs. (1.2.8) and (1.2.9) are rewritten as

$$p = P^{\frac{1}{2}}, \quad p_0 = P_0^{\frac{1}{2}}, \quad p_a = P_a^{\frac{1}{2}} \tag{A.9}$$

respectively, where P's represent incompressible pressure. Using the pressure distribution for an incompressible fluid of Eq. (1.3.7), the compressible solution can be obtained as follows;

$$\begin{aligned} p &= \sqrt{K_{1(k)}\,\Phi(R,\theta) + K_{2(k)}} \\ &= \sqrt{\frac{p_0^2 - p_a^2}{\Phi(R_a - R_s, 0)}\,\Phi(R,\theta) + p_a^2} \\ &= \sqrt{(p_0 + p_a)(P - p_a) + p_a^2} \end{aligned} \tag{A.10}$$

where $$\Phi(R,\theta) = \log \frac{R_a^{2k}R^{2k} + 1 - 2R_a^k R^k \cos k\theta}{R^{2k} + R_a^{2k} - 2R_a^k R^k \cos k\theta} \tag{A.11}$$

and P is incompressible solution.

When the pressure $(P - p_a)$ in the bearing clearance is small enough compared with p_a, the pressure p can be expanded in series as

$$p - p_a = \sqrt{(p_o + p_a)(P - p_a) + p_a^2} - p_a$$

$$= \frac{p_o + p_a}{2p_a}(P - p_a) - \frac{(p_o + p_a)^2}{8p_a^3}(P - p_a)^2 - \cdots \qquad (A.12)$$

Neglecting the terms with higher order than $(P - p_a)^2$, one can approximate the compressible pressure distribution as

$$p - p_a \cong \frac{p_o + p_a}{2p_a}(P - p_a) \qquad (A.13)$$

Then, the load capacity with a compressible fluid is

$$W_{comp.} = \int_0^{r_i}\int_0^{2\pi}(p - p_a)r\,dr\,d\theta \cong \frac{p_o + p_a}{2p_a}\int_0^{r_i}\int_0^{2\pi}(P - p_a)r\,dr\,d\theta$$

$$= \frac{p_o + p_a}{2p_a} \times W_{incomp.} \qquad (A.14)$$

The error of approximation of Eq. (A.13) increases with increase of P . But, the externally pressurized thrust gas-bearing as analyzed here has the point supply holes so that higher bearing pressure may be bounded in comparatively small region near the supply holes, which shows that the approximation of load capacity of Eq. (A.14) is rather reasonable as long as the supply pressure is not so high.

Appendix VI

At section C, the momentum of the fluid for a unit breadth is as follows by considering that the flow velocity profile is uniform;

$$J_c = \int_0^h \rho u^2 dz = \rho u_m^2 h \qquad (A.15)$$

where J : momentum of the fluid

h : bearing clearance

ρ : density of the fluid

u : velocity of the fluid

u_m : average velocity at section C

z : ordinate normal to bearing surface

At section F where the fully developed flow profile may be expected, that is $u = 4u_0(1-\frac{z}{h})(\frac{z}{h})$, where u_0 is flow velocity at the middle of bearing clearance. The momentum of the fluid is

$$J_F = \int_0^h \rho u^2 dz = \int_0^h \rho\{4u_0(1-\frac{z}{h})\frac{z}{h}\}^2 dz$$

$$= \frac{8}{15}\rho u_0^2 h \qquad (A.16)$$

From the continuity of the flow,

$$\int_0^h u_m dz = \int_0^h 4u_0(1-\frac{z}{h})\frac{z}{h} dz \qquad (A.17)$$

where density change between sections C and F is neglected. Then

$$u_0 = \frac{3}{2} u_m \qquad (A.18)$$

Using this equation and the momentum equation, the pressure loss for the change of velocity profile is

$$p_o' - p_o'' = \frac{1}{\hbar}(J_F - J_c)$$

$$= \frac{1}{5}\rho u_m^2 \qquad (A.19)$$

Appendix VII

The pressure loss at supply holes due to the flow profile change is obtained in the followings with consideration of the friction loss at the entrance length. It is assumed that the fluid is incompressible because the pressure change may be comparatively small, and that the flow may be such as between two parallel surfaces though it is a radial flow from a point supply hole.

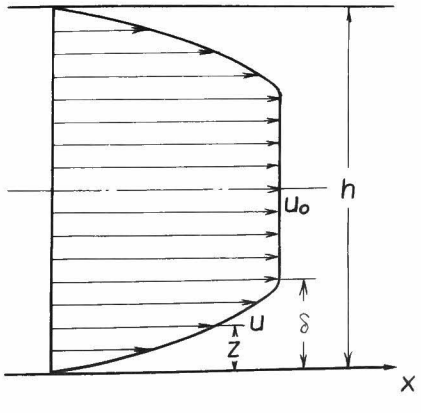

Fig. A.1 Partly developed flow pattern between two parallel surfaces

partly
In Fig. A.1 ∧ -developed flow pattern is shown in which

Z : ordinate normal to bearing surface

h : bearing clearance

δ : thickness of boundary layer

u : flow velocity of fluid

u_o : flow velocity at the middle plane of bearing clearance

Now, assuming the flow velocity distribution in the boundary layer as

$$\frac{u}{u_o} = 2\left(\frac{Z}{\delta}\right) - \left(\frac{Z}{\delta}\right)^2 \tag{A.20}$$

then, the frictional stress τ_b at the bearing surface is

$$\tau_b = \mu \left.\frac{du}{dZ}\right|_{Z=0}$$

$$= \mu \frac{2u_o}{\delta} \tag{A.21}$$

Letting $\bar{u}$ be average flow velocity,

$$\bar{u}h = 2\int_o^{\frac{h}{2}} u\,dZ$$

$$= 2\int_o^{\delta} u\,dZ + u_o(h - 2\delta)$$

$$= u_o h\left[1 - \frac{2}{3}\left(\frac{\delta}{h}\right)\right] \tag{A.22}$$

then,

$$\bar{u} = u_o\left[1-\frac{2}{3}\left(\frac{\delta}{h}\right)\right] \tag{A.23}$$

Denoting J to be momentum of the fluid which flows through any section of unit width of bearing clearance in unit time,

$$\begin{aligned} J &= \rho\int_o^h u^2\,dz \\ &= 2\rho\int_o^\delta u^2\,dz + \rho u_o^2(h-2\delta) \\ &= \rho u_o^2 h\left[1-\frac{14}{15}\left(\frac{\delta}{h}\right)\right] \end{aligned} \tag{A.24}$$

From the momentum theory along the flow direction (x-axis),

$$\frac{dJ}{dx} = -h\frac{dp}{dx} - 2\tau_b \tag{A.25}$$

Considering that the flow in the central part has a uniform velocity distribution so that the effect of viscosity may be neglected, Bernoulli's theorem can be applied

$$-\frac{1}{\rho}\frac{dp}{dx} = u_o\frac{du_o}{dx} \tag{A.26}$$

From Eqs. (A.20)-(A.26) and assuming ρ = constant, one can obtain the following differential equation:

$$\frac{d}{dx}\left\{\left(\frac{u_o}{\bar{u}}\right)^2\left[\frac{1}{2}-\frac{14}{15}\left(\frac{\delta}{h}\right)\right]\right\} = -\frac{2}{hR_e}\left(\frac{u_o}{\bar{u}}\right)\left(\frac{h}{\delta}\right) \tag{A.27}$$

where $R_e = 2h\bar{u}\rho/\mu$: Reynolds number

Integrating Eq. (A.27) by using Eq. (A.23),

$$\frac{x}{hR_e} = 1.4\frac{\delta}{h} + 4.8\log\left(1-\frac{2}{3}\frac{\delta}{h}\right) + \frac{2.7}{1-\frac{2}{3}\frac{\delta}{h}} - 2.7 \qquad (A.28)$$

where the following boundary condition is used:

$$\delta = 0 \quad \text{at} \quad x = 0 \qquad (A.29)$$

The entrance length l_e can be obtained by substituting $\delta = h/2$ into the above solution, resulting

$$\frac{l_e}{hR_e} = 0.01297 \qquad (A.30)$$

For the region of $x > l_e$, the fully viscous flow can be formed, then

$$\bar{u} = -\frac{h^2}{12\mu}\frac{dp}{dx} \qquad (A.31)$$

Integrating this under the condition that $p = p_l$ at $x = l_e$,

$$p_l - p = \frac{12\mu\bar{u}}{h^2}(x - l_e) \qquad (A.32)$$

Then

$$\frac{p_l - p}{\frac{1}{2}\rho\bar{u}^2} = \frac{48(x-l_e)}{hR_e} \qquad (A.33)$$

The equivalent pressure fall at the entrance length is

$$\frac{p_o' - p_o''}{\frac{1}{2}\rho\bar{u}^2} = 0.6226 \qquad (A.34)$$

These results are shown in chart in Fig. A.2.

When this theory is applied, the coefficient of pressure loss at supply holes is

$$\lambda = 1.623$$

For practial bearing dimensions, for example

$\bar{u}$ = 340 m/sec

h = 40 microns

ν = 0.15 cm^2/sec (air)

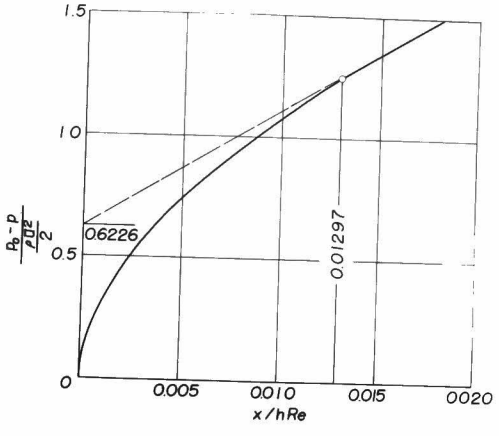

Fig. A-2. Pressure drop in entrance region with consideration of development of boundary layer

Reynolds number is

Re = 1810

The entrance length is

ℓ_e = 0.94mm

This length is fairly small compared with the diameter of supply hole so that the assumption of one dimensional flow may be reasonable.

The compressible and radial flow with consideration of the development of the boundary layer is analyzed in

Reference (9), but the entrance length cannot be calculated numerically so easily, hence this theory can be approximately applied.

Appendix VIII

Logarithmic function of complex number is calculated as follows;

$$\log(x+iy) = \frac{1}{2}\log(x^2+y^2) + i\cos^{-1}\frac{x}{\sqrt{x^2+y^2}} \qquad (A.35)$$

or $$\log(re^{i\theta}) = \log r + i(\theta + 2j\pi) \qquad (j = 0, \pm 1, \pm 2, \ldots) \qquad (A.36)$$

Using equation (A.36),

$$w_o = w(r_o e^{i\theta})$$

$$= \frac{g}{2\pi}\log\left[\sin\frac{\pi\log r_o/a}{2\log r_o/r_i}\cosh\frac{\pi(\theta+2j\pi)}{2\log r_o/r_i} + i\cos\frac{\pi\log r_o/a}{2\log r_o/r_i}\sinh\frac{\pi(\theta+2j\pi)}{2\log r_o/r_i}\right]$$

$$-\frac{g}{2\pi}\log\left[\sin\frac{\pi\log a/r_o}{2\log r_o/r_i}\cosh\frac{\pi(\theta+2j\pi)}{2\log r_o/r_i} + i\cos\frac{\pi\log a/r_o}{2\log r_o/r_i}\sinh\frac{\pi(\theta+2j\pi)}{2\log r_o/r_i}\right]$$

$$= \frac{g}{2\pi}\log\frac{\sin A_o\cosh B_j + i\cos A_o\sinh B_j}{\sin(-A_o)\cosh B_j + i\cos(-A_o)\sinh B_j}$$

$$= \frac{g}{2\pi}\log\frac{(-\sin^2 A_o\cosh^2 B_j + \cos^2 A_o\sinh^2 B_j) - 2i\sin A_o\cos A_o\sinh B_j\cosh B_j}{\sin^2 A_o\cosh^2 B_j + \cos^2 A_o\sinh^2 B_j} \qquad (A.37)$$

where

$$A_o \equiv \frac{\pi\log r_o/a}{2\log r_o/r_i}, \qquad B_j \equiv \frac{\pi(\theta+2j\pi)}{2\log r_o/r_i}$$

Using equation (A.35), real part of function w_o is as follows.

$$\mathcal{R}(w_o) = \frac{q}{4\pi} \log\left[\left(\frac{-\sin^2 A_o \cosh^2 B_j + \cos^2 A_o \sinh^2 B_j}{\sin^2 A_o \cosh^2 B_j + \cos^2 A_o \sinh^2 B_j}\right)^2 + \left(\frac{2 \sin A_o \cos A_o \sinh B_j \cosh B_j}{\sin^2 A_o \cosh^2 B_j + \cos^2 A_o \sinh^2 B_j}\right)^2\right]$$

$$= \frac{q}{4\pi} \log(1) = 0 \qquad \text{(A.38)}$$

Thus w_o has only imaginary part determined by A_o and B_j.

Appendix IX

Similarly

$$w_1 = w(r_1 e^{i\theta})$$

$$= \frac{q}{2\pi} \log\left[\sin \frac{\pi \log r_1/a}{2 \log r_o/r_1} \cosh \frac{\pi(\theta + 2j\pi)}{2 \log r_o/r_1} + i \cos \frac{\pi \log r_1/a}{2 \log r_o/r_1} \sinh \frac{\pi(\theta + 2j\pi)}{2 \log r_o/r_1}\right]$$

$$- \frac{q}{2\pi} \log\left[\sin \frac{\pi \log (ar_1/r_o^2)}{2 \log r_o/r_1} \cosh \frac{\pi(\theta + 2j\pi)}{2 \log r_o/r_1} + i \cos \frac{\pi \log (ar_1/r_o^2)}{2 \log r_o/r_1} \sinh \frac{\pi(\theta + 2j\pi)}{2 \log r_o/r_1}\right]$$

$$\sin \frac{\pi \log (ar_1/r_o^2)}{2 \log r_o/r_1} = \sin\left[\frac{\pi \log a/r_1}{2 \log r_o/r_1} - \pi\right] = \sin \frac{\pi \log r_1/a}{2 \log r_o/r_1}$$

$$\cos \frac{\pi \log (ar_1/r_o^2)}{2 \log r_o/r_1} = -\cos \frac{\pi \log r_1/a}{2 \log r_o/r_1} \qquad \text{(A.39)}$$

Putting A_1 to be

$$A_1 \equiv \frac{\pi \log (r_1/a)}{2 \log (r_o/r_1)}$$

Using Eq. (A.35) and the above equations, one obtains

$$w_1 = \frac{g}{2\pi} \log \frac{\sin A_1 \cosh B_j + i \cos A_1 \sinh B_j}{\sin A_1 \cosh B_j - i \cos A_1 \sinh B_j}$$

$$= \frac{g}{2\pi} \log \frac{(\sin^2 A_1 \cosh^2 B_j - \cos^2 A_1 \sinh^2 B_j) + 2i \cos A_1 \sin A_1 \cosh B_j \sinh B_j}{\sin^2 A_1 \cosh^2 B_j + \cos^2 A_1 \sinh^2 B_j}$$

$$= i \frac{g}{2\pi} \Psi_1(A_1, B_j) \qquad (A.40)$$

Appendix X

(i) $\sigma \equiv \frac{r}{\bar{a}} > 1$ or $r > \bar{a}$

Consider the complex integral of $\overline{w}(Z)$ on the contour Γ as shown in Fig. A.3, where

$$\overline{w}(Z) = \frac{\log(\sigma - Z)}{Z} \qquad (A.41)$$

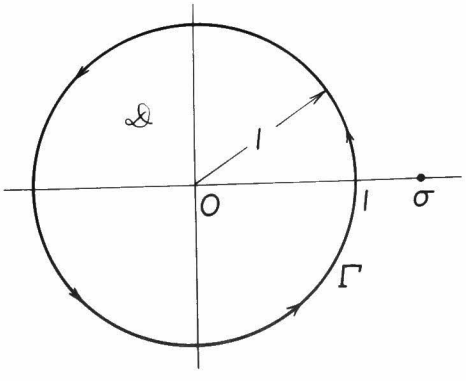

Fig. A.3 Contour of complex integral ($\sigma > 1$)

$\overline{w}(z)$ is analytical in the domain $\mathcal{D}$ enclosed by the circ except at the origin, where $\overline{w}(z)$ has an isolated singulari whose residue is calculated as

$$\lim_{z\to 0} z\,\overline{w}(z) = \log\sigma \tag{A.42}$$

Then, by the theorem of complex integral

$$\oint_\Gamma \overline{w}(z)\,dz = 2\pi i \log\sigma \tag{A.43}$$

The left-hand side of this equation is

$$\oint_\Gamma \overline{w}(z)\,dz = \oint_\Gamma \frac{\log(\sigma - z)}{z}\,dz = \int_0^{2\pi} \frac{\log(\sigma - e^{i\theta})}{e^{i\theta}} \cdot e^{i\theta} \cdot i\,d\theta$$

$$= i\int_0^{2\pi} \left\{ \frac{1}{2}\log\left[(\sigma-\cos\theta)^2 + \sin^2\theta\right] + i\cos^{-1}\frac{\sigma-\cos\theta}{\sqrt{(\sigma-\cos\theta)^2+\sin^2\theta}} \right\} d\theta \tag{A.44}$$

From the imaginary part of this equation, one can obtain

$$\int_0^{2\pi} \log(\sigma^2 - 2\sigma\cos\theta + 1)\,d\theta = 4\pi\log\sigma \tag{A.45}$$

(ii) $\sigma \equiv \frac{r}{a} < 1$ or $r < a$

Now, consider the complex integral of $\overline{w}(z)$ along the contour shown in Fig. A.4. Similarly as the above section

$$\oint_\Gamma \overline{w}(z)\,dz = 2\pi i \log\sigma \tag{A.46}$$

The left-hand side of this equation is

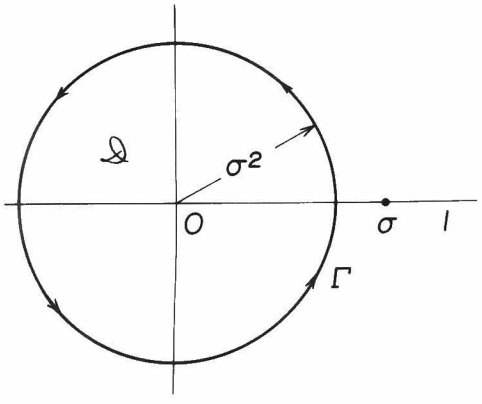

Fig. A.4 Contour of complex integral ($\sigma < 1$)

$$\oint_\Gamma \overline{w}(\overline{z})\,d\overline{z} = \oint_\Gamma \frac{\log(\sigma - z)}{\overline{z}}\,d\overline{z}$$

$$= \int_0^{2\pi} \frac{\log(\sigma - \sigma^2 e^{i\theta})}{\sigma^2 e^{i\theta}} \cdot \sigma^2 e^{i\theta} \cdot i\,d\theta$$

$$= 2\pi i \log\sigma + i\int_0^{2\pi} \left\{ \frac{1}{2}\log\left[(1-\sigma\cos\theta)^2 + (\sigma\sin\theta)^2\right] \right.$$

$$\left. + i\cos^{-1}\frac{1-\sigma\cos\theta}{\sqrt{(1-\sigma\cos\theta)^2 + (\sigma\sin\theta)^2}} \right\} d\theta \qquad \text{(A.47)}$$

Then from the imaginary part of this equation, one can obtain

$$\int_0^{2\pi} \log(\sigma^2 - 2\sigma\cos\theta + 1)\,d\theta = 0 \qquad \text{(A.48)}$$

Appendix XI

Using the formulae concerning the infinite product,

namely

$$\pi z \prod_{\beta=1}^{\infty} \left(1 + \frac{z^2}{\beta^2}\right) = \sinh \pi z$$

$$\prod_{\beta=1}^{\infty} \left(1 + \frac{z^2}{(2\beta-1)^2}\right) = \cosh \frac{\pi z}{2} \tag{A.49}$$

Then

$$\sum_{\beta=-\infty}^{\infty} \left\{ \log\left[z - 2\alpha B - 2i\beta L - a\right] - \log\left[z - (2\alpha+1)B - 2i\beta L + \tilde{a}\right] \right.$$

$$= \log\left[z - 2\alpha B - a\right] + \sum_{\substack{\beta=-\infty \\ \beta \neq 0}}^{\infty} \log\left[\frac{z - 2\alpha B - a}{2\beta L} - i\right]$$

$$- \log\left[z - (2\alpha+1)B + \tilde{a}\right] - \sum_{\substack{\beta=-\infty \\ \beta \neq 0}}^{\infty} \left[\frac{z - (2\alpha+1)B + \tilde{a}}{2\beta L} - i\right]$$

$$= \log\left\{(z - 2\alpha B - a) \prod_{\beta=1}^{\infty} \left[1 + \frac{(z - 2\alpha B - a)^2}{4\beta^2 L^2}\right]\right\}$$

$$- \log\left\{\left[z - (2\alpha+1)B + \tilde{a}\right] \prod_{\beta=1}^{\infty} \left[1 + \frac{[z - (2\alpha+1) + \tilde{a}]^2}{4\beta^2 L^2}\right]\right\}$$

$$= \log \sinh \frac{\pi[z - 2\alpha B - a]}{2L} - \log \sinh \frac{\pi[z - (2\alpha+1)B + \tilde{a}]}{2L} \tag{A.50}$$

Similarly,

$$\sum_{\beta=-\infty}^{\infty} \left\{ \log\left[z - (2\alpha+1)B - i(2\beta+1)L + a\right] - \log\left[z - 2\alpha B - i(2\beta+L) - \tilde{a}\right] \right.$$

$$= \log \cosh \frac{\pi[z - (2\alpha+1)B + a]}{2L} - \log \cosh \frac{\pi[z - 2\alpha B - \tilde{a}]}{2L} \tag{A.51}$$

Summing up these terms with respect to α from minus infinity to infinity, one can obtain Eq. (1.5.3).

Appendix XII

Transforming the coordinates so that the source may locate at the origin, namely

$$x \longrightarrow x + \bar{a}_x \quad , \quad y \longrightarrow y + \bar{a}_y$$

Then the integration of Eq. (1.5.11) becomes

$$\overline{W} = \int_{-\frac{B}{2}-\bar{a}_x}^{\frac{B}{2}-\bar{a}_x} \int_{-\frac{L}{2}-\bar{a}_y}^{\frac{L}{2}-\bar{a}_y} \frac{\rho}{4\pi} \log \frac{x^2+y^2}{\bar{a}_x^2+\bar{a}_y^2} \, dx dy$$

$$= \frac{\rho}{4\pi} \int_{x_0}^{x_1} \int_{y_0}^{y_1} \log \frac{x^2+y^2}{\bar{a}_x^2+\bar{a}_y^2} \, dx dy \qquad (A.52)$$

where

$$\left.\begin{aligned} x_0 &= -\frac{B}{2} - \bar{a}_x \quad , \quad x_1 = \frac{B}{2} - \bar{a}_x \\ y_0 &= -\frac{L}{2} - \bar{a}_y \quad , \quad y_1 = \frac{L}{2} - \bar{a}_y \end{aligned}\right\} \qquad (A.53)$$

For the first, the integration with x is

$$\int_{x_0}^{x_1} \log (x^2+y^2) \, dx = \left[x \log (x^2+y^2) - 2x + 2y \tan^{-1} \frac{x}{y} \right]_{x_0}^{x_1}$$

$$= \left\{ x_1 \log (x_1^2+y_1^2) - x_0 \log (x_0^2+y^2) - 2(x_1 - x_0) \right.$$

$$\left. + 2y \left[\tan^{-1} \frac{x_1}{y} - \tan^{-1} \frac{x_0}{y} \right] \right. \qquad (A.54)$$

Each term of this equation, now, is integrated with respect to y from y_0 to y_1, namely

$$\int_{y_0}^{y_1} \log (x_j^2+y^2)\,dy$$

$$= y_1 \log (x_j^2+y_1^2) - y_0 \log (x_j^2+y_0^2) - 2(y_1-y_0)$$

$$+ 2x_j\left[\tan^{-1}\frac{y_1}{x_j} - \tan^{-1}\frac{y_0}{x_j}\right] \qquad \text{(A.55)}$$

where $j = 0$ or 1.

$$\int_{y_0}^{y_1} 2(x_1-x_0)\,dy = 2(x_1-x_0)(y_1-y_0) \qquad \text{(A.56)}$$

By using the formula of

$$\tan^{-1}\frac{x_j}{y} = -\tan^{-1}\frac{y}{x_j} + \frac{\pi}{2} \qquad \left(\frac{y}{x_j} \geqq 0\right)$$

$$= -\tan^{-1}\frac{y}{x_j} - \frac{\pi}{2} \qquad \left(\frac{y}{x_j} < 0\right)$$

then,

$$\int_{y_0}^{y_1} y \tan^{-1}\left(\frac{x_j}{y}\right) dy = \int_{y_0}^{y_1} y\left\{\pm\frac{\pi}{2} - \tan^{-1}\frac{y}{x_j}\right\} dy$$

$$= \pm\frac{\pi}{2}\int_{y_0}^{y_1} y\,dy - \int_{y_0}^{y_1} y\tan^{-1}\frac{y}{x_j}\,dy$$

$$= \pm\frac{\pi}{2}\left[\frac{y^2}{2}\right]_{y_0}^{y_1} - \left[\frac{x_j^2+y^2}{2}\tan^{-1}\frac{y}{x_j} - \frac{x_j y}{2}\right]_{y_0}^{y_1}$$

$$= \pm\frac{\pi}{4}(y_1^2-y_0^2) - \frac{1}{2}\left[(x_j^2+y_1^2)\tan^{-1}\frac{y_1}{x_j}\right.$$

$$\left. - (x_j^2+y_0^2)\tan\frac{y_0}{x_j} - x_j(y_1-y_0)\right]$$

$$= -\frac{1}{2}\left[x_j^2\tan^{-1}\frac{y_1}{x_j} - x_j^2\tan^{-1}\frac{y_0}{x_j}\right.$$

$$\left. - y_1^2\tan^{-1}\frac{x_j}{y_1} + y_0^2\tan^{-1}\frac{x_j}{y_0} - x_j(y_1-y_0)\right] \qquad \text{(A.57)}$$

Substituting the results of Eqs. (A55)-(A.57) into Eq. (A.5. then,

$$\overline{W} = \frac{g}{4\pi}\Big[x_i^2(\tan^{-1}\frac{y_i}{x_i} - \tan^{-1}\frac{y_o}{x_i}) - x_o^2(\tan^{-1}\frac{y_i}{x_o} - \tan^{-1}\frac{y_o}{x_o})$$
$$+ y_i^2(\tan^{-1}\frac{x_i}{y_i} - \tan^{-1}\frac{x_o}{y_i}) - y_o^2(\tan^{-1}\frac{x_i}{y_o} - \tan^{-1}\frac{x_o}{y_o})$$
$$+ x_i y_i \log(x_i^2+y_i^2) - x_i y_o \log(x_i^2+y_o^2) - x_o y_i \log(x_o^2+y_i^2) + x_o y_o \log(x_o^2$$
$$- 3(x_i - x_o)(y_i - y_o) - (x_i - x_o)(y_i - y_o)\log(\bar{a}_x^2 + \bar{a}_y^2)\Big] \qquad (A.58)$$

Substituting the relations of Eq. (A.53), one can obtain Eq. (1.5.11). In these equations, the value of arctangent should evidently take its principal one.

Appendix XIII

Before the reduction of Eq. (2.4.1), the approximations of Eq. (1.3.23) in Chapter 3 in Part I, and Eq. (A.13) in Appendix V are studied here again in order to know the meaning of the approximation of pressure distribution and load capacity.

At the first, the transformation from an incompressible solution P to a compressible solution p is as follows (see Appendix V):

$$p - p_a = \sqrt{(p_o + p_a)(P - p_a) + p_a^2} - p_a \qquad (A.59)$$

where the isothermal condition is assumed. This is shown

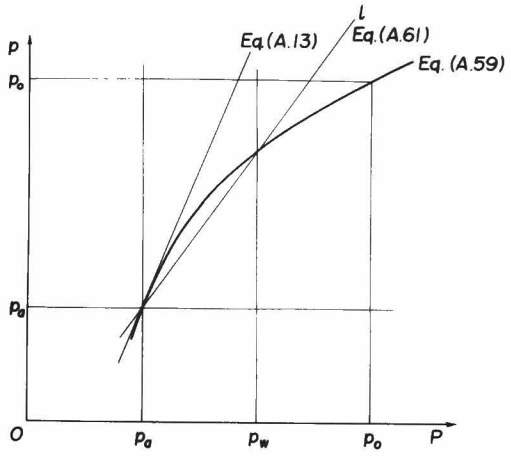

Fig. A.5 Transformation of P into p

in chart in Fig. A.5.

The approximation of the bearing pressure by Eq. (A.13) in Appendix V is represented by the tangent of this curve at $P=p_a$ because Eq. (A.13) is the first term of Taylor expansion of the pressure near the ambinet pressure p_a.

Now, denoting $S(P)$ as the projected area enclosed by a constant pressure line of P, then, the load capacity can be obtained by the following calculation by using Fig. A.6:

$$W = \int_{\text{bearing area}} (p - p_a)\, dS = \int_{p_a}^{p_o} (p - p_a)\left(-\frac{dS}{dP}\right) dP \qquad (A.60)$$

where minus sign represents that $S(P)$ decreased when P increases. $-\frac{dS}{dP}$ in the last term of the integration can be considered as a distribution function or a density function

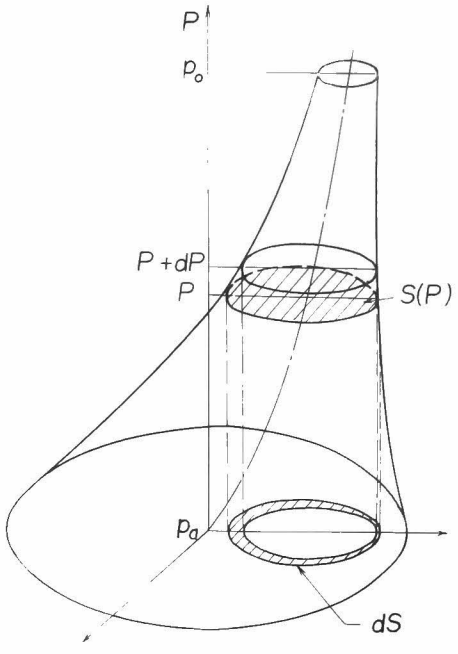

Fig. A.6 Schematic expression of obtaining load capacity

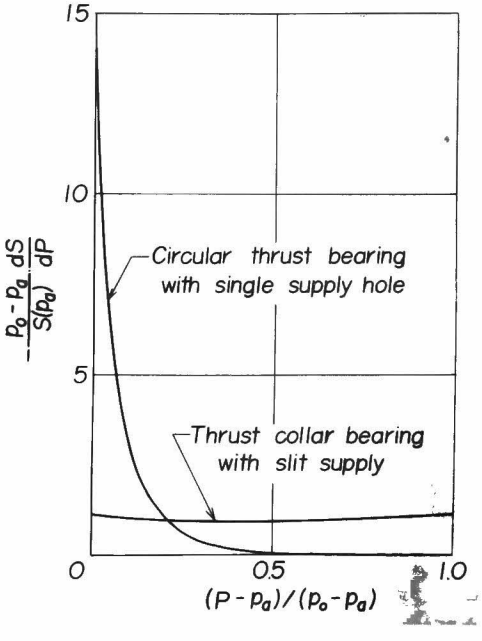

Fig. A.7 Distribution function in integration of load capacit;

of the bearing pressure P at the calculation of load capacity, while the term of $(p-p_a)$ is to be a weight function. The load capacity can be obtained by the integration of the product of weight function $(p-p_a)$ and density function $(-\frac{dS}{dP})$ with respect to the pressure range.

In Fig. A.7, the distribution functions are shown in dimensionless form; one is a circular thrust bearing with single supply hole with dimensions of $R_a = 1/2$ and $R_s = 1/100$ as shown in Fig. 1.3.13 in Chapter 3 in Part I, the other a thrust collar bearing with single slit supply with dimensions of $R_o = 1/3$ and $R_a = 2/3$. $S(P_a)$ represents the bearing area according to the difinition of $S(P)$.

For the former bearing, the circular thrust bearing with single supply hole, $-\frac{P_o - P_a}{S(P_a)} \cdot \frac{dS}{dP}$ takes very large value for lower pressure, while for higher pressure (near the pressure P_o) it falls down very much nearly to zero, which means that most of the bearing area is occupied by comparatively lower pressure than P_o. Then for the calculation of the compressible load capacity of this bearing, the accurate approximation of the compressible pressure, which is considered to be the weight function, is demanded especially for lower pressure region, because this part may be main for the load capacity. This is the reason

why the approximation of Eq. (1.3.23) is used accurately for the presumption of compressible effect.

In the other hand, for the thrust collar bearing with slit-supply, the density or distribution of the pressure is formed to be almost uniform as shown in Fig. A.5. Then, compressible pressure, which is the weight function, must be fairly accurate even for higher part.

Now, the following function may be considered as the weight function p instead of Eq. (A.13) :

$$p = \frac{\sqrt{(p_o + p_a)(p_w - p_a) + p_a^2} - p_a}{p_w - p_a}(P - p_a) + p_a \qquad (A.61)$$

This equation represents a straight line ℓ which intersects with the real transforming function Eq. (A.59) at two points of $P = p_a$ (ambient pressure) and $P = p_w$ in the $P \sim p$ plane of Fig. A.5, where $p_w \left[= W/\pi(r_i^2 - r_o^2) \right]$ is the specific load of the bearing. The load capacity can be obtained by this approximation of the weight function in integration of Eq. (A.60), resulting

$$\begin{aligned} W &= \int_{\text{bearing area}} (p - p_a)\, dS \\ &= \int_{\text{bearing area}} \frac{\sqrt{(p_o + p_a)(p_w - p_a) + p_a^2} - p_a}{p_w - p_a}(P - p_a)\, dS \\ &= \frac{\sqrt{(p_o + p_a)(p_w - p_a) + p_a^2} - p_a}{p_w - p_a} \int_{\text{bearing area}} (P - p_a)\, dS \\ &= \frac{\sqrt{(p_o + p_a)(p_w - p_a) + p_a^2} - p_a}{p_w - p_a} \times W_{\text{incomp.}} \end{aligned} \qquad (A.62)$$

This pressumption of compressible effect may be fiarly accurate as shown in the experimental results in the body.

Appendix XIV

The complementary functions of Eq. (3.2.21) is given by the following forms.

$$\left.\begin{aligned} p &= M_1 I_0(\alpha_1 r) + M_2 I_0(\alpha_2 r) + M_3 K_0(\alpha_1 r) + M_4 K_0(\alpha_2 r) \\ p' &= N_1 I_0(\alpha_1 r) + N_2 I_0(\alpha_2 r) + N_3 K_0(\alpha_1 r) + N_4 K_0(\alpha_2 r) \end{aligned}\right\} \quad (A.63)$$

These functions can be made to satisfy Eq. (3.2.21) by substituting it into the differential equations and equating the coefficients in I_0 and K_0 to zero. From this, the following equations are obtained

$$\left.\begin{aligned} (\alpha_i^2 - A'^2) N_j + B'^2 M_j &= 0 \\ (\alpha_i^2 - D'^2) M_j + D'^2 N_j &= 0 \end{aligned}\right\} \quad (A.64)$$

where $j = 1$ or 3 when $i = 1$, and $j = 2$ or 4 when $i = 2$. Both of M_j and N_j are not zero in Eq. (A.64), hence

$$\begin{vmatrix} \alpha_i^2 - A'^2 & B'^2 \\ B'^2 & \alpha_i^2 - D'^2 \end{vmatrix} = 0 \quad (A.65)$$

This determinant yields Eq. (3.2.24).

Then, from Eq. (A.64), one can obtain the relation of Eq. (3.2.25). Since the particular solution of Eq. (3.2.21) is

$$p = p' = p_s \tag{A.66}$$

the general solutions are obtained as Eqs. (3.2.22) and (3.2.23).

Appendix XV

For the former case of ΔW_1, the load capacity is

$$W_1 = (p_s - p_a)\int_0^{\pi} \frac{-2ra_1\cos\theta}{b_1 + (\frac{1}{B_0})^3(1+\varepsilon\cos\theta)^3}\, d\theta$$

$$= -\frac{2ra_1(p_s-p_a)}{b_1}\int_0^{\pi} \frac{B_0^3\cos\theta}{B_0^3+(1+\varepsilon\cos\theta)^3}\, d\theta$$

or

$$F_{W_1} = -\int_0^{\pi} \frac{B_0^3\cos\theta}{B_0^3+(1+\varepsilon\cos\theta)^3}\, d\theta \tag{A.67}$$

The bearing stiffness is

$$\frac{\partial F_{W_1}}{\partial \varepsilon} = \int_0^{\pi} \frac{3B_0^3\cos^2\theta(1+\varepsilon\cos\theta)^2}{[B_0^3+(1+\varepsilon\cos\theta)^3]^2}\, d\theta \tag{A.68}$$

At the design, the bearing stiffness near non-eccentric state is important, that is

$$\left.\frac{\partial F_{W_1}}{\partial \varepsilon}\right|_{\varepsilon=0} = \int_0^{\pi} \frac{3B_0^3\cos^2\theta}{(B_0^3+1)^2}\, d\theta = \frac{3\pi B_0^3}{2(B_0^3+1)^2} \tag{A.69}$$

In order to obtain the appropriate design parameter which maximizes the stiffness,

$$\frac{\partial}{\partial B_0}\left(\left.\frac{\partial F_{W_1}}{\partial \varepsilon}\right|_{\varepsilon=0}\right) = \frac{9\pi B_0^2(1-B_0^3)}{2(B_0^3+1)^4} = 0 \tag{A.70}$$

Thus the maximum bearing stiffness can be obtained when

$B_o = 1.0$.

For the case of ΔW_2, the similar deductions are applied resulting

$$\frac{\partial F_{W_2}}{\partial \varepsilon} = \int_0^{\pi} \frac{2\kappa^2 B_o^2 \cos^2\theta(1+\varepsilon\cos\theta)}{[\kappa^2 B_o^2 + (1+\varepsilon\cos\theta)^2]^2} d\theta$$

$$\left.\frac{\partial F_{W_2}}{\partial \varepsilon}\right|_{\varepsilon=0} = \int_0^{\pi} \frac{2\kappa^2 B_o^2 \cos^2\theta}{(\kappa^2 B_o^2 + 1)^2} d\theta = \frac{\pi \kappa^2 B_o^2}{(\kappa^2 B_o^2 + 1)^2}$$

Then

$$\frac{\partial}{\partial(\kappa B_o)}\left(\left.\frac{\partial F_{W_2}}{\partial \varepsilon}\right|_{\varepsilon=0}\right) = \frac{2\pi\kappa B_o(1-\kappa^2 B_o^2)}{(\kappa^2 B_o^2 + 1)^4} = 0 \qquad (A.71)$$

The maximum bearing stiffness for this case can be obtained when $\kappa B_o = 1.0$.

References

(1) T. Sasaki and H. Mori, "Survey of Gas-Lubricated Bearing Research in Japan with Recent Developments in the Study of Externally-Pressurized Bearings," First International Symposium on Gas-Lubricated Bearings, Washington D.C., Oct. 26-28, (1959).

(2) S. Raynor and A. Charnes, "Flow Parameters in Hydrostatic Lubrication for Several Bearing Shapes" ASME Trans. 82 p.257 (1960).

(3) H. Mori, "A Theoretical Investigation of Pressure Depression in Externally Pressurized Gas-Lubricated Circular Thrust Bearings", ASME. Trans. 83 p.201 (1961)

(4) L. Licht, D.D. Fuller and B. Sternlicht, "Self-Excited Vibrations of an Air Lubricated Thrust Bearing", ASME Trans. 80, p.411 (1958)

(5) S.A. Sheinberg and V.G. Shuster, "Vibration-proof Hydrostatic Porous Air Bearing" Machine and Instrument, No.11, p.23, (1960) (in Russian)

(6) W.A. Gross, Gas Film Lubrication, John Wiley & Sons, Inc., New York, N.Y., (1962).

(7) C.H. Robinson and F. Sterry, "The Static Strength of Pressure Fed Gas Journal Bearings, Porous Bearings," Atomic Energy Research Establishment, Harwall, Berkshire, ED/R 1672, (1958).

(8) H. Mori, H. Yabe, and T. Shibayama, "Theoretical Solution as a Boundary Value Problem for Externally Pressurized Porous Gas-Bearings", ASME-ASLE International Lubrication Conference, Washington, D.C., Oct. 13-16, 1964.

(9) H. Mori, Y. Miyamatsu and S. Sakata, "Theory on the Pressure Depression in Externally Pressurized Thrust Gas Bearing with Consideration of the Growth of Boundary Layers" Journal of JSLE, 9 p.113 (1964).